
Nonuniversal features of turbulent systems

Vasil Bratanov



München 2015

Nonuniversal features of turbulent systems

Vasil Bratanov

Dissertation
an der Fakultät für Physik
der Ludwig-Maximilians-Universität
München

vorgelegt von
Vasil Bratanov
aus Burgas, Bulgarien

München, den 19.03.2015

Erstgutachter: Prof. Dr. Erwin Frey
Zweitgutachter: Prof. Dr. Frank Jenko
Tag der mündlichen Prüfung: 10.07.2015

Contents

Abstract	vii
Zusammenfassung	viii
1 Introduction	1
1.1 The numerous faces of turbulence	1
1.2 The idealised picture of turbulence	2
1.3 Real-life turbulent systems	6
1.4 Structure of the thesis	8
2 Classical Navier-Stokes turbulence	11
2.1 Navier-Stokes equations	14
2.2 Fourier representation and Kolmogorov's theory	18
2.3 The role of dimensionality	26
2.4 A note on universality	30
3 Importance of linear effects in plasmas	35
3.1 Gyrokinetic theory	36
3.2 Effects of damped modes on plasma turbulence	41
3.3 Role of velocity hyperdiffusion	43
3.4 Conclusion	49
4 Modified Kuramoto-Sivashinsky model	51
4.1 Spectral formulation	53
4.2 Modification of the linear part	56
4.3 Numerical implementation	58
4.4 Energy transfer between scales	60
4.5 Closure approximation and energy spectrum	67
4.6 Conclusion	73
5 Turbulence in living fluids	75
5.1 Fourier representation	79
5.2 Spectral shell decomposition	84
5.3 Quasi-normal approximation	88
5.4 Navier-Stokes nonlinearity	94

5.5	Variable spectral exponent	97
5.6	Conclusion	100
6	Summary and outlook	103
A	Relations involving the plasma dispersion function Z	107
B	Range of the disparity parameter S	109
C	Symmetries of the shell-to-shell coupling terms	111
D	Derivation of Eqs. (5.25)	113

Abstract

Turbulence is one of the most widespread phenomena in nature occurring in fluids and plasmas at all scales - from the blood flow in the human body, via the Earth's atmosphere to the remnants of supernovas at astrophysical scales. Despite its frequent occurrence, constructing a theory of turbulent motion, which provides reliable quantitative predictions, represents one of the unsolved problems of classical physics. Most of the research efforts in the past have been focused on studying the Navier-Stokes model of simple fluids and trying to understand the Fourier spectrum of velocity fluctuations. Due to this common restriction to the Navier-Stokes equations, turbulence is usually associated with power-law spectra of universal form which arise only at scales where both driving and dissipation mechanisms are inactive. However, recent studies reveal that many active systems which do not possess a true inertial range can, nevertheless, exhibit power-law spectra. Furthermore, those spectra are not of universal form which contradicts the classical theory of turbulence.

One of the turbulent models we shall consider in this work derives from the Kuramoto-Sivashinsky equation. It describes a simple one-dimensional active system where energy is injected at large scales and dissipated at small scales. Based on observations from plasma physics we modify the linear part of the equation such that the large scales remain practically intact but the damping rate at high wave numbers approaches a constant. We construct a semi-analytical approximation for the modified equation which predicts a power-law form for the energy spectrum in the range where the ratio between the characteristic linear and nonlinear frequencies is scale-independent. Furthermore, we conclude that the steepness of this power law is not universal but depends on the frequency ratio. These results are confirmed by numerical simulations. Our analysis could also be relevant for kinetic Alfvén-wave turbulence in the solar wind where similar conditions might occur.

Further in this work we present the first systematic study of another active system which provides a continuum model aimed at the coarse-grained description of the dynamics observed in dense bacterial suspensions. The model extends the framework of the familiar Navier-Stokes equations by including additional linear and nonlinear terms in order to emulate energy injection and dissipation as well as the flocking tendency of bacteria. The resulting dynamics has been described as 'low-Reynolds-number turbulence' and the corresponding energy spectrum exhibits nonuniversal power laws at large scales. With the aid of extensive numerical simulations we study the scale-to-scale energy flow in spectral space. The physical insight gained this way helped us to develop an approximation for the spectral energy balance equation. Its solution provides an energy spectrum of a power-law form at small wave numbers. Furthermore, we derive a functional dependence of the steepness of this power law on the system parameters. A comparison with data from numerical simulations verifies our results.

Zusammenfassung

Turbulenz stellt eines der meist verbreiteten Phänomene in der Natur dar, das in Fluiden und Plasmen auf diversen Längenskalen auftritt - von den Blutgefäßen im menschlichen Körper, über die Erdatmosphäre bis hin zu den Überbleibseln von Supernovae im Weltall. Trotz des häufigen Auftretens von turbulenten Strömungen gehört die Entwicklung einer systematischen Theorie, die zuverlässige quantitative Vorhersagen liefert, zu den ungelösten Problemen der klassischen Physik. Ein Großteil der bisherigen Forschungsarbeit auf dem Gebiet wurde der Untersuchung einfacher Fluide gewidmet, indem man versuchte, das Fourierspektrum der Geschwindigkeitsfluktuationen zu verstehen. Aufgrund dieser Einschränkung auf die Navier-Stokes-Gleichungen ist Turbulenz meistens mit potenzgesetzartigen Spektren assoziiert, die eine universale Form haben und auf Längenskalen entstehen, auf denen weder Antrieb- noch Dissipationsmechanismen aktiv sind. Jüngste Studien haben jedoch offenbart, dass viele aktive Systeme, die keinen echten Inertialbereich aufweisen, trotzdem spektrale Potenzgesetze vorweisen können. Außerdem haben diese Potenzgesetze keine universelle Form, was der klassischen Theorie der Turbulenz widerspricht.

Eines der turbulenten Modelle, die wir in dieser Arbeit betrachten werden, beruht auf der Kuramoto-Sivashinsky-Gleichung. Sie beschreibt ein einfaches, eindimensionales aktives System, wo Energie auf großen Skalen eingeführt und auf kleinen Skalen dissipiert wird. Auf der Basis von Beobachtungen aus der Plasmaphysik modifizieren wir den linearen Teil der Gleichung so, dass die großen Skalen praktisch unverändert bleiben, aber die Dämpfungsrate bei großen Wellenzahlen konstant wird. Anschließend konstruieren wir eine Näherung für die modifizierte Gleichung, die ein Potenzgesetz als Energiespektrum in dem Bereich vorhersagt, wo der Quotient zwischen der charakteristischen linearen und nichtlinearen Frequenz skalenundependent ist. Weiterhin folgern wir, dass die Steigung dieses Potenzgesetzes von dem Frequenzquotienten abhängt. Diese Resultate bestätigen wir durch numerische Simulationen. Unsere Analyse könnte auch für Turbulenzregimes relevant sein, die in dem Sonnenwind durch kinetische Alfvénwellen zustande kommen.

Weiter im Laufe dieser Arbeit legen wir die erste systematische Untersuchung von einem anderen aktiven System vor. Es stellt ein Kontinuumsmodell dar, das die großskalige Dynamik von bakteriellen Suspensionen beschreibt. Das Modell erweitert den Rahmen der geläufigen Navier-Stokes-Gleichungen, indem es zusätzliche lineare und nichtlineare Terme enthält, die Energiezufuhr und Energiedissipation so wie das Schwarmverhalten von Bakterien nachahmen. Die daraus resultierende Dynamik wurde als „Turbulenz bei kleinen Reynoldszahlen“ bezeichnet und das entsprechende Energiespektrum weist nicht-universelle Potenzgesetze auf großen Skalen auf. Mithilfe von umfangreichen numerischen Simulationen studieren wir den Energiefluss zwischen verschiedenen Skalen im Fourier-Raum. Die dadurch gewonnen physikalischen Erkenntnisse helfen uns, eine Näherung der spektralen Energiebilanzgleichung zu entwickeln. Ihre Lösung für das Energiespektrum liefert ein Potenzgesetz bei kleinen Wellenzahlen. Weiterhin leiten wir auch die funktionale Abhängigkeit der Steigung dieses Potenzgesetzes von Systemparametern her. Der Vergleich mit Daten aus numerischen Simulationen bekräftigt unsere Resultate.

Chapter 1

Introduction

1.1 The numerous faces of turbulence

Turbulence, the irregular and chaotic motion of fluids, is an ubiquitous phenomenon in Nature. Its understanding represents not only a problem of academic and scientific interest but also underlines its importance for many practical engineering applications. One encounters turbulence at various spatial scales: from branch points in large arteries in the human body to the motion of the oceans and the atmosphere. Turbulent flows play a major role in the heat transfer in nuclear reactors, drag forces around air planes, cars or in oil pipelines which makes its quantitative characterisation an engineering challenge with far-reaching implications. The high cruising speed of aeroplanes excites the air flowing past their wings creating turbulent boundary layers. The properties of the latter control the aerodynamic drag experienced by the aeroplane. Thus, a better understanding of turbulence would provide an improved wing design allowing for a more stable flight with less fuel consumption. The impact of turbulent flows can be immediately felt not only by fast moving objects but also on the ground. Strong winds create turbulent wakes behind large buildings further increasing the wind load and undermining their structural integrity. Additionally, effective city planning relies heavily on the dispersion of pollutants from chimney stacks and cars which happens largely due to turbulent flows in the surrounding air presenting an example where the effect of turbulence has to be enhanced rather than mitigated. Another case where the impact of turbulence plays a decisive and positive role present internal combustion engines. There, the explosive ignition of the fuel leads to highly turbulent flows in the combustion chamber which enhance the mixing between the fuel component and the oxygen in the air thereby improving the combustion efficiency. As a result, developing a better understanding together with means for control of turbulent flows would potentially allow for a considerable reduction in the world's energy consumption.

Besides its practical importance, turbulence is one of the fundamental problems of classical physics and deserves attention in its own right. Quantitative understanding of turbulent

flows will shed light on many important processes in Nature. A crucial example from geophysics presents the geodynamo which generates the Earth's magnetic field. Heat produced in the inner Earth's core, mainly due to the decay of radioactive elements, induces turbulent convection flows in the liquid and electrically conducting outer core. Thus, gaining insight into the intrinsic properties of turbulent flows will provide understanding of the dynamo processes controlling Earth's magnetic field and can translate directly to the generation of magnetic fields inside and around stars.

Turbulent motion can arise not only in fluids but also in plasmas which comprise more than 99% of the visible Universe. Thus, turbulence constitutes an important phenomenon at astrophysical scales governing physical processes such as solar flares, solar eruptions, or accretion disks around compact massive objects like neutron stars or black holes. The former present an example of large-scale plasma turbulence that can have a direct impact on Earth. Solar prominences constitute large arc-shaped plasma filaments anchored in the Sun's photosphere and extending outwards into the Sun's corona. The shape of those filaments is governed by the Sun's magnetic field which traps plasma from the photosphere that is much cooler and denser than the surrounding coronal plasma. Such high temperature and density gradients trigger strong turbulence in the coronal plasma around the prominence often leading to magnetic reconnection and inducing solar flares and coronal mass ejections. The latter generate the solar wind, consisting of highly energetic charged particles moving outward from the Sun. When such a solar-wind shock wave reaches the Earth it can produce turbulence in the Earth's magnetosphere leading to geomagnetic storms. These storms can increase electric currents in Earth's magnetosphere and ionosphere which can have severe negative effects on radio communication as well as on the hardware of satellites. More intense geomagnetic storms have the potential to damage satellite-based navigation systems, such as GPS, and cause large-scale electrical blackouts. According to the modern cosmological models, turbulence, as produced by the multidimensional Burgers equation, might have played an essential role even in the early Universe shortly after the recombination of atomic nuclei and electrons, i.e., when photons decoupled from the baryonic matter.

1.2 The idealised picture of turbulence

Due to its frequent occurrence in natural phenomena, turbulence has very early drawn the attention of natural scientist. Before the development of advanced calculus the study remained rather qualitative. Some of the earliest and most prominent examples are the drawings of Leonardo da Vinci, e.g., Fig. 1.1. It was him who introduced the term 'turbolenza' which translates roughly as 'the random motion of the crowd'. Already back then he recognised that turbulent motion is characterised by fairly chaotic features suggesting an apparent randomness in its structures. Later, with the development of mechanics on the basis of differential and integral calculus and its success in describing the motion of mass points and rigid bodies, physicists focused on deriving the equations of motion of continu-

ous media. Pioneers in that direction were, among others, Leonhard Euler, Claude-Louis



Figure 1.1: A sketch of a turbulent water flow found in da Vinci's notes. The chaotic nature of the flow is immediately evident. One can also recognise the feature of scale-invariance, i.e., a small portion of the turbulent fluid looks statistically the same as a much larger one.

Navier and George Gabriel Stokes who, by applying Newton's laws of motion together with the condition that fluid cannot be created or destroyed, were able to derive the equations governing the motion of fluids which we shall discuss in more detail in the next chapter. The advancements in the study of turbulence, and fluid dynamics in general, remained rather limited due to the mathematical complexity of the equations involved. In contrast to the motion of point particles where we have a system of three (for the case of three spatial dimensions) coupled second-order ordinary differential equations with respect to time, in the case of continua, one has to solve a system of three coupled partial second-order differential equations, i.e., we have to solve for the three components of the fluid velocity as functions of both space and time. Hence, analytical solutions were possible only in a limited number of cases where many, often unrealistic, assumptions about the behaviour of the fluid were made. Such simplified cases, however, lead to smooth and usually steady flow patterns which are qualitative different from the turbulent regime.

Indeed, turbulent flows display a clear chaotic behaviour which varies rapidly in space and time, and exhibits strong sensitivity on initial conditions. Moreover, the turbulent structures seem to continually evolve and never exactly repeat. This chaotic character impeded the analytical studies which for a long time remained on a rather qualitative basis. However, the myriad of practical problems involving turbulence demand for reliable quantitative predictions for which a qualitative theory is not sufficient. Furthermore, the rapid and chaotic fluctuations of the turbulent velocity field calls for a statistical description. One should abandon the idea to compute the exact fluid velocity in every point in space

and time, but instead focus on predicting the statistical properties of turbulent flows. Such a statistical theory of turbulence might not appear satisfactory compared to the success of celestial mechanics but it has proved useful in other fields of physics, e.g., thermodynamics. There, the computation of the position and velocity of every atom or molecule in a macroscopic quantity of matter is practically impossible even from the view of classical physics. However, statistical properties of such many-body systems have provided the possibility of exact quantitative predictions leading to the solution of many real-life problems. However, an important difference between turbulence and thermodynamics that prevents successful concepts and ideas from the latter to be directly applied to the former is the fact that thermodynamical systems are usually in equilibrium. On the other hand, one of the essential features of turbulent fluids is that their degrees of freedom are not in equilibrium, i.e., there is no equipartition of energy among them. This lack of energy equilibrium is another manifestation of the fact that turbulence is only possible in open systems which interact with their environment and, thereby, ensuring a continuous energy flow through the system.

For a turbulent fluid there is always a kind of energy source which is often in the form of an external force acting on the system. In a turbulent wake behind the fast-spinning propeller of an aeroplane this is the motion of the propeller itself which sets the fluid into motion and acts as an external stirring mechanism providing energy to the fluid. In the case of an aeroplane wing, the fast movement of the wing pushes the air sideways forcing it to flow around the wing. This disturbance of the air movement causes the turbulent wake behind the wing.¹ The energy for the excitation of turbulence comes from the kinetic energy of the wing. Thus, the drag acting on objects moving in a fluid medium is entirely due to the turbulence they produce in that medium. Furthermore, the mathematical analysis tells us that a smooth fluid flow around objects of arbitrary form produces no drag force on them.

While the mechanism of energy injection is often external, energy is dissipated by entirely internal processes. All fluids consist of molecules attracting with each other, unless the distance between them becomes very small and the force becomes repulsive. This mutual attraction keeps the molecules together creating effectively a friction mechanism. If two neighbouring layers of a fluid move with different speeds, this intermolecular attraction will speed up the slower layer while slowing down the faster one and, thereby, equalising their speeds. The result of this effective inter-fluid friction is heat. Hence, the kinetic energy of the turbulent motion, where velocity varies rapidly in space, is transformed via friction in thermal energy that heats the fluid.

The description given above provides one of the main concepts of classical turbulence theory which has played a major role for the motivation of the present work, namely the idea of scale separation. In the classical examples of turbulence the kinetic energy is injected into

¹The entire process is much more complicated and not completely understood. An essential role play adhesion forces between air molecules and the molecules at the boundary of the wing. This allows for the creation of boundary layers around rigid objects in a fluid and the properties of those layers determine the extent and intensity of the turbulent wake behind the wing.

the fluid by external forces and this happens at very large spatial scales, usually the largest allowed by the system size, e.g., the size of the object around which the fluid flows. On the other hand, the kinetic energy of the turbulent motion is extracted and transformed into heat at very small scales where the friction between fluid layers moving at different speeds becomes important. Hence, there is a flow of kinetic energy from large through intermediate to small spatial scales. The nonlinear character of the equations of motion provides the coupling between different scales ensuring the continuous flow of kinetic energy. It is the intermediate scales that transport the energy in a conservative manner and act as a mediator between energy injection and dissipation. Often it is only these scales which are called turbulent and at which the velocity field exhibits scale-invariant structures that are characteristic of turbulence.

Quantitative description of turbulence in realistic examples is often mathematically too involved. For that reason one usually considers simplified situations where certain symmetries apply at least in a statistical manner. Such a simplification represents the case of homogeneous and isotropic turbulence, i.e., we assume that the turbulent fluid looks statistically the same in every point in space and in every direction. These conditions are, in general, not fulfilled at very large scales, e.g., at scales comparable with the size of the object moving through the fluid. However, the intermediate scales, which transfer kinetic energy in a conservative manner, are much smaller than the system size and there the conditions of homogeneity and isotropy are well satisfied. Thus, if one regards the largest scales of the system simply as an energy source and is interested only in the dynamics of the intermediate, turbulent, scales, one can usually consider them to be statistically homogeneous and isotropic, thereby, simplifying the mathematical description considerably and still retaining the essential turbulence features.

Since the efforts for deriving exact mathematical turbulent solutions of the equations of motion have proved to be futile, the development of the energy picture described above has led to important physical insights. It has stimulated the main advancement in the quantitative understanding of turbulence since the derivation of the governing equations by Navier and Stokes. The notion that a turbulent flow represents a system out of equilibrium where kinetic energy flows in one direction from large to small spatial scales serves as a basis for the Kolmogorov theory. The latter, which we shall describe in greater detail in Chapter 2, assumes a constant flow of kinetic energy together with statistical homogeneity and isotropy. Based on that one derives the average intensity of the turbulent fluctuations at different scales. Thus, it provides the first and, according to many, the most successful attempt of developing a statistical theory of turbulence. It is important to emphasise that the flow of kinetic energy discussed above does not happen from one region of the turbulent system to another. It occurs simultaneously in every turbulent region and presents a flow of energy between spatial structures of different size. Large structures break up giving rise to many smaller structures which inherit their energy. This is the mechanism behind the energy exchange among different scales and, in three dimensional systems, its nett effect is one-directional. Thus, structures in the turbulent velocity field break apart over and over again until the resulting formations reach the spatial scales at which friction between

fluid layers moving at different velocities becomes strong enough to dissipate a substantial amount of their energy before they break even further. The Kolmogorov theory represents a hallmark in turbulence research, since it is the first systematic approach that led to experimentally measurable predictions. Indeed, the theory successfully passed the early experimental tests serving as a foundation for further developments. More refined experiments, however, showed that real turbulent systems display small but consistent deviations from the predictions of Kolmogorov providing the stimulation for further theoretical research. The theory of Kolmogorov is, however, in many aspects, heuristic. It relies on assumptions which are sound, physically motivated and can be tested experimentally, but it is not derived in a mathematically rigorous manner from the Navier-Stokes equations. This mathematical bridge between the exact fluid equations of motion and the Kolmogorov theory still remains an open problem in turbulence research.

1.3 Real-life turbulent systems

The idealised picture of turbulence, described in the previous section, is often not valid for real-life turbulent systems. The most restrictive of the idealisations discussed so far is the picture of energy injection and transfer between different spatial scales. While the concept behind the mechanism of energy dissipation is based on sound physical grounds and well-tested, the notion that energy injection is entirely due to external forces, localised at the largest scales of the system and completely uncorrelated with the fluid motion, does not find much confirmation in realistic examples. Frequently, energy injection mechanisms are internal with respect to the system under study and due to intrinsic instabilities of the flow, e.g., induced by the corresponding geometrical setting. In the case of the solar prominences discussed in Section 1.1 as well as of fusion devices using magnetic confinement we have adjacent layers of plasma with very different temperature and density. Such large temperature and density gradients correspond to a state with lower entropy. Thus, mixing between the different layers occurs which increases the entropy of the system. On the mathematical level of description this gives rise to linear instabilities, i.e., arbitrarily small perturbations of a certain type, i.e., modes, tend to grow unboundedly in the linear regime. Eventually nonlinear effects become important, providing coupling between fluctuations of different scales and allowing for energy exchange. Thus, in real-life turbulence energy injection emanates from internal mechanisms which are directly connected to the fluctuations of the velocity field and it is not simply a Gaussian noise in time as in many idealised models. Such temperature and density gradients represent a source of free energy which is then transformed into kinetic energy of the turbulent fluctuations.

Another class of examples where internal instabilities give rise to turbulence provides the Rayleigh-Taylor instability, one the most prominent manifestation of which can be often seen in the breaking of large waves. It arises when a heavier fluid lies on top of a lighter one in a gravitational field or when a lighter fluid is accelerated into a heavier one. Such a situation occurs also often in plasmas, e.g., in concepts of both inertial and magnetic

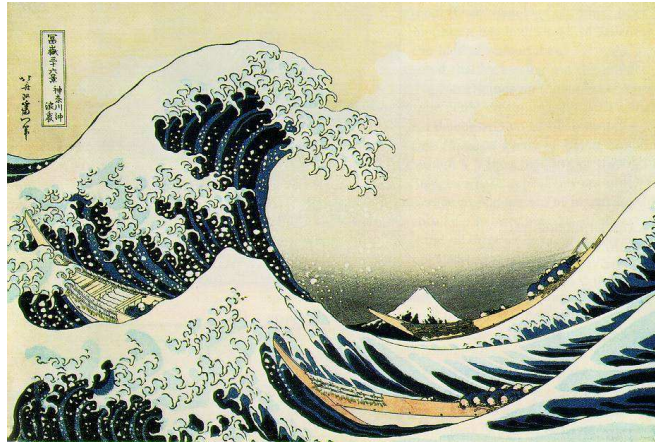


Figure 1.2: An example of the Rayleigh-Taylor instability as painted by Katsushika Hokusai. At the wave crest we have a heavier fluid (water) on top of a lighter one (air). This leads rapidly to instabilities producing via mixing the typical white colour of the crest and making the water flow turbulent.

confinement fusion. A more dense fluid on top of a less dense one represents an energetically unstable configuration. The resulting instability rearranges the fluid, thereby, transforming the stored potential energy into kinetic energy. The importance of this example lies in the fact that the Rayleigh-Taylor instability favours small-scale fluctuations. Thus, in such systems energy is injected at small scales which fundamentally contradicts the paradigm of classical turbulence. Nevertheless, the small scale fluctuations manage to excite turbulence in the whole system, i.e., although energy is injected at small scales, it eventually reaches the largest scales available. Such an inverse energy flow in three dimensional systems challenges the Kolmogorov theory of turbulence and calls for a generalisation that can take such processes into account, since they are common in Nature.

Furthermore, real-life turbulent systems often exhibit instabilities at various spatial scales. Thus, the simple picture of energy injection concentrated at the largest scales represents an unrealistic extreme case. In reality the flow of energy appears to be multi-scale and considerably more complicated. The spatial scales at which different injection mechanisms are active can even overlap leading to a situation where instabilities will interact not only with damped modes but also with other instabilities leading to a more complicated physical picture. Additionally, in the case of plasmas the large-scale linear instabilities coexist with damped linear eigenmodes. It is still an open problem in plasma turbulence research to determine unambiguously if, or in which parameter regimes, the coupling between unstable and damped eigenmodes at different scales will dominate, thus leading to an energy flux across scales similarly to the classical theory of turbulence, and when the dominant coupling will be between unstable and damped modes at the same scale resulting in an entirely different paradigm. The issue regarding the nonlinear interaction between linear eigenmodes in the case of magnetised plasmas and its dependence on system parameters will be discussed in greater detail in Section 3.2. Furthermore, the classical theory of turbulence

relies inevitably on the concept of scale separation, i.e., the mechanism of energy injection and dissipation should be active at very distant spatial scales while the intermediate scales provide simply a conservative energy channel. However, this assumption contradicts what we observe in many practical examples where the ranges of energy injection and dissipation overlap, thereby, invalidating the basis of the Kolmogorov theory.

1.4 Structure of the thesis

In the present work we shall not try to improve the classical theory of turbulence in order to account for the small deviations in the Kolmogorov spectrum, nor shall we focus on a particular engineering example, like predicting the drag force experienced by a wing of a particular shape as a function of velocity. Instead, we will study some basic turbulent models where the assumptions of the Kolmogorov theory are not satisfied. The classical theory of turbulence predicts an universal form for the intensity of velocity fluctuations as a function of scale, the so-called Kolmogorov spectrum. It is universal in the sense that it does not depend on system parameters or on injection or dissipation mechanisms. Real-life turbulence, however, often exhibits clear non-universality, i.e., the form of the energy distribution among scales depends on various system parameters. Such non-universal features appear to be rather the rule than the exception in plasma physics and can also be observed in biophysics as we shall see in Chapter 5. Our goal is to study the range of scales where nonuniversality occurs, the structure of the terms that are active in that range as well as their interdependence. This way we will deduce the physical conditions of the nonuniversal behaviour and derive an analytic expression for its dependence on system parameters.

While turbulence is the main topic discussed in this thesis, its immensely manifold nature makes it virtually impossible to consider all of its aspects. Thus, the present text focuses on the work that the author has done in the course of his PhD at the Max Planck Institute for Plasma Physics in Garching, Germany, and the issues which have arisen in the course of this research. In order to facilitate a smooth transition to some of the open problems in fundamental turbulence research, this thesis is structured as follows.

In Chapter 2 we shall give a general description of classical Navier-Stokes turbulence in fluids. The first part of the chapter provides the basic phenomenology of turbulence focusing also on the transition from a laminar to a turbulent flow and introducing the parameter that governs such a transition connecting it to the mixing properties of the fluid. Next, we give the mathematical form of the Navier-Stokes equations together with their physical interpretation. The important quantities for the statistical description of turbulence are established emphasising the mathematical difficulties attributed to the Navier-Stokes equations and the terms they arise from. Section 2.2 introduces the Fourier representation in the framework of turbulence and discusses the theory of Kolmogorov. The latter is one of the most important advances in the understanding of three-dimensional turbulence and provides insight into the quantitative form of some statistical properties of turbulent flows.

The next section deals with the critical exception of the two-dimensional version of the Navier-Stokes equations. It emphasises how fundamentally different such two-dimensional systems are compared to their three-dimensional counterparts in terms of energy dynamics at different spatial scales. In the last section of Chapter 2 we discuss some of the features, usually thought of to be universally exhibited by turbulent flows, but actually absent in the dynamics of many real-life turbulent systems. Examples of such a departure from the orthodox view come from many different areas, e.g., plasma physics or biophysics. They commonly belong to the class of active systems where energy is injected by means of internal linear instabilities and not external forces.

Chapter 3 deals with the importance of linear effects in plasma physics. In contrast to the Navier-Stokes equations, the linearised versions of the equations governing the time evolution of the particle distribution functions in plasmas display much greater complexity and a myriad of nontrivial solutions. The reason for this lies in the fact that the dynamics considered in the kinetic theory of plasmas takes place both in configuration and velocity space. The important differences being that they allow for linearly unstable eigenmodes coexisting with countably infinitely many damped modes at the same wave vector. While the importance of the unstable modes is immediately evident, we elaborate on recent studies which have shown that also the damped eigenmodes can have a considerable effect on the nonlinear behaviour of the system. Section 3.3 presents some of the early work of the author regarding the linear physics in some drift-kinetic models used in plasma physics. Since eigenmodes (both unstable and damped) are essential for the full nonlinear evolution of the system, it is natural to ask what effect on them have operators of simplified form used to model collision processes. The example of such a simplified collision operator considered here is the hyperdiffusion term used extensively in numerical simulations.

The mathematical formulation of the models used in plasma physics is even more intricate than that of classical fluid turbulence and does not allow a transparent analytical investigation, since already the linearised problem provides a considerable challenge for physical interpretation. Thus, in Chapter 4 we consider a simplified one-dimensional model exhibiting spatio-temporal chaos. Although it was originally introduced in the field of plasma physics, it has been developed independently for the description of chemical reactions of the Belousov-Zhabotinsky type as well as for flame-front propagation. Motivated by observations from plasma physics we shall modify the linear terms of the model which will lead to fundamental changes in the form of the energy spectrum. Section 4.4 is then devoted to the study of the nonlinear interactions between different Fourier modes which are responsible for the exchange of energy between them. Based on these observations we propose a closure scheme aimed at modelling the small-scale structure of the system. Hence, for this range of the spectrum we obtain a closed differential equation that is solved analytically. Its solutions confirm the form produced by numerical simulations and provide an analytic expression for its functional dependency on systems parameters. This dependency compares also favourably against numerical computations.

In Chapter 5 we investigate another model that exhibits turbulent behaviour. It is for-

mulated in two spatial dimensions and has been put forward to describe the dynamics of bacterial suspensions. The model contains the basic features of the Navier-Stokes equations. However, due to the interactions between bacteria, it also includes additional terms which give rise to internal instabilities acting as a mechanism for energy injection. In addition, there are also nonlinear terms of order higher than two which aim to model flocking behaviour as observed in such biological systems. Examining this higher-order nonlinearity with the aid of the spectral shell decomposition used in the analysis of classical turbulence, we find that, in contrast to the familiar Navier-Stokes nonlinearity, it cannot be interpreted as a mean for transfer of energy between different spatial scales. The result of such a coupling mechanism consists mostly in the dissipation of the same amount of energy from both scales. In Section 5.3 we study the probability distribution of the Fourier-transformed velocity field at small wave numbers and conclude that it is very close to a Gaussian distribution which is a similar result as the one obtained for the classical two-dimensional Navier-Stokes model. This allows for the construction of a large-scale approximation of the higher-order nonlinearity which compares favourably to numerical simulations. Section 5.4 deals with the effect of the classical Navier-Stokes nonlinearity. We find that it transports energy mostly from intermediate (where instabilities are most prominent) to large scales. Such an effect is due to the two-dimensional setting in which the model is considered. There is no cascade of energy, i.e., a constant energy flux through scales, instead at large scales the characteristic shear rate is constant with respect to the wave number. This provides a heuristic closure of the nonlinearity leading to a closed differential equation for the energy spectrum as explained in Section 5.5. The solution of this differential equation gives an energy spectrum of a power-law form at small wave numbers which we also verify numerically. Moreover, the steepness of this power law is not universal but depends on system parameters which is also observed in the numerical simulations.

Chapter 2

Classical Navier-Stokes turbulence

Historically, the recognition of turbulence and its qualitative study dates back to the 15th century to the time of Leonardo da Vinci who left in his notes many drawings of turbulent flows, e.g., Fig. 1.1. Already then two characteristic features of turbulence were recognised which paved the way for a more quantitative study centuries later. The first one regards the chaotic and, apparently, random patterns produced in a turbulent fluid while the second one refers to the collective effects which play an essential role for the fluid motion. Another keen observation that put da Vinci ahead of his time was the coexistence of a myriad of circular flow structures, i.e., eddies or whirls, and the influence which the larger eddies exert on the smaller ones. This qualitative picture describing the interaction of vortical structures was rediscovered later (1926) by Lewis Fry Richardson and became the standard perception of turbulence that persists also today. In Richardson's words [1]:

‘Big whorls have little whorls
That feed on their velocity,
And little whorls have lesser whorls
And so on to viscosity.’

The modern description of this notion is that of a cascade of energy from large to small scales. It is important to note, however, that it applies only to three-dimensional turbulence. In three dimensions the large-scale vortices are unstable and break up into smaller ones of roughly half their size. (This corresponds to $q = 1/2$ in Fig. 2.1.) The smaller eddies, on their part, break again into even smaller whirls again half their size. This process continues until the dissipation scale η where the eddy size is small enough such that viscous effects become important and damp the flow converting its kinetic energy into heat. The energy cascade is presented schematically in Fig. 2.1 where the notation on the left denotes the characteristic size of the eddies at each level. The factor q is always smaller than one and quantifies the space-filling property of the eddies.

Another direction of research that dominated the investigation of turbulent flows in the second half of the 19th and first half of the 20th century was the question of how turbulence

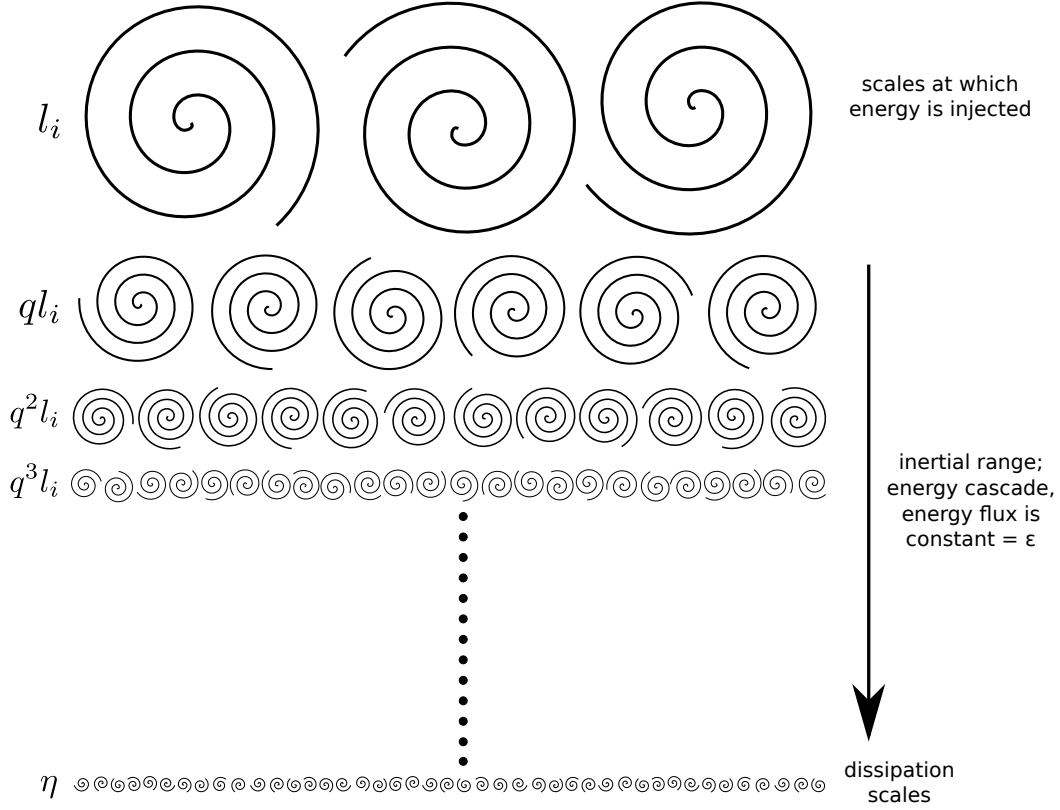


Figure 2.1: Schematic picture of the energy cascade in fully-developed turbulence. Energy is injected at large scales and transported conservatively by nonlinear interactions to small scales where it is dissipated by viscosity. (The figure was inspired by Fig. 7.2 in Ref. [2].)

arises in the first place. One of the pioneers in that direction was Osborne Reynolds who investigated experimentally the transition from a laminar to a turbulent flow. He identified an important quantity, subsequently called the ‘Reynolds number’, defined as

$$Re = \frac{UL}{\nu}, \quad (2.1)$$

where L is the typical size of the flow, U the typical fluid velocity at that scale and ν the kinematic viscosity, i.e., the physical viscosity divided by the fluid density ρ . Fig. 2.2 displays schematically Reynolds’ experiments. There water flows through a transparent circular pipe driven by a pressure difference and dye is injected in the middle of the pipe to visualise the flow. The diameter of the pipe gives the flow scale L and U is a typical flow velocity along the pipe induced by the pressure difference, e.g., the maximal velocity at the centre of the pipe or an average over the velocity profile. By controlling the latter one can control the Reynolds number. As an illustrative example, for water ($\nu \approx 0.01 \text{ cm}^2/\text{s}$ at a temperature of 20°C and pressure of $101,325 \text{ Pa}$) flowing through a pipe with a diameter of 5 cm with a speed of 10 m/s we have a Reynolds number of $Re \approx 5 \cdot 10^5$. When U is small enough the flow is laminar and the dye jet remains confined, i.e., its spreading is

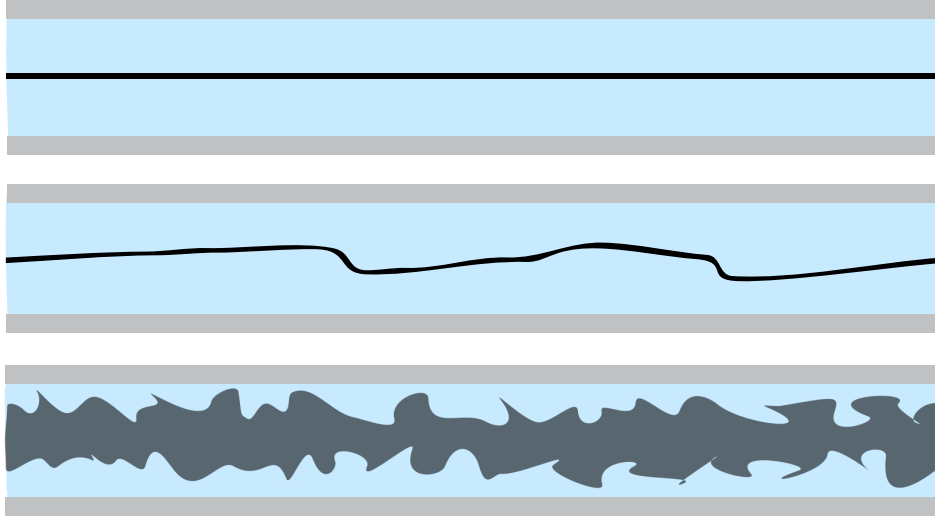


Figure 2.2: Schematic representation of the transition from laminar to turbulent fluid motion in a pipe flow. The fluid velocity increases from top to bottom.

due only to the molecular diffusion which is an extremely slow process. Increasing Re induces oscillations in the jet which become increasingly irregular. Nevertheless, the dye remains relatively confined. At large Re , however, the fluid motion becomes chaotic and the dye is evenly spread along the cross section of the pipe, i.e., we have fully developed turbulence. For a pipe with a circular cross section the critical value of the Reynolds number, where the transition happens, amounts nearly $Re \approx 2000$ although this number can vary between 1000 and 50,000 depending on the initial conditions and the roughness of the wall.[3] Hence, in the simple numerical example above involving normal every-day conditions the water flow is highly turbulent.

Here the Reynolds number was introduced in a rather *ad hoc* way. However, one can provide a more physical motivation for Eq. (2.1) by thinking in terms of the time scales determining the flow evolution. Given the typical flow size L and velocity U , one can easily construct the time scale $t_c = L/U$. It represents the time needed for a passive tracer to be convected by the typical flow velocity at distances comparable to the size of the flow domain. On the other hand, recalling the physical units of the kinematic viscosity, one can immediately form another time scale, namely $t_d = L^2/\nu$. The latter expresses the time molecular diffusion needs in order to transport fluid at distances again comparable to the size of the flow domain. Forming the ratio of both gives the large-scale Reynold number from Eq. (2.1), i.e., $t_d/t_c = Re$. In physical terms, the Reynolds number essentially embodies the ratio between the diffusive and the convective time, i.e., it shows how fast is the mixing due to macroscopic flows compared to the intrinsic diffusive transport. This large-scale mixing effect at high Re , greatly surpassing the molecular diffusion, is one of the main features characterising turbulence. It provides another reason for the importance of turbulence in engineering since enhanced mixing of different fluids plays an essential role in combustion processes and is one of the major hurdles preventing the commercial

realisation of controlled nuclear fusion.

Regarding the experimental study of homogeneous isotropic turbulence, which will be defined in the next section, one has to mention the Taylor's hypothesis [4] which played for a long time an essential role in the quantitative analysis of turbulent fluctuations. Since measuring the simultaneous velocity distribution in space presented for a long time an insurmountable challenge, one makes use of high mean flow velocities as produced in wind tunnels. Turbulence can be generated by a regular grid perpendicular to the mean flow. Far away from the grid and its edges the flow possesses a high degree of homogeneity and isotropy. When those states are reached one can conduct time-resolved hot-wire measurements of the velocity field at one point in space. When mean flow velocity is much larger than the turbulent velocity fluctuations, one can apply the Taylor's 'frozen-turbulence' hypothesis and argue that the turbulent structures are simply convected by the mean flow without change. Thus, the time-resolved measurement can be translated into a single-time spatial velocity distribution along the line of the mean flow. Recent developments in experimental techniques, however, has made possible to measure much more diverse quantities. Holographic methods allow to determine the full three-dimensional structure of the velocity field at a given time with high resolution.[5] Other methods allow the time-resolved measurement of the full three-dimensional velocity gradient tensor making possible the determination of local vorticity and energy dissipation.[6] The latter plays a pivotal role in studying energy cascades and intermittency as will be discussed in the next section. Techniques borrowed from high-energy physics have even allowed the tracking of a single small passive tracer in a fluid making possible the time-resolved measurement of many Lagrangian properties of the flow.[7]

2.1 Navier-Stokes equations

The quantitative study of turbulence begins with the formulation of the Navier-Stokes equations in the middle of the 19th century which, under the assumption of the continuum hypothesis, describe the motion of a fluid, both laminar and turbulent. For an incompressible flow of constant mass density ρ they read

$$\frac{\partial \mathbf{v}}{\partial t} + (\mathbf{v} \cdot \nabla) \mathbf{v} = -\nabla p + \nu \Delta \mathbf{v} + \mathbf{f} \quad (2.2a)$$

$$\nabla \cdot \mathbf{v} = 0, \quad (2.2b)$$

where \mathbf{x} belongs to a given spatial domain Ω , $\mathbf{v}(\mathbf{x}, t)$ is the velocity field of the fluid, p denotes the kinematic pressure, i.e., pressure divided by the density ρ , and the vector field $\mathbf{f}(\mathbf{x}, t)$ represents the external forces acting on a fluid element. For the above equations to be complete, they need to be supplemented by prescribing an initial velocity field $\mathbf{v}(\mathbf{x}, t = 0)$ on the whole spatial domain and appropriate boundary conditions, i.e., $\mathbf{v}(\mathbf{x}, t)$ on $\mathbf{x} \in \partial\Omega$ for all $t \in \mathbb{R}_+$. The physical content of the Navier-Stokes equations is simple -

they represent the Newton's second law for a continuous medium combined with the constraint for conservation of mass. The left-hand side embodies the acceleration acting on a fluid element. It contains the additional advection term $(\mathbf{v} \cdot \nabla)\mathbf{v}$ which arises mathematically through the coordinate transformation from a reference frame moving with the fluid (Lagrangian description) to a reference frame that is fixed in space (Eulerian description). From a physical point of view, it illustrates the acceleration of a fluid element due to the collective motion of the whole fluid. The right-hand side of Eq. (2.2) gives the different forces acting on a fluid element: the pressure force, viscous friction between different fluid elements and external forces. Despite the apparently simple form of the equations, the nonlinear term has the potential to excite fluctuations at many different spatial and temporal scales giving rise to highly complicated dynamics. Solutions of the Navier-Stokes equations are, in general, sensitive to initial conditions, meaning that very similar initial conditions can, in short time, develop into very different flows. Those difficulties lie at the core of the fact that up to date a general, exact solution of the Navier-Stokes equations is not known. The only exact solutions found so far correspond to simplified cases where usually the nonlinearity either vanishes or takes a simpler form due to geometric simplifications. (See, for example, the reviews [8, 9] and references therein.) In the two-dimensional case it has been proved that a unique smooth strong solution of Eq. (2.2) exists given that the initial condition is also smooth.[10] Furthermore, the solution remains global in time. The corresponding three-dimensional version of the problem, however, remains unsolved. To the best of our knowledge, so far only partial results have been obtained guarantying a smooth, unique and global in time solution only if the initial velocity is small enough with respect to an appropriate norm. Without the smallness condition a solution with the desired properties is known to exist only up to a given time T , which depends on the initial condition. For a relatively complete and up-to-date overview of the results obtained so far (both for a general domain in the form of a smooth manifold \mathcal{M} as well as in the special case of \mathbb{R}^N) the reader is referred to Ref. [11]. Providing a mathematically rigorous answer to the problem of existence and uniqueness of a smooth solution for the three-dimensional version of the incompressible Navier-Stokes equations presents one of the six still unsolved Millennium Prize Problems posed by the Clay Mathematics Institute. However, even if such a solution is actually found, its usefulness for the physical investigation of turbulent flows might be rather limited. A good example in this regard presents the Burgers' equation [12, 13], often viewed as a one-dimensional model for turbulence although it possesses several different physical features, e.g., allowing for the development of shock waves. In this case, the Cole-Hopf transformation [14, 15] transforms the equation into the linear diffusion equation which can be readily solved for a given initial condition. The result can then be transformed back obtaining a unique velocity field which adheres to the original nonlinear equation. Nevertheless, the exact solution constructed that way is so complicated that one can hardly gain any physical insight into the processes modelled by the Burgers' equation.

Although the transition from a laminar to a turbulent flow in simple geometrical settings as in Reynolds' experiments has been studied for a long time and an informal notion of

turbulence is well established, there is up to date no mathematically precise definition of turbulence. The problematic point is that both the laminar and turbulent flows are solutions of the same Navier-Stokes equations and the parameter, controlling the transition, is continuous. This gave rise to the Landau-Hopf theory [16, 17] that increasing the Reynolds number leads to an infinite number of successive bifurcations of the flow pattern giving rise to different spatial and temporal scales. Eventually, this produces an apparently random flow. Later, Ruelle and Takens [18] introduced the concept of a strange attractor. In the dynamical systems' framework developed in their paper, the flow undergoes only few bifurcations before the chaotic state, represented by the strange attractor, emerges. Experimentally, one has never managed to observe the numerous bifurcations of the Landau-Hopf theory but the variety of bifurcations observed was often greater than the one suggested by Ruelle and Takens, e.g., the period-doubling subharmonic sequence of Feigenbaum [19] or transitions involving 'phase-locking'. [20] Although proposing a universal definition of turbulence is a rather controversial issue, the dominant perception of turbulence is that it describes solutions of the three-dimensional Navier-Stokes equations which display irregular and chaotic behaviour both in space and in time. Such a depiction successfully captures the main characteristic of the turbulent flow, namely its chaotic structure. Nevertheless, it is too restrictive and cannot encompass the immense variety of practical situations in which chaotic flows arise, e.g., solutions of the two-dimensional Navier-Stokes equations at high Reynolds number or the dynamics produced by the Hasegawa-Mima model. Another important example that goes beyond the scope of such a definition would also be turbulence in plasmas as in stars, accretion disks around compact and massive objects or nuclear fusion devices on Earth to name a few. Thus, in this thesis we shall use the term 'turbulence' in a more general manner denoting chaotic (both in space and time) fields which arise as solutions of nonlinear evolution equations and possess a large number of interacting degrees of freedom.

Although finding a general exact solution of the Navier-Stokes equations, or even proving the existence and uniqueness of a solution, presents an open mathematical problem, the main effort in the study of turbulence from a physical point of view is dedicated to determining the statistical properties of the turbulent field in space and time. A central role in this investigation play velocity correlation functions, also called velocity moments. The general definition of an n -point, n -time velocity moment reads

$$Q_{i_1 i_2 \dots i_n}(\mathbf{x}_1, \mathbf{x}_2, \dots, \mathbf{x}_n; t_1, t_2, \dots, t_n) := \langle v_{i_1}(\mathbf{x}_1, t_1) v_{i_2}(\mathbf{x}_2, t_2) \dots v_{i_n}(\mathbf{x}_n, t_n) \rangle, \quad (2.3)$$

which is a tensor of rank n and the brackets $\langle \cdot \rangle$ denote a suitable averaging procedure. In situations where the physical features of the flow are expected to change, e.g., in the case of decaying turbulence where energy should decrease with time, an ensemble average is needed. It corresponds to an average over the functional space of all possible different initial conditions, which are still allowed by the mathematical formulation of the problem. However, such an average procedure is computationally very demanding. In the case where energy is constantly supplied to the system, after some intrinsic time a statistically stationary state emerges where the total energy merely fluctuates around some constant value.

Then, one can substitute the ensemble average with a time average. From a mathematical point of view this is supported by the so-called ergodicity assumption which, roughly speaking, states that the system will come arbitrarily close to every possible state given one waits long enough. Although the ergodicity hypothesis has, to the best of our knowledge, never been rigorously proved for the Navier-Stokes equations, it is suggested by the high degree of disorder characteristic to turbulence. While such an averaged quantity as in Eq. (2.3) still contains a lot of information, the irregular fluctuations due to the chaotic nature of the turbulent velocity field are averaged out and we are left with a more regular structure telling us how the velocity of the different fluid elements is correlated in space and time. The complexity of such velocity moments grows rapidly when the number of fields is increased, so practical applications usually involve moments of only up to fourth order. Despite their apparent simplicity, the Navier-Stokes equations in a general setting are still too complex and investigations of the fundamental features of turbulence make use of two important simplifications. First, one considers flows which are spatially homogeneous, i.e., their statistical properties do not depend on the absolute position in the flow, implying that the velocity moments are functions of relative position only, i.e.,

$$Q_{ij}(\mathbf{x}, \mathbf{x}') = Q_{ij}(\mathbf{x} - \mathbf{x}') = Q_{ij}(\mathbf{x}' - \mathbf{x}), \quad (2.4)$$

where we have suppressed the temporal arguments for the ease of notation. The second important simplification is the assumption of isotropy which implies independence of direction, i.e., all velocity moments are invariant under rotations of the coordinate frame and under reflections of its axes. Mathematically, the latter means that velocity moments depend only on the absolute value of the relative positions and not on their orientation, i.e.,

$$Q_{ij}(\mathbf{x} - \mathbf{x}') = Q_{ij}(|\mathbf{x} - \mathbf{x}'|). \quad (2.5)$$

Velocity correlations play an essential role in determining the turbulent flow since they represent the nonlinear interaction of the velocity field with itself. The condition of homogeneity demands that the velocity field has zero mean, i.e., $\langle v_j(\mathbf{x}, t) \rangle = 0$ for every j , \mathbf{x} and t which yields for the evolution of the velocity field in terms of correlations

$$\frac{\partial v_i(\mathbf{x}, t)}{\partial t} = \sum_{j,k} M_{ijk}(\nabla)(v_j(\mathbf{x}, t)v_k(\mathbf{x}, t) - Q_{jk}(\mathbf{x}, \mathbf{x}; t, t)) + \nu \Delta v_i(\mathbf{x}, t), \quad (2.6)$$

with $M_{ijk}(\nabla)$ being an integral operator arising from the incompressibility constraint of the Navier-Stokes equations in the following way. Let $G(\mathbf{x}, \mathbf{x}')$ be the solution of the Poisson's equation

$$\Delta G(\mathbf{x}, \mathbf{x}') = \delta(\mathbf{x} - \mathbf{x}') \quad (2.7)$$

with a delta function as a source term and periodic boundary conditions. Then we define the operator D_{ij} as

$$(D_{ij}(\nabla)f)(\mathbf{x}) := \delta_{ij}f(\mathbf{x}) - \frac{\partial^2}{\partial x_i \partial x_j} \int_V G(\mathbf{x}, \mathbf{x}') f(\mathbf{x}') d^3 x'. \quad (2.8)$$

The importance of the latter consists in projecting out the part of the vector field that is not divergence free and thereby ensuring that the incompressibility condition is satisfied. We will usually use D_{ij} in Fourier space where it takes a much simpler form. With the aid of the expression in Eq. (2.8) $M_{ijk}(\nabla)$ can be readily constructed as

$$M_{ijk}(\nabla) := -\frac{1}{2} \left(\frac{\partial}{\partial x_j} D_{ik}(\nabla) + \frac{\partial}{\partial x_k} D_{ij}(\nabla) \right). \quad (2.9)$$

Recalling the definition of the second-order velocity moment, it is straightforward to derive from the Navier-Stokes equations the evolution equation for $Q_{ij}(\mathbf{x}, \mathbf{x}'; t, t')$ which reads

$$\frac{\partial}{\partial t} Q_{ij}(\mathbf{x}, \mathbf{x}'; t, t') = \nu \Delta Q_{ij}(\mathbf{x}, \mathbf{x}'; t, t') + M_{ikl}(\nabla) Q_{klj}(\mathbf{x}, \mathbf{x}, \mathbf{x}'; t, t, t'). \quad (2.10)$$

Thus, solving the equation for the second-order velocity correlation would require a third-order moment as an input which, however, is unknown. Further, an equation for the latter would incorporate a still unknown fourth-order velocity correlation and so forth. An infinite hierarchy of moment equations arises which never terminates naturally. This is usually referred to as the ‘closure problem’ in turbulence theory. What is described as a ‘closure’ is an *ad hoc* relation expressing a velocity correlation of a certain order as a function of lower-order velocity moments. This creates a system of finitely many coupled equations that can, at least in principle, be solved.

2.2 Fourier representation and Kolmogorov’s theory

The mathematical complexity of the Navier-Stokes equations and the relation between the pressure and the velocity field suggest the search for different representations of the quantities involved. One such choice for representing the velocity field offer Fourier series which are suitable for studying turbulence under periodic boundary conditions. This type of analysis was pioneered by Taylor [4] and largely adopted by the turbulence community with the advent of the pseudo-spectral method employed in numerical simulations.[21, 22] Assuming we have the vector field $\mathbf{v}(\mathbf{x}, t)$ defined on the N -dimensional torus Ω (usually a rectangular N -dimensional box) with volume V we can write

$$\mathbf{v}(\mathbf{x}, t) = \sum_{\mathbf{k}} \hat{\mathbf{v}}(\mathbf{k}, t) e^{i\mathbf{k} \cdot \mathbf{x}} \text{ or equivalently } \hat{\mathbf{v}}(\mathbf{k}, t) = \frac{1}{V} \int_{\Omega} \mathbf{v}(\mathbf{x}, t) e^{-i\mathbf{k} \cdot \mathbf{x}} d^N x, \quad (2.11)$$

where \mathbf{k} is an N -dimensional wave number vector determined by the box size in each direction as $\mathbf{k} = 2\pi(n_1/L_1, n_2/L_2, \dots, n_N/L_N)$ and $n_i \in \mathbb{N}_0$. Note, however, that modelling isotropic flows demands for equal box size in all directions. An additional computational advantage of the Fourier representation consists in the fact that the tensors $D_{\alpha\beta}$ and $M_{\alpha\beta\gamma}$ arising from the incompressibility condition take much simpler forms, namely

$$D_{\alpha\beta}(\mathbf{k}) = \delta_{\alpha\beta} - \frac{k_{\alpha} k_{\beta}}{k^2}, \quad M_{\alpha\beta\gamma}(\mathbf{k}) = -\frac{1}{2} i (k_{\beta} D_{\alpha\gamma}(\mathbf{k}) + k_{\gamma} D_{\alpha\beta}(\mathbf{k})). \quad (2.12)$$

The more transparent structure makes the symmetries of $D_{\alpha\beta}$ and $M_{\alpha\beta\gamma}$ immediately evident, i.e.,

$$D_{\alpha\beta}(\mathbf{k}) = D_{\beta\alpha}(\mathbf{k}) , \quad (2.13a)$$

$$D_{\alpha\beta}(-\mathbf{k}) = D_{\alpha\beta}(\mathbf{k}) , \quad (2.13b)$$

$$M_{\alpha\beta\gamma}(\mathbf{k}) = M_{\alpha\gamma\beta}(\mathbf{k}) \text{ and} \quad (2.13c)$$

$$M_{\alpha\beta\gamma}(-\mathbf{k}) = -M_{\alpha\beta\gamma}(\mathbf{k}). \quad (2.13d)$$

Thus, in Fourier space the incompressible Navier-Stokes equations can be combined in a straightforward way in one single equation that reads

$$\frac{\partial}{\partial t} \hat{v}_\alpha(\mathbf{k}, t) = \sum_{\rho, \gamma=1}^N M_{\alpha\rho\gamma}(\mathbf{k}) \sum_{\mathbf{p}} \hat{v}_\rho(\mathbf{p}, t) \hat{v}_\gamma(\mathbf{k} - \mathbf{p}, t) - \nu k^2 \hat{v}_\alpha(\mathbf{k}, t) + \hat{f}_\alpha(\mathbf{k}, t), \quad (2.14)$$

where for now we leave the spatial dimension N arbitrary and bear in mind that the physically relevant cases are usually $N = 2$ or 3 . The incompressibility condition transforms into $\mathbf{k} \cdot \hat{\mathbf{v}}(\mathbf{k}, t) = 0$ and is automatically fulfilled by the equation above due to the properties of the tensor $M_{\alpha\beta\gamma}$. The convolution sum over \mathbf{p} results from a Fourier transformation of the quadratic nonlinearity in Eq. (2.2a). Since we are interested in statistical features of the velocity field, it is important to investigate the velocity correlation in Fourier space, i.e., $\langle \hat{v}_\alpha(\mathbf{k}, t) \hat{v}_\beta(\mathbf{p}, t') \rangle$, and relate it to the correlation functions in real space. Under the condition of spatial homogeneity, which is a prerequisite for isotropy, a straightforward computation gives

$$\langle \hat{v}_\alpha(\mathbf{k}, t) \hat{v}_\beta(\mathbf{p}, t') \rangle = \delta_{\mathbf{k}+\mathbf{p},0} \frac{1}{V} \int_{\Omega} Q_{\alpha\beta}(\mathbf{r}; t, t') e^{-i\mathbf{k} \cdot \mathbf{r}} d^N r. \quad (2.15)$$

Similarly, omitting the time argument for brevity, one derives for a velocity correlation of arbitrary order M

$$\langle \hat{v}_{\alpha_1}(\mathbf{k}_1) \hat{v}_{\alpha_2}(\mathbf{k}_2) \dots \hat{v}_{\alpha_M}(\mathbf{k}_M) \rangle = 0 \text{ if } \sum_{j=1}^M \mathbf{k}_j \neq 0. \quad (2.16)$$

Of course, the existence of a box with a given size destroys the complete homogeneity even in a statistical sense due to the presence of boundaries. However, far away from the walls, i.e., outside the boundary layer they induce, the turbulent flow approaches closely the homogeneous and isotropic idealisation. Restoring strict homogeneity and isotropy requires taking the limit of the box length L going to infinity. In this limit the wave number components k_i become continuous variables and the sums over wave numbers change over to integrals. Formally, we have $\mathbf{k} \in \mathbb{R}^N$ and

$$\lim_{L \rightarrow \infty} \left(\frac{2\pi}{L} \right)^N \sum_{\mathbf{k}} = \int_{\mathbb{R}^N} d^N k, \quad (2.17)$$

where a quadratic box is assumed. Additionally, the Kronecker delta becomes a Dirac delta function and $\langle \hat{v}_\alpha(\mathbf{k}, t) \hat{v}_\beta(\mathbf{p}, t') \rangle \rightarrow \delta(\mathbf{k} + \mathbf{p}) Q_{\alpha\beta}(\mathbf{k}; t, t')$ with $Q_{\alpha\beta}(\mathbf{k}; t, t')$ being the continuous spectral density tensor. Omitting the time argument for ease of notation and following Ref. [23], one can argue that in the isotropic case

$$Q_{\alpha\beta} = g_1(k) \delta_{\alpha\beta} + g_2(k) k_\alpha k_\beta. \quad (2.18)$$

Taking into account that $\sum_\beta k_\beta Q_{\alpha\beta}(\mathbf{k}) = 0$, which results from the incompressibility condition, we derive that the spectral density tensor is proportional to the projection operator $D_{\alpha\beta}$, i.e., $Q_{\alpha\beta}(\mathbf{k}; t, t') = Q(\mathbf{k}; t, t') D_{\alpha\beta}(\mathbf{k})$. In the case of an instantaneous velocity correlation, i.e., time arguments being the same, the spectral density Q depends only on the absolute value of \mathbf{k} , i.e., $Q(\mathbf{k}; t, t) = Q(k; t)$.

Given that in this thesis we will work mostly in Fourier space, it is helpful to illustrate the closure problem in spectral space where the structure of the equations is more transparent. Multiplying Eq. (2.14) with $\hat{v}_\beta(-\mathbf{k}, t)$, adding to it the evolution equation for $\hat{v}_\beta(-\mathbf{k}, t)$ multiplied by $\hat{v}_\alpha(\mathbf{k}, t)$, summing over α and taking the continuous limit gives

$$\begin{aligned} \frac{\partial Q(k; t)}{\partial t} = & -\frac{2}{N-1} \int_{\mathbb{R}^N} \sum_{\alpha, \rho, \gamma=1}^N \Re(M_{\alpha\rho\gamma}(\mathbf{k}) Q_{\alpha\rho\gamma}(\mathbf{k}, \mathbf{p}, -\mathbf{k} - \mathbf{p}; t)) d^N p - 2\nu k^2 Q(k; t) + \\ & + \frac{2}{N-1} \sum_{\alpha=1}^N \Re(\langle \hat{f}_\alpha(\mathbf{k}, t) \hat{v}_\alpha(-\mathbf{k}, t) \rangle), \end{aligned} \quad (2.19)$$

where we have used the simplification of homogeneous and isotropic turbulence and the property that $M_{\alpha\beta\gamma}(-\mathbf{k}) = -M_{\alpha\beta\gamma}(\mathbf{k})$. From Eq. (2.19) it becomes immediately clear that the evolution equation for second-order velocity correlations depends on third-order correlations which are *a priori* unknown. One can, of course, employ the Navier-Stokes equation in spectral space to derive the evolution equation for $Q_{\alpha\rho\gamma}(\mathbf{k}, \mathbf{p}, -\mathbf{k} - \mathbf{p}; t)$ in analogy to what we did in the previous section in real space. However, the resulting equation will involve unknown fourth-order correlation functions. An iterative application of the above procedure creates an infinite system of coupled equations and leads to conceptually the same closure problem as encountered earlier.

The nonlinear character of the Navier-Stokes equations complicates immensely their quantitative analysis. In order to gain some insight into the physics of turbulent flows they describe, it has proven useful to look at the representation of some physically relevant quantities in spectral space. An example of such an important physical quantity is the energy E of the system, defined as

$$E(t) = \frac{1}{2} \frac{1}{V} \int_{\Omega} |\mathbf{v}(\mathbf{x}, t)|^2 d^N x. \quad (2.20)$$

Strictly speaking, the above equation gives the energy of the system per unit mass. However, since we consider fluids with constant density, we shall refer to this quantity simply as

energy, which is a common abuse of notation in turbulence literature. Similarly, the energy of mode \mathbf{k} is given by $\langle |\hat{\mathbf{v}}(\mathbf{k}, t)|^2 \rangle / 2$. In the limit $L \rightarrow \infty$ one derives for a homogeneous and isotropic flow

$$E(t) = \frac{1}{2} \sum_{\alpha=1}^N \int_{\mathbb{R}^N} Q_{\alpha\alpha}(\mathbf{k}; t) d^N k = (N-1) \frac{\sqrt{\Pi}^N}{\Gamma(\frac{N}{2})} \int_0^\infty Q(k; t) k^{N-1} d^N k \quad (2.21)$$

with Γ denoting the Gamma function. The above calculation suggests expressing the energy at scale $1/k$ as

$$E(k, t) = (N-1) \frac{\sqrt{\Pi}^N}{\Gamma(N/2)} k^{N-1} Q(k; t), \quad (2.22)$$

which relates the second-order velocity correlation function to the energy of a given scale. $E(k, t)$ is usually referred to as the energy spectrum. Multiplying Eq. (2.19) with the appropriate factors, one arrives at

$$\frac{\partial E(k, t)}{\partial t} = T(k, t) - 2\nu k^2 E(k, t) + P(k, t), \quad (2.23)$$

where the first term on the right-hand side denotes the nonlinear transfer of energy between different scales and is given by

$$T(k, t) = -2 \frac{\sqrt{\Pi}^N}{\Gamma(N/2)} k^{N-1} \int_{\mathbb{R}^N} \sum_{\alpha, \rho, \gamma=1}^N \Re(M_{\alpha\rho\gamma}(\mathbf{k}) Q_{\alpha\rho\gamma}(\mathbf{k}, \mathbf{p}, -\mathbf{k} - \mathbf{p}; t)) d^N p. \quad (2.24)$$

The second term on the right-hand side quantifies the energy dissipation due to viscous effects and the last term represents the power input arising from the external forces acting on the fluid. It can be expressed as

$$P(k, t) = 2 \frac{\sqrt{\Pi}^N}{\Gamma(N/2)} k^{N-1} \Re \left(\langle \hat{\mathbf{f}}(\mathbf{k}, t) \cdot \hat{\mathbf{v}}(-\mathbf{k}, t) \rangle \right). \quad (2.25)$$

Eq. (2.23) can be viewed as the energy balance equation at scale $1/k$. It manifests quantitatively that the rate of change of energy at a given wave number results from the balance between energy input via external forces, energy dissipation due to viscosity and the interaction between different modes. Note that the dissipation $D(k) := -\nu k^2 E(k)$ is local in spectral space, i.e., it depends only on quantities at the scale under consideration, and the mode-to-mode interaction does not change the total energy of the system, i.e.,

$$\int_0^\infty T(k, t) dk = 0. \quad (2.26)$$

Thus, the nonlinearity merely redistributes energy among different modes without any total effect for the system as a whole. Hence, the time evolution of the total energy is given by

$$\frac{dE(t)}{dt} = \int_0^\infty P(k, t) dk - \nu \int_0^\infty k^2 E(k, t) dk. \quad (2.27)$$

The second term on the left-hand side plays an important role in the analysis that follows and we shall refer to it as energy dissipation ε , i.e.,

$$\varepsilon := \nu \int_{\mathbb{R}^N} \langle |\nabla \mathbf{v}(\mathbf{x}, t)|^2 \rangle d^N x = \nu \int_0^\infty k^2 E(k) dk, \quad (2.28)$$

where we have taken the limit of infinite real-space domain. In a statistically stationary state, the form of the turbulent energy spectrum adjusts such that the viscous dissipation balances the energy injection by the external forces. As seen by the above definition, the dissipation rate ε will, in general, depend on the Reynolds number ($\propto 1/\nu$) of the turbulent system. However, a remarkable feature of three-dimensional turbulence ($N = 3$) is that in the limit $\nu \rightarrow 0$ the dissipation rate does not tend to zero but instead to a fixed positive value. In mathematical terms,

$$\lim_{\nu \rightarrow 0} \varepsilon(\nu) = \text{const} > 0, \quad (2.29)$$

where the constant shall be denoted as ε_0 . For the above limit to be realised the spatial derivatives of the velocity field have to scale as $1/\sqrt{\nu}$ when ν is small. Physically, this means that in the limit of infinite Reynolds numbers the velocity field develops rough structures and loses its regularity. To the best of our knowledge, no rigorous mathematical proof of the dissipation anomaly in three dimensions exists up to date. Nevertheless, there are many experimental [24, 25, 26] and numerical [27, 28, 29, 26, 30] results indicating its validity. Furthermore, as we will see, it serves as a foundation for the modern theory of turbulence.

One of the most important theoretical contributions for understanding the physical aspects of fluid turbulence was developed by Kolmogorov [31] and it provides a quantitative foundation for the notion of energy cascade introduced earlier by Richardson. In his papers, Kolmogorov formulated his ideas in real space but due to didactic reasons here we shall follow [32] and present a spectral type of analysis which will facilitate a better understanding. The Kolmogorov theory considers the limit of infinite Reynolds numbers and relies on three major assumptions:

- In the limit $Re \rightarrow \infty$ the symmetries of the Navier-Stokes equations are restored in a statistical sense for the scales that are not directly influenced by the forcing mechanism and are large compared to the dissipation scale.

- The increments of the turbulent velocity field defined as $\delta \mathbf{v}(\mathbf{x}, \mathbf{r}) := \mathbf{v}(\mathbf{x} + \mathbf{r}) - \mathbf{v}(\mathbf{x})$ exhibit self-similarity (again in the statistical sense) of the form

$$\delta \mathbf{v}(\mathbf{x}, \lambda \mathbf{r}) = \lambda^h \delta \mathbf{v}(\mathbf{x}, \mathbf{r}). \quad (2.30)$$

- The mean energy dissipation rate tends to a positive constant in the limit of vanishing viscosity, i.e., there is an anomalous energy dissipation.

In order to make the physical picture more transparent, one should first clarify the different spatial scales which arise naturally in the flow. The maximal eddy size that can exist in the system is limited by the box size which gives the smallest wave number $k_{\min} = 2\pi/L$. Since external forces act usually at scales comparable to the box size, we shall associate k_{\min} with the forcing wave number. Viscosity, on the other hand, tries to equalise the velocity of adjacent fluid elements providing the effect of momentum diffusion. Hence, viscous effects become important only at spatial scales that are small enough for such a diffusion to be appreciable. The scale η at which this takes place depends only on two physical quantities: kinematic viscosity ν and the rate of energy dissipation ε . Dimensional analysis gives

$$\eta \sim \left(\frac{\nu^3}{\varepsilon} \right)^{1/4}, \quad (2.31)$$

which represents the scale at which viscous energy dissipation becomes important and starts dominating the flow. The corresponding wave number is $k_d \sim 1/\eta$. The above reasoning provides the constraints for the range of the energy cascade that is displayed in Fig. 2.1 and characteristic for three-dimensional turbulence. It spreads over spatial scales ℓ satisfying the condition $\eta \ll \ell \ll L$. A schematic illustration of this process is shown in Fig. 2.3 (a) which represents a more quantitative view on the physics displayed already in Fig. 2.1. The solid black curve represents the time-averaged nonlinear term in Eq. (2.23) for a statistically stationary state where the time average of the left-hand side is zero. At small wave numbers the viscous term is negligible due to the k^2 -factor in front of it and the power input $P(k)$ (red line) has to be balanced by the nonlinear interactions alone. As a result, the cumulative effect of the coupling to the higher modes resembles an effective energy sink for the large scales, i.e., the contribution of $T(k)$ is negative. k_i denotes the scales where the external forcing is most effective and is usually of the same order as k_{\min} . The effect of the forcing typically drops rapidly with decreasing the scale under consideration. If also the Reynolds number is large enough, i.e., ν small enough, then there are scales where both energy injection and dissipation are negligible, requiring that $T(k)$ is nearly zero. Nevertheless, the latter does not imply that at those scales, referred to as inertial range, the nonlinear term is not active. The condition $T(k) = 0$ suggests merely that the net effect of the nonlinear interactions for the corresponding wave numbers equals zero. Indeed, in this range only the nonlinear term is active transferring energy between different scales in a conservative way, i.e., all the energy that a scale $1/k_0$ received from wave numbers $k < k_0$ is transferred to $k > k_0$ which leads to a zero energy balance for the

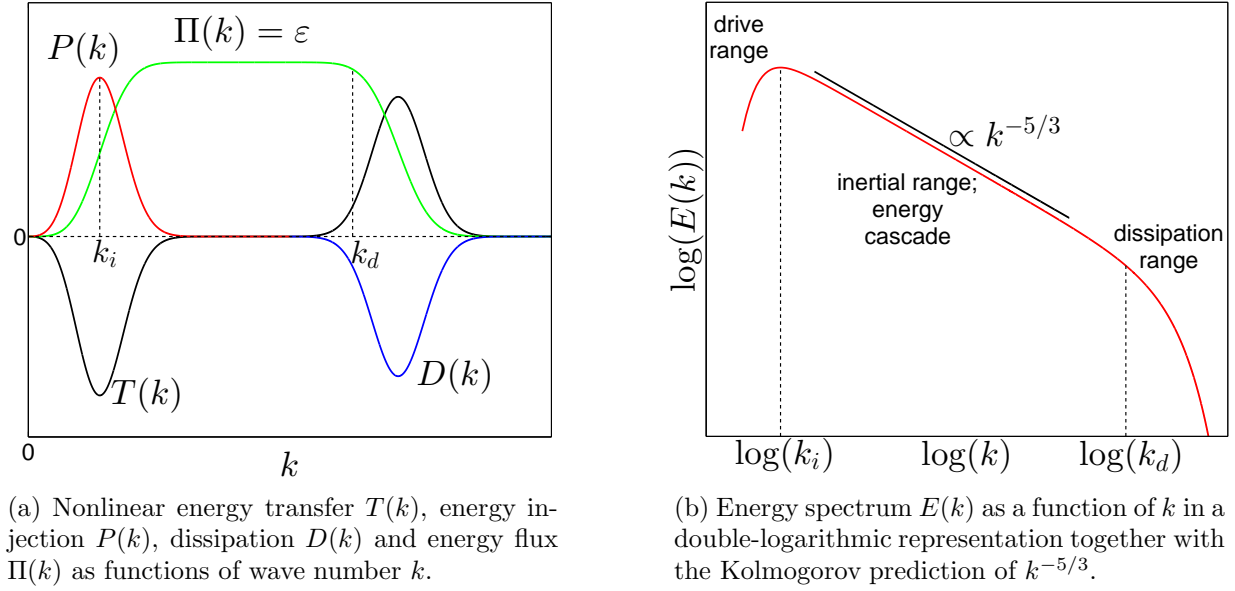


Figure 2.3: Schematic representation of energy related quantities in spectral space for fully-developed three-dimensional Navier-Stokes turbulence according to the Kolmogorov theory.

scale $1/k_0$. To further clarify this, let us introduce the notion of spectral energy flux $\Pi(k)$ defined as

$$\Pi(k) := - \int_0^k T(p) dp, \quad (2.32)$$

which plays an essential role in the analysis of turbulent flows. The schematic form of the energy flux is shown in Fig. 2.3 (a) in green. Clearly, a range where $T(k) = 0$ implies a constant energy flux emphasising again the conservative nature of the nonlinear interactions and supporting the analogy of a ‘cascade’ of energy from larger to smaller scales. This invariance of energy flux represents the most characteristic feature of the inertial range. Going to small enough scales the contribution from the viscous dissipation (blue line in Fig. 2.3 (a)) increases and eventually starts influencing the energy balance of those scales. At this point we say that we have reached the dissipation scale k_d . The nonlinearity still transports energy to even smaller scales in a conservative way but in the same time the viscous term drains energy from every scale leading to a decrease of the energy flux.

The essential problem in the theoretical analysis of turbulence reduces to finding the form of the energy spectrum $E(k)$, i.e., how the energy of the flow is distributed among scales. The importance of the contribution of Kolmogorov consists in providing such an expression in the limit of infinitely large Reynolds numbers. Following the basic assumptions in Ref. [31] one can argue that there are only three independent quantities that the spectrum $E(k)$ can be a function of (in the statistically stationary state and in the spectral range that is

not directly influenced by the external forcing mechanism): viscosity ν , energy dissipation rate ε and the wave number k itself. Hence, one can write that

$$E(k) = \nu^{5/4} \varepsilon^{1/4} g\left(\frac{k}{k_d}\right), \quad (2.33)$$

at least up to a numerical constant which can be incorporated into the function g . Note that k_d can be computed from ν and ε and does not constitute a fourth independent quantity in Eq. (2.33). Next, note that in the limit $\nu \rightarrow 0$ the spectrum should not depend on the viscosity, i.e., the dissipation-dominated part in Fig. 2.3 (a) moves to the right and the flat part where $T(k) = 0$ extends to infinity. Due to the $\nu^{5/4}$ factor in the spectrum and since k_d is the only other quantity depending on ν , independence from viscosity can be achieved only if in this limit $g \propto (k/k_d)^q$. Recalling that $k_d \sim 1/\eta$ and Eq. (2.31) one can easily compute the form of $k_d(\nu, \varepsilon)$. Dimensional arguments then yield $q = -5/3$ which is necessary in order to compensate for the $\nu^{5/4}$ -term in the equation above. Thus, outside the forcing range the turbulent energy spectrum takes the form

$$E(k) = C_K \varepsilon^{2/3} k^{-5/3} F\left(\frac{k}{k_d}\right), \quad (2.34)$$

where C_K is a numerical constant and $F(k/k_d)$ a non-dimensional function capturing the effect of viscous dissipation. Given the previous considerations $F(0) = 1$ and it stays close to one until $k \approx k_d$. A schematic picture of the energy spectrum in fully developed three-dimensional Navier-Stokes turbulence is displayed in Fig. 2.3 (b). $E(k)$ initially increases with wave number as k^2 or k^4 (depending on the initial conditions [33, 34]) for very small arguments while eventually attaining its maximum at the scales where external forcing is most active. Going to smaller spatial scales, one enters the inertial range where the energy spectrum drops off as a power law, $E(k) \propto k^{-5/3}$, constituting a straight line in a double logarithmic representation as in Fig. 2.3 (b). Eventually, for every finite Reynolds number Re at some point the dissipation scale k_d is reached where the viscous term becomes important accelerating the drop off of the energy spectrum. Given the limited experimental capabilities and the lack of systematic theoretical understanding, there has been some controversy for the form of the spectrum in the far dissipation range. Various forms have been argued for, ranging from an algebraic fall-off [35] via exponential fall-off to a faster-than-exponential decay, more specifically as $\exp(-k^{4/3})$ [36, 37] or $\exp(-k^2)$. [38] The exponential fall-off, up to algebraic prefactors, was suggested already by von Neumann [39] who made the remark that every analytic function in L^1 which decays sufficiently fast at infinity has a Fourier transform that falls off exponentially at large k . However, since the mathematical problem of proving existence and uniqueness of the solution of the three-dimensional Navier-Stokes equation together with clarifying its properties is still open, one cannot state with certainty that the velocity field is an analytic function in space. Later mathematical analysis showed that, given that a strong solution exist, it falls-off at large k as $o(e^{-k})$. [40] A more recent work [41] even provided an analytic form specifying all the parameters of the exponential decay including the algebraic prefactors by taking the Kolmogorov form of the velocity increments in the inertial range as given.

At this point let us remark that the problem of finding the form of the energy spectrum in the inertial range is still not solved completely. Although the Kolmogorov form $k^{-5/3}$ appears to be a good approximation, there are some systematic deviations. In general, the Kolmogorov theory gives for the velocity increments the form $\langle |\delta \mathbf{v}(r)|^n \rangle \propto r^{\xi(n)}$ with $\xi(n) = n/3$. Extensive data from experimental measurements of the function $\xi(n)$ (even today a difficult task for $n \geq 10$) revealed that it does not depend linearly on n . [42] Instead it displays a concave form meaning that velocity increments increase more slowly than expected with increase of separation. There are several ideas for deriving the correction to the linear form $\xi(n) = n/3$. (See Chapter 8 in Ref. [2] for a detailed description.) One of the most recent approaches for deriving the correct form of $\xi(n)$ and, to the best of our knowledge the most mathematically consistent one, is due to Ruelle. [43] However, so far none of the suggested approaches has managed to provide a functional form of $\xi(n)$ that is consistent with the known analytical constraints: $\xi(n=3) = 1$ and the curve $\xi(n)$ should increase monotonically with n but less than linear, i.e., it is convex. The first restriction derives from the Kolmogorov 4/5-law [31], which is exact as long as the energy flux is constant, while the second follows from a Hölder-type of inequality. [2]

2.3 The role of dimensionality

It is necessary to emphasise that most of the discussion above applies to three-dimensional turbulence. The lowest number of dimensions where we can have an incompressible fluid is two, since the incompressibility condition allows only for trivial solutions in one dimension. However, in two dimensions the physical picture is in many aspects quite different compared to the three-dimensional one. An extensive discussion on homogeneous and isotropic turbulence (both two- and three-dimensional) is provided in the book of Batchelor [23] while a more modern review can be found in the article by Boffetta. [44] Here we shall give only a basic description of the differences arising due to constraining the velocity field to only two spatial dimensions. The important recognition that two-dimensional flows behave fundamentally different than three-dimensional ones dates back to a paper by Førtøft [45] who showed that in two dimensions the nonlinear term in the Navier-Stokes equations transports kinetic energy predominantly towards large spatial scales. This effect was recognised later independently by Batchelor and by Kraichnan [46] who managed to draw some quantitative conclusions from it regarding the turbulent energy spectrum. The different direction of the energy flux results from the fact that in two dimensions there is an additional energy-like quantity, the enstrophy, which is conserved in the inviscid limit. In order to clarify this, let us first introduce the concept of vorticity $\boldsymbol{\omega}$ defined as the curl of the velocity field, i.e., $\boldsymbol{\omega} := \nabla \times \mathbf{v}$. Taking the curl of the Navier-Stokes equations given by Eq. (2.2a), one arrives at

$$\frac{\partial \boldsymbol{\omega}}{\partial t} + (\mathbf{v} \cdot \nabla) \boldsymbol{\omega} = (\boldsymbol{\omega} \cdot \nabla) \mathbf{v} + \nu \Delta \boldsymbol{\omega} + \nabla \times \mathbf{f}, \quad (2.35)$$

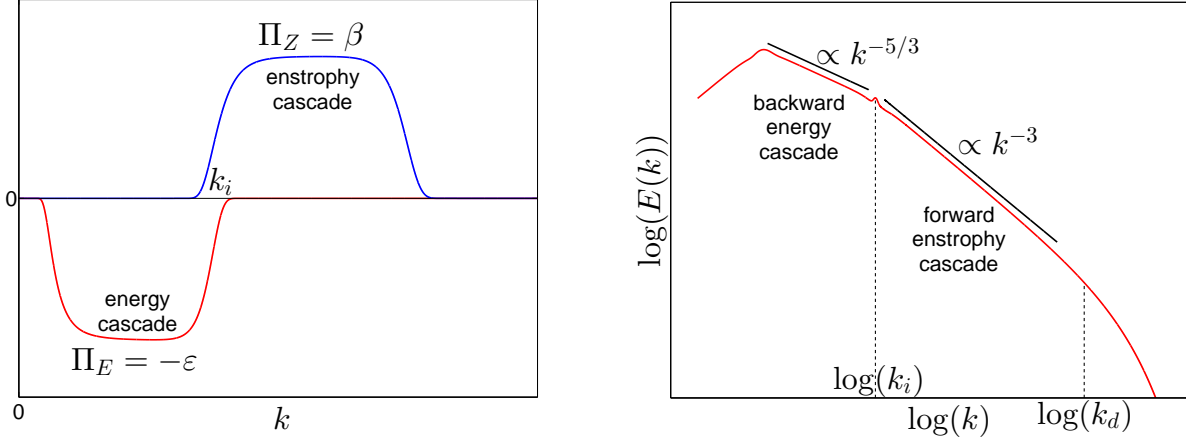
which gives the vorticity evolution equation and also has to be supplemented by the incompressibility constraint in Eq. (2.2b). By constructing Eq. (2.35) one eliminates the pressure term since the curl of every gradient term is zero. However, Eq. (2.35) incorporates two nonlinear terms. The one on the left-hand side describes the advection of vorticity by the velocity field, while the nonlinearity on the right-hand side represents the advection of velocity by the vorticity field, also called vorticity stretching. We will see that only the latter can contribute to the global enstrophy balance. The notion of enstrophy Z relates to the vorticity field in the same way as that of kinetic energy to the velocity field, namely

$$Z(t) := \frac{1}{2} \frac{1}{V} \int_{\Omega} |\boldsymbol{\omega}(\mathbf{x}, t)|^2 d^N x = \frac{1}{2} \sum_{\mathbf{k}} k^2 |\hat{\boldsymbol{\omega}}(\mathbf{k}, t)|^2. \quad (2.36)$$

Multiplying Eq. (2.35) by $\boldsymbol{\omega}$ and integrating over space yields

$$\frac{dZ}{dt} = \frac{1}{V} \int_{\Omega} \boldsymbol{\omega} \cdot (\boldsymbol{\omega} \cdot \nabla) \mathbf{v} d^N x + \nu \frac{1}{V} \int_{\Omega} |\nabla \boldsymbol{\omega}|^2 d^N x + \frac{1}{V} \int_{\Omega} \boldsymbol{\omega} \cdot (\nabla \times \mathbf{f}) d^N x, \quad (2.37)$$

where $\nabla \boldsymbol{\omega}$ denotes the tensor gradient of $\boldsymbol{\omega}$. The term proportional to $\boldsymbol{\omega} \cdot ((\mathbf{v} \cdot \nabla) \boldsymbol{\omega})$ does not contribute since it integrates to zero due to the periodic boundary conditions. Eq. (2.37) gives the different terms which can influence the enstrophy balance of the system. In contrast to the energy balance which is determined only by viscous dissipation and external forcing, the rate of change of the total enstrophy depends in general also on the nonlinearity. Thus, for an arbitrary dimension and no external forces, one arrives in the inviscid limit ($\nu = 0$) at a system where energy is conserved but enstrophy is not. However, the two-dimensional case presents an important exception, since in this setup the vorticity-stretching term equals zero. For $N = 2$ the vorticity reduces to a (pseudo) scalar quantity and $(\boldsymbol{\omega} \cdot \nabla) \mathbf{v} = \omega \partial_z \mathbf{v}$. Since in two dimensions \mathbf{v} does not have a z -component, the advection of the velocity field by vorticity is zero. This distinctiveness of the $N = 2$ case leads to an additional dynamical constraint - enstrophy conservation - which enforces the radically different flow behaviour. In the ideal case where external forcing is confined only to a few intermediate wave numbers and there is a considerable scale separation between forcing and dissipation a dual cascade emerges: a forward (towards small scales) cascade of enstrophy and an inverse (towards large scales) cascade of energy. Hence, the energy flux is constant and negative at wave numbers to the left of the forcing range, and decreases rapidly to zero at larger k , while the enstrophy flux is constant and positive at large k and zero at large scales, as shown schematically in Fig. 2.4 (a). Strictly speaking, this idealisation holds only in the limit of vanishing viscosity. For any finite viscosity there is still a small amount of energy cascading forwards and, accordingly, enstrophy going backwards. The value of ν sets the scale at which the enstrophy flux (blue line in Fig. 2.4 (a)) starts to decrease at large k . In the limit $\nu \rightarrow 0$ Π_Z will stay constant till infinity. On the other hand, the k -value where the amplitude energy flux (red line) starts to decrease (left from the plateau) is not stationary in an infinitely large system but becomes smaller with time. This is due to the fact that the viscosity term dissipates energy very ineffectively in



(a) Energy and enstrophy fluxes, $\Pi_E(k)$ and $\Pi_Z(k)$, respectively, as functions of the wave number k .

(b) Energy spectrum $E(k)$ as a function of the wave number k in a double-logarithmic representation.

Figure 2.4: A schematic representation of energy related quantities in spectral space for fully-developed two-dimensional Navier-Stokes turbulence.

two dimensions. Thus, energy moves to larger and larger scales. Using the requirement of constant fluxes of energy and enstrophy in the corresponding ranges, one can derive [46, 47, 48] the form of the energy spectrum by means of dimensional analysis, as done in the previous section. At large scales, where the energy cascade prevails, it yields

$$E(k) \propto \varepsilon^{2/3} k^{-5/3}, \quad (2.38)$$

which is surprising since in two dimensions the physical processes which lead to the energy cascade have a fundamentally different character given the fact that there is no vortex stretching. At large k (enstrophy cascade) the spectrum attains the form

$$E(k) \propto \beta^{2/3} k^{-3} \quad (2.39)$$

with β being the mean enstrophy transfer rate. A schematic representation of the energy spectrum is given in Fig. 2.4 (b). There one can see the position of the power-law parts - left ($\propto k^{-5/3}$) and right ($\propto k^{-3}$) from the wave number k_i at which energy injection by the external force is localised. For any non-zero viscosity, $E(k)$ eventually reaches dissipation range where the decay is faster than polynomial. Note, however, that, in contrast to the three dimensional case discussed in the previous section, in two dimensions this part of the Fourier space is predominantly responsible for the dissipation of enstrophy and not energy. It happens at $k \approx k_d \sim (\beta/\nu^3)^{1/6}$. In an infinite system the peak of the spectrum will move gradually to the left to lower k . Note that in two dimensions there is no anomalous dissipation. Consider the evolution equation for the total energy in enstrophy in the case

of a curl-free external force which read

$$\frac{dE}{dt} = -2\nu Z = -\nu \frac{1}{V} \int_{\mathbb{R}^N} |\omega|^2 d^N x \quad (2.40a)$$

$$\frac{dZ}{dt} = -\nu \frac{1}{V} \int_{\mathbb{R}^N} |\nabla \omega|^2 d^N x. \quad (2.40b)$$

According to Eq. (2.40b) the enstrophy decreases with time, which means that the rate of energy dissipation goes to zero in the limit of vanishing viscosity, i.e., there is no energy anomaly. On the other hand, the enstrophy dissipation is observed to tend to a positive constant, i.e., in two dimensions there is an enstrophy anomaly. The absence of an energy anomaly is thought to be connected to the observation that the two-dimensional Navier-Stokes model does not exhibit any intermittency. Indeed, there is no evidence for correction for the exponent in Eq. (2.38). On the other hand, Eq. (2.39) is only an approximate expression even in the idealised case. A subsequent analysis of Kraichnan [49] yielded a logarithmic correction for the energy spectrum at large wave numbers as

$$E(k) \propto \beta^{2/3} k^{-3} \left[\ln \left(\frac{k}{k_i} \right) \right]^{-1/3}, \quad (2.41)$$

where $k_i \ll k$.

One should note that the idealised picture of inverse energy cascade can be true only in a system of infinite size. Only in such a setup energy can flow steadily to larger scales without any impediment and a quasi-stationary state can be reached. In this case a ‘quasi-stationary state’ means that the scales where the cascade-induced spectral power laws have been established are statistically stationary and the energy inertial range constantly keeps extending to smaller wave numbers. In reality, one always considers systems of finite size where energy cannot flow indefinitely to larger scales. It will eventually reach the largest scale of the system given by the box size. In such a case the kinetic energy will ultimately accumulate at a few of the lowest wave numbers. Given a steady energy input, the amount of this accumulated energy will increase indefinitely since the only term in the Navier-Stokes equations capable of dissipating energy is the viscous term which, however, is active only at small scales. This is, clearly, not a physical situation. The resolution comes from the fact that no physical system is truly two-dimensional. One of the simplest ways to take this into account is to include a linear term of the form $-\alpha \mathbf{v}$, $\alpha > 0$, on the right-hand side of Eq. (2.2a). Such a term has the effect of friction/drag and is usually referred to as Ekman term. The physical picture behind such a modification is that the flow has to interact in some way with the matter enclosing it in the third dimension, e.g., horizontal winds in the atmosphere are subject to friction with the Earth’s surface, and will thereby transfer some of its momentum¹ and energy to it. The version of Eqs. (2.2) modified in this way is often referred to as Ekman-Navier-Stokes or Navier-Stokes with drag. It

¹Note that adding the term $-\alpha \mathbf{v}$ to Eq. (2.2a) violates momentum conservation.

is noteworthy that the new system of equations possesses some fundamentally different features compared to the traditional two-dimensional Navier-Stokes model. For instance, the drag term violates the anomaly of enstrophy dissipation, i.e., for every $\alpha > 0$ the rate of enstrophy dissipation in the limit $\nu \rightarrow 0$ tends to zero instead to a positive constant.[50, 51] Another important change is the form of the energy spectrum in the enstrophy inertial range. Instead of the k^{-3} -factor we have $k^{-3-\delta}$ where δ is a positive linear function of α , for α small enough.[52] Regarding the form of the energy spectrum in the enstrophy dissipation range, i.e., $k \gg k_d$, one can invoke the von Neumann argument in a similar way as for three-dimensional systems. A solution which possesses enough regularity should decay exponentially in the limit $k \rightarrow \infty$. Assuming that such a solution exist and taking the k^{-3} spectrum as granted, one can derive the precise form of the exponential decay including the factors in the exponent.[53]

2.4 A note on universality

In Sec. 2.2 we discussed briefly the physical picture of fully-developed three-dimensional turbulence. One of its most eminent manifestations is the form of the nonlinear energy spectrum in the inertial range, $E \propto k^{-5/3}$. It is essential to remark that Eqs. (2.2) depend only on one free parameter, namely the viscosity, which relates to the Reynolds number as $\nu \propto 1/Re$. Nevertheless, neither the form of the energy spectrum at the turbulent scales (inertial range) nor its position depend on the viscosity. The (lack of) dependency on the constant C_K has not been completely clarified yet from a theoretical point of view, but experimental studies show that the dependence on ν , if any, is very weak.²[54] Thus, the Kolmogorov form of the energy spectrum seems to be an universal feature that is characteristic to turbulence. Varying the viscosity in Eqs. (2.2) influences only the extent in Fourier space over which the turbulent energy spectrum is observed. Essentially the same picture applies also to the two-dimensional version of the Navier-Stokes equations. There the energy spectrum in the energy and enstrophy inertial ranges is again independent of the value of the viscosity. The reason for this universality is generally related to the fact that the Kolmogorov and Kraichnan spectra arise at scales where both external forces and viscous dissipation are negligible. Therefore, the energy spectrum is determined solely by the nonlinear interactions which, however, do not depend on viscosity. Since the incompressible Navier-Stokes equations represent the earliest model for turbulence, the results derived from their study shaped the perception of turbulent flows. Hence, a universal power-law form of the spectrum of energy-like quantities is often regarded as an intrinsic feature of turbulence. However, there is an increasing number of examples for turbulence in a general sense suggesting that such a universality might not be a characteristic trait of all turbulent systems but instead - only a consequence of the particular form of the Navier-Stokes equations. One such example, which stimulated most of the work presen-

²Note that the quantity denoted by C_K in Ref. [54] is not the same as the C_K used here. They are related as $C_K = (55/18)C'_K$, where the prime designates the result reported in the reference.

ted here, emanates from the area of plasma physics. In the case of magnetically confined

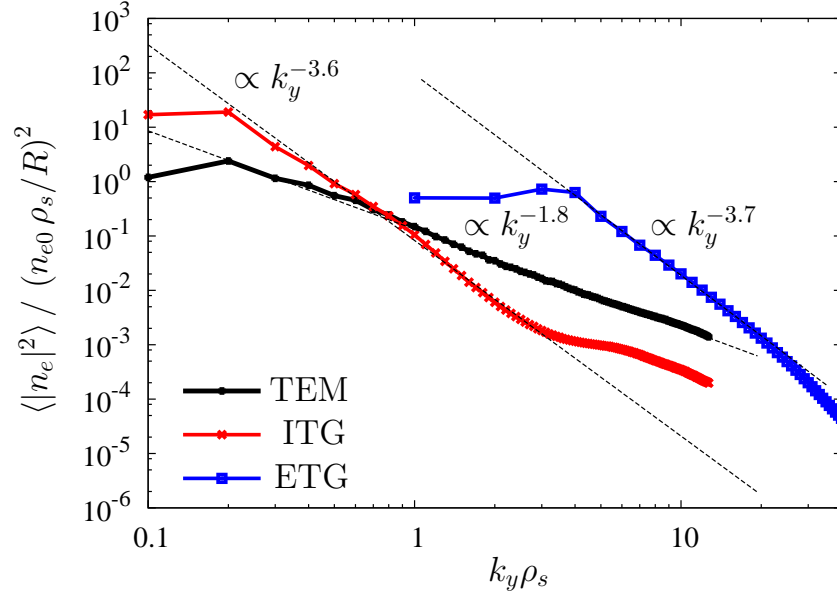


Figure 2.5: Nonlinear spectrum of particle density produced by numerical gyrokinetic simulations performed with the GENE code.[55] ρ_s denotes a typical scale in physical space and is directly proportional to the ion gyroradius to be defined in Section 3.1. (Reproduced with permission from Görler *et al.*, Phys. Plasmas 10, 102508 (2008). Copyright 2008, AIP Publishing LLC.)

plasmas for the purpose of controlled nuclear fusion research the strong magnetic fields imposed on the plasma restrain dramatically the motion of both ions and electrons. The latter are forced to gyrate rapidly around magnetic field lines. If one is interested only in phenomena involving time scales much larger than the periods of gyration of ions and electrons, averaging over the gyromotion is justified and one derives a reduced description of the plasma referred to as gyrokinetic theory.³ In this framework one solves for the time evolution of the particle distribution functions of ions and electrons which are defined over a five-dimensional phase space and are subject to complex nonlinear evolution equations determining both the distribution function and the electromagnetic fields self-consistently. The coupling between the plasma and its intrinsic electromagnetic fields resembles in many ways the nonlinear nature of the Navier-Stokes equations and produces chaotic spatio-temporal behaviour which in the plasma physics community is generally referred to as turbulence. In analogy to fluid turbulence one can define similar energy-like quantities, e.g., free energy or electrostatic energy. The latter is directly related to the ion/electron density which can be measured in experiments. Solving the evolution equations numerically, one observes that the nonlinear spectra of many of the energy-like quantities also display power-laws for some spectral ranges. An example for such a nu-

³A modern account of gyrokinetics is given in Ref. [56].

merical result regarding the electron density is displayed in Fig. 2.5 which can be found in Ref. [57]. The different colours represent different types of linear instabilities driving the plasma turbulence. Evidently, the same energy-like quantity exhibits different features depending on which linear instability is active. The main result of the analysis in Ref. [57] supports the idea that the features of turbulent spectra in plasmas are not universal but instead depend considerably on the linear physics of the problem under consideration. The

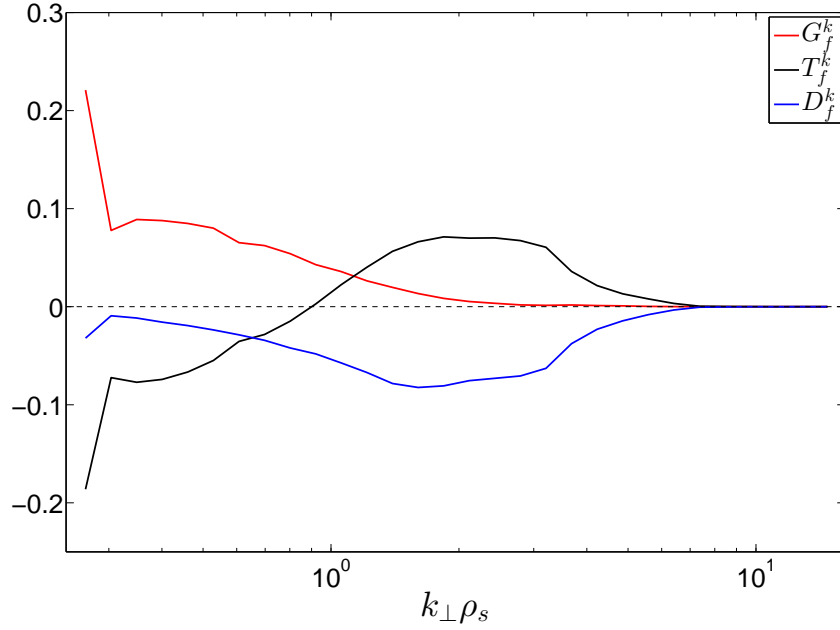


Figure 2.6: Nonlinear spectrum of the different terms in the gyrokinetic equation as a function of spatial scale in slab geometry. G^k (red) denotes the energy injection term, D^k (blue) stands for dissipation effects and T^k (black) represents the nonlinearity. Summing the three contributions gives $G^k + T^k + D^k \approx 0$, as is to be expected in the statistically stationary state. The numerical simulations were performed with GENE. (courtesy of Dr. Alejandro Bañón Navarro)

difference between plasma physics and fluid dynamics becomes even more prominent when analysing the structure of the different terms in the gyrokinetic equation. We shall not discuss here the particular structure of the equation, modelling plasma turbulence, since this is done in Chapter 3. It is sufficient to note that one solves not for a vector field over real space as in fluid dynamics but instead for a particle distribution function f defined over (a reduced) phase space. The energy-like quantity usually considered is the free energy which is given by the integral of $|f|^2$ over all velocity coordinates. In analogy to Eq. (2.23) one can derive a free-energy-balance equation in Fourier space which, in condensed form, is expressed as

$$\frac{\partial \mathcal{E}_f^k}{\partial t} = G_f^k + T_f^k + D_f^k, \quad (2.42)$$

where \mathcal{E}_f^k denotes the free energy at the scale k . On the left-hand side we have the rate of change of free energy which, in a statistically stationary state, will average to zero. G_f^k denotes the injection rate of free energy at a given scale.⁴ In contrast to the Navier-Stokes case it does not result from external forces but arises due to various internal instabilities present in magnetised plasmas. The second term on the right-hand side represents the nonlinear coupling between different Fourier modes. Similarly as for the incompressible Navier-Stokes equations, integrated over all scales T_f^k gives zero. Thus, we have the same physical interpretation, i.e., the nonlinearity in the gyrokinetic model does not inject/dissipate free energy in/from the system. It merely redistributes it in a conservative manner among the different scales. An important difference between classical Navier-Stokes turbulence and gyrokinetic turbulence presents the notion of locality which can be computed on the basis of the nonlinear coupling. Interactions between different Fourier modes are said to be local if all tree modes involved in them have a similar magnitude. This idea can be made quantitative by introduction of the so-called disparity parameter to be discussed in Section 4.4. At this point we shall only note that in Navier-Stokes turbulence energy is transferred mainly with the aid of local interactions, while in the gyrokinetic theory the result can vary depending on the type of instability which is active. Overall, the transfer of free energy in plasma turbulence seems to be less local than in classical fluids. The case where turbulence is driven by an ion temperature gradient exhibits a much smaller degree of locality compared to a drive due to an electron temperature gradient.[59] The last term on the right-hand side models dissipation effects resulting from collisions. D_f^k is negative definite and its precise form depends on the collision operator used. In the statistically stationary state the time average of the left-hand side vanishes causing the three contributions on the right-hand side to add up to zero. Despite the apparent similarity to Navier-Stokes turbulence, however, an explicit numerical computation of the individual terms reveals substantial differences in their structure as seen in Fig. 2.6. The (free) energy injection term is again active only at large scales but the form of the other two terms (blue and black curve) deviates considerably from the case of fully-developed fluid turbulence as in Fig. 2.3 (a). There is, for instance, a non-negligible amount of dissipation at low wave numbers which represents an important and distinctive feature of plasma turbulence and will be discussed in more detail in the next chapter. Additionally, the nonlinear term cannot be disregarded for any range of scales. It is positive at low wave numbers, decreases continually and becomes negative at small scales. Thus, in plasma turbulence there does not necessarily exist an inertial range with a conservative cascade of free energy. Nevertheless, as evident from Fig. 2.5 the nonlinear evolution of the system leads to power-laws in the spectra of energy-like quantities which is often regarded as a manifestation of self-similarity. Such an observation can be made not only in plasma turbulence but also in many other areas where nonlinear dynamics play an essential role. The study of the emer-

⁴In a general geometry of the magnetic-line configuration there are also terms resulting from curvature effects. However, their magnitude is usually much smaller than that of the injection term. Hence, for the purpose of elucidating the essential idea of this discussion we have added the curvature effects to the term G_f^k . For a more detailed discussion, the reader is referred to Ref. [58].

gence of such structures without a conservative nonlinear cascade constitutes the main goal of this work. Since we are interested in understanding the fundamental reasons for such a behaviour, we shall study it in simplified models which pose more modest computational challenges.

Chapter 3

Importance of linear effects in plasmas

So far our main attention was dedicated to fluids and fluid turbulence. However, there exist many real-life systems capable of exhibiting the multi-scale spatio-temporal chaos characteristic for turbulence. One such example is represented by plasmas. Due to their wide abundance in Nature it is of great importance from scientific point of view to develop a reliable theoretical description of the turbulent phenomena occurring in ionised gases. Their main difference from classical Navier-Stokes fluids arises from the fact that their microscopic constituents are free charged particles in contrast to normal fluids where we have electrically neutral molecules. This fundamental difference opens the possibility for long-ranged interactions between the particles due to the electromagnetic forces they produce and in the same time also react to. An important bridge between plasmas and neutral fluids represents the theory of magnetohydrodynamics which describes fluids similar to the classical ones but which are in the same time metals and, therefore, electrically conducting. The importance of the metallicity condition lies in the fact that charge carriers in metals are the electrons which, however, carry a negligible part of the fluid momentum. This allows the creation of large electric currents and magnetic fields which in the same time influence the macroscopic fluid motion. The condition for a large mass ratio between particles of different electric charge distinguishes fluids like water, the turbulent motion of which can be described sufficiently well by classical hydrodynamics, from liquid metals, e.g., mercury or liquid sodium, which demand for a generalisation of the Navier-Stokes equations in order to include the effect of the self-consistently generated magnetic forces acting on the electrically conducting fluid. Magnetohydrodynamics can also be viewed as a limit case of the kinetic theory of magnetised plasmas when the magnetic field is strong enough such that the gyroradius of the electron is negligibly small compared to the spatial scales under considerations.

In this chapter we shall give a brief description of the basic ideas of the gyrokinetic theory of magnetised plasmas which we already addressed in Section 2.4. Although the research

presented in this work does not extend to the gyrokinetic theory, the latter played an essential role by providing an example of important physical systems that display spectral nonuniversality and, thereby, motivated this work. The gyrokinetic description of plasmas is applicable in cases when there is a strong magnetic field that is imposed on the ionised gas and guides the particle motion. On the scale of approximation it lies between the full kinetic theory and magnetohydrodynamics, i.e., it incorporates less phenomena than the kinetic theory but more compared to magnetohydrodynamics. For the sake of completeness, a brief summary and a heuristic motivation of the gyrokinetic equations is given in Section 3.1. It provides a connection to the numerical results discussed in Section 2.4. Section 3.2 deals with the importance of linear effects for the understanding of the turbulent motion in plasmas. While in classical Navier-Stokes turbulence the linear physics is completely erased with the formation of the turbulent state, in gyrokinetic theory linear eigenmodes, both unstable and damped, can have a significant impact on turbulent quantities like heat or particle fluxes. Thus, understanding the effects arising from those linear modes plays an important role in modelling plasma turbulence. In Section 3.3 we investigate the linear physics emerging in a drift-kinetic model of magnetised plasmas. Such an approximation of the kinetic theory of plasmas contains less details than the gyrokinetic description but still incorporates more physical phenomena compared to magnetohydrodynamics. We study quantitatively the linear eigenmodes focusing on the role of the collisional parameter and the particular role of the specific operator chosen to model collisional effects.

3.1 Gyrokinetic theory

The statistical description of plasmas relies on the notion of the so-called particle distribution function, $f = f(\mathbf{x}, \mathbf{v}, t)$ giving the probability $f(\mathbf{x}, \mathbf{v}, t)d^3x d^3v$ that a particle of a certain species occupies the position $[\mathbf{x}, \mathbf{x} + d\mathbf{x}]$ and has a velocity in the interval $[\mathbf{v}, \mathbf{v} + d\mathbf{v}]$ at the time t . Since f is a particle density in phase space, it has to satisfy the continuity equation which, in the case of no particles being created or destroyed, reads

$$\frac{\partial f}{\partial t} + \nabla_{\mathbf{z}}(\dot{\mathbf{z}}f) = 0, \quad (3.1)$$

where \mathbf{z} denotes a six-dimensional phase-space vector combining position and momentum of the form $\mathbf{z} = (\mathbf{x}, \mathbf{p})$, with $\mathbf{p} = m\mathbf{v}$ being the momentum of the particle and m - the particle mass, which is constant in the non-relativistic case. Note that Eq. (3.1) conserves entropy. Due to the form of the Hamilton's equations the phase-space flow velocity is divergence free, i.e.,

$$\nabla_{\mathbf{z}} \cdot \dot{\mathbf{z}} = \frac{\partial \dot{\mathbf{x}}}{\partial \mathbf{x}} + \frac{\partial \dot{\mathbf{p}}}{\partial \mathbf{p}} = \frac{\partial^2 \mathcal{H}}{\partial \mathbf{x} \partial \mathbf{p}} - \frac{\partial^2 \mathcal{H}}{\partial \mathbf{p} \partial \mathbf{x}} = 0, \quad (3.2)$$

where \mathcal{H} denotes the Hamiltonian function of a given charged particle in the plasma with $\partial/\partial \mathbf{x}$ and $\partial/\partial \mathbf{p}$ representing an alternative notation for $\nabla_{\mathbf{x}}$ and $\nabla_{\mathbf{p}}$. The above equation combined with the form of Eq. (3.1) provides a mathematical structure quite similar to

that of the Navier-Stokes equations. This similarity is not coincidental but results from the pivotal role of the continuity equation. In the Navier-Stokes case the divergence-free velocity field is advected by itself in real space, while in the case of plasmas the particle distribution function is being advected in phase space by the phase-space flow velocity $\dot{\mathbf{z}}$. In fluid dynamics friction forces between fluid elements are modelled by including a viscosity term on the right-hand side. Here, the intrinsic forces are due to particle collisions which can also be taken into account by introducing a term on the right-hand side. The resulting equation is called the Boltzmann equation and has the form

$$\frac{\partial f}{\partial t} + \mathbf{v} \cdot \nabla_{\mathbf{x}} f + \frac{\mathbf{F}}{m} \cdot \nabla_{\mathbf{v}} f = C(f), \quad (3.3)$$

where we have substituted $\dot{\mathbf{x}}$ with \mathbf{v} and denoted by \mathbf{F} the large-scale (compared to the Debye length) forces acting on the plasma particles, i.e., gravitational or electromagnetic forces resulting from the collective behaviour of the plasma. Forces fluctuating rapidly at small spatial scales arise from collisions and their combined effect results in the term on the right-hand side. The particular form of $C(f)$ has to be such as to fulfil Boltzmann's H-theorem, i.e., the quantity $H := \int f \ln(f/f_0) d^3v$ should not decrease in time, where f_0 is simply a constant that makes the argument of the logarithm a non-dimensional quantity. It can be easily shown that H is, up to a constant term, proportional to $-S$ with S being the entropy of the system. Under the condition of constant total energy, i.e., we consider a closed system, the only distribution function which maximises the entropy is a Maxwellian. Thus, the energy distribution among particles in a plasma follows the same form as in normal gases.

Despite its at first sight simple form, Eq. (3.3) encompasses a huge variety of complex, nonlinear phenomena and its general solution presents a formidable computational challenge. Note that one such equation should be written for every particle species s , i.e., f in Eq. (3.3) should be substituted by f_s and m by m_s . This gives us a system of coupled equations the number of which equals the number of particle species. The different distribution functions f_s are coupled to each other via the force \mathbf{F} which is in this case simply the Lorentz force acting on a particle with charge $Z_s e$ moving with the velocity \mathbf{v} . Mathematically, we have that $\mathbf{F} = Z_s e (\mathbf{E} + \mathbf{v} \times \mathbf{B})$, where Z_s denotes the charge number of the corresponding species and e is the elementary charge. The electric \mathbf{E} and magnetic \mathbf{B} fields provide the coupling mechanism between the different species and are computed with the aid of the Maxwell's equations as

$$\nabla \cdot \mathbf{E} = \frac{1}{\varepsilon_0} \sum_s Z_s e \int_{\mathbb{R}^3} f_s d^3v, \quad (3.4a)$$

$$\nabla \cdot \mathbf{B} = 0, \quad (3.4b)$$

$$\nabla \times \mathbf{E} = -\frac{\partial \mathbf{B}}{\partial t}, \quad (3.4c)$$

$$\nabla \times \mathbf{B} = \frac{1}{\varepsilon_0 c^2} \sum_s Z_s e \int_{\mathbb{R}^3} \mathbf{v} f_s d^3v + \frac{1}{c^2} \frac{\partial \mathbf{E}}{\partial t}, \quad (3.4d)$$

where c denotes the speed of light and ε_0 - the vacuum permittivity. Recall that \mathbf{E} and \mathbf{B} represent the large-scale variations of the corresponding fields, since their small-scale structure is incorporated in the particular form of the collision operator $C(f_s)$. In this chapter we assume that magnetic fields induced by fluctuations of the current are negligible compared to the background magnetic field. Such an approximation is referred to as the electrostatic limit. The motion of a single charged particle in a magnetic field is schematically presented in Fig. 3.1. It gyrates around a given magnetic field line while keeping

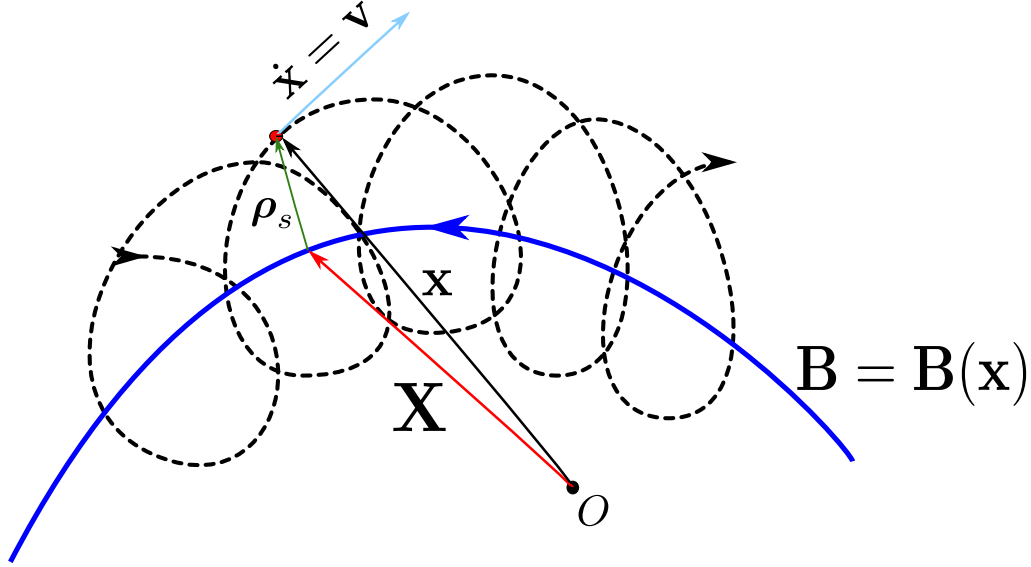


Figure 3.1: A schematic representation of the motion of a charged particle under the influence of a magnetic field. The gyro-averaging corresponds to an average of the gyro-vector $\boldsymbol{\rho}$ over one rotation.

its velocity along the magnetic field constant. The particle position can be expressed either directly by \mathbf{x} or by the position of its guiding centre \mathbf{X} combined with its position with respect to the latter, i.e., $\boldsymbol{\rho}_s$. In the following, when we say ‘perpendicular’ or ‘parallel’ we shall mean with respect to the direction of the magnetic field at the corresponding point. Hence, the velocity can be decomposed as

$$\mathbf{v} = v_{\parallel} \mathbf{b} + v_{\perp} \mathbf{a}, \quad (3.5)$$

where $\mathbf{b} = \mathbf{b}(\mathbf{x})$ represents a unit vector that points locally in the direction of \mathbf{B} and \mathbf{a} is its orthogonal complement. The gyroradius ρ_s of the species s is given by

$$\rho_s = \frac{v_{\perp s}}{\omega_{gs}}, \quad (3.6)$$

where ω_{gs} stands for the frequency of the gyration expressed as

$$\omega_{gs} = \frac{Z_s e B}{m_s}. \quad (3.7)$$

In strongly magnetised plasmas, that we shall discuss in this chapter, the magnetic field is strong enough such that the gyroradii of the particles are much smaller than the typical scale on which \mathbf{B} varies, i.e.,

$$\frac{\rho_s \nabla B}{B} \sim \epsilon_B \ll 1. \quad (3.8)$$

This provides a natural smallness parameter in powers of which one can expand the full equations. The main idea of gyrokinetics is that the particle motion can be effectively decomposed into a fast part given by its gyromotion around the guiding centre and a slow part, i.e., the motion of the guiding centre itself. If we are interested in processes in the plasma which evolve on time scales much larger than $1/\omega_{gs}$, then we can average over the gyromotion and effectively reduce the degrees of freedom of the system. Expressing $\boldsymbol{\rho}_s = v_\perp \mathbf{a}/\omega_{gs} = v_\perp (\cos(\theta) \mathbf{e}_1 + \sin(\theta) \mathbf{e}_2)/\omega_{gs}$ one can define the gyro-averaging procedure for an arbitrary quantity $Q(\mathbf{x})$ as

$$\overline{Q(\mathbf{x})} := \frac{1}{2\pi} \int_0^{2\pi} Q(\mathbf{X} + \boldsymbol{\rho}) d\theta. \quad (3.9)$$

Due to the large scale on which the magnetic field changes compared to the particle gyroradius, we have that its magnetic moment

$$\mu = \frac{m_s v_\perp^2}{2B(\mathbf{X})} \quad (3.10)$$

is approximately a constant of motion (also called adiabatic invariant). Thus, the gyro-averaging procedure gives us the possibility to reduce the original six-dimensional phase space (\mathbf{x}, \mathbf{v}) to a five-dimensional one, namely $(\mathbf{X}, v_\parallel, \mu)$, the gyro-centre phase space. Pictorially speaking, the gyrokinetic theory substitutes the charged point particles with charged ‘rings’ which possess a magnetic moment. The latter is, however, not fixed but can change due to particle collisions, since it is directly proportional to v_\perp^2 , i.e., depends on the particle energy. Hence, after averaging out the gyro-angle θ we can transform Eq. (3.3) into gyro-centre coordinates yielding

$$\frac{F_s}{\partial t} + \dot{\mathbf{X}} \cdot \nabla F_s + v_\parallel \frac{\partial F_s}{\partial v_\parallel} = \overline{C}(F_s), \quad (3.11)$$

where F_s denotes the gyro-centre distribution of species s . It does not depend on θ and μ , since we averaged out the first, i.e., $\partial F_s / \partial \theta = 0$ and the second is an approximate constant of motion, i.e., $\dot{\mu} \approx 0$. Further, we shall consider the case where there are only two particle species, i.e., electrons ($s = e$) and single charged ions ($s = i$), with temperatures T_e and T_i , respectively. Such an assumption provides a realistic approximation for the conditions in the core of most of the present-day fusion devices using magnetic confinement, for the description of which the gyrokinetic theory was originally developed. The lightest possible ions are protons, i.e., the nuclei of hydrogen. Even in this case the mass ratio between the ions and electrons is $m_i/m_e \approx 1836 \sim 10^3$, implying that practically all

the momentum is carried by the ions. Thus, we adopt the so-called adiabatic-electron approximation according to which the electrons react almost instantly to the changes of potential created by the ion dynamics. Therefore, we need to solve only one equation of the form of Eq. (3.11), namely that for the ions. Subsequently, the electron distribution can be determined with the aid of Eq. (3.4a). Additionally, one can write the distribution function of ion gyro-centres, which is now the only one we need to solve for, as a sum of an equilibrium part F_{i0} and a deviation f_{i1} , i.e., $F_i(\mathbf{X}, v_{\parallel}, \mu, t) = F_{i0}(\mathbf{X}, v_{\parallel}, \mu) + f_{i1}(\mathbf{X}, v_{\parallel}, \mu, t)$. Due to the quasi-neutrality condition the latter is the only part which contributes to the gyro-averaged electrostatic potential $\bar{\phi}_1$ on the right-hand side of Eq. (3.4a). Assuming that the distribution function is close to its equilibrium form, one can write that

$$\frac{|f_{i1}|}{F_{i0}} \sim \frac{e\bar{\phi}_1}{T_e} \sim \epsilon_{\delta}, \quad (3.12)$$

which gives us another smallness parameter. Using the decomposition of F_i into a constant equilibrium background and a small perturbation in the collisionless form of Eq. (3.11), we group together terms of the same order with respect to ϵ_{δ} and demand that they vanish separately. The 0th-order part yields

$$v_{\parallel} \mathbf{b} \cdot \left(\nabla F_{i0} - \frac{\mu}{m_i v_{\parallel}} \nabla B \frac{\partial F_{i0}}{\partial v_{\parallel}} \right) = 0, \quad (3.13)$$

which determines the form of the equilibrium part F_{i0} . The solution of the above equation is given by a Maxwellian of the form

$$F_{i0}(\mathbf{X}, v_{\parallel}, \mu) = \frac{n_{i0}(\mathbf{X})}{\pi^{3/2} v_{th,i}} \exp \left(-\frac{m_i v_{\parallel}^2 / 2 + \mu B}{k_B T_{i0}(\mathbf{X})} \right), \quad (3.14)$$

where the $n_{i0}(\mathbf{X})$ and $T_{i0}(\mathbf{X})$ stand for the density and temperature of the ions, respectively, which can, in general, be functions of the position \mathbf{X} . Hence, we have a local thermal equilibrium. Strictly speaking, the thermal velocity of the ions $v_{th,i} := \sqrt{2k_B T_{i0}/m_i}$ is also a function of the coordinate \mathbf{X} , since it involves the ion temperature. k_B represents the Boltzmann constant and is not related to the magnetic field. After determining the background ion distribution, we go one step further and equate the part proportional to ϵ_{δ} to zero. This gives

$$\begin{aligned} \frac{\partial f_{i1}}{\partial t} + \left[\omega_{in} + \left(v_{\parallel} + \mu B - \frac{3}{2} \right) \omega_{iT} \right] F_{i0} \frac{\partial \bar{\phi}_1}{\partial y} + \frac{T_{i0}(2v_{\parallel} + \mu B)}{q_i B} \left(K_x \frac{\partial h_i}{\partial x} + K_y \frac{\partial h_i}{\partial y} \right) + \\ + \{ \bar{\phi}_1, f_{i1} \}_{xy} + \frac{1}{2} v_{th,i} \{ v_{\parallel}^2 + \mu B, h_i \}_{zv_{\parallel}} = D[f_{i1}], \end{aligned} \quad (3.15)$$

where K_x and K_y result from the curvature of the magnetic field \mathbf{B} and their detailed form can be seen in Ref. [58]. In the above equation we have set the coordinate system such that \mathbf{b} lies in the z -direction. h_i is a first-order quantity which is related to f_{i1} as

$$h_i = f_{i1} + Z_i F_{i0} \bar{\phi}_1 / T_{i0}. \quad (3.16)$$

Note that the Poisson brackets $\{\bar{\phi}_1, f_{i1}\}_{xy}$ in Eq. (3.15), which represent the nonlinear term are only of order ϵ_δ , although they involve the product of two first-order quantities. The reason is that they contain derivatives with respect to x and y . The latter lead to contributions scaling as $1/\epsilon_\delta$, thereby, reducing the order of the nonlinearity by one. The terms ω_{in} and ω_{iT} take into account the effects of the variation of temperature and density in space and are roughly proportional to the inverse of the corresponding gradient lengths. In Eq. (3.15) we have used the so-called local gradient approximation described in more detail in Section 3.3. It requires that the variation of temperature and density happens on spatial scales that are much larger than the ion gyroradius. Such temperature and density gradients act as a source of free energy driving the plasma turbulence. The term $D[f_{i1}]$ on the right-hand side in Eq. (3.15) represents collisional effects which try to change the perturbation f_{i1} to a Maxwellian of the same temperature as F_{i0} . Note that D is simply a physically reasonable model for the collisional effects, since gyro-averaging of the full Landau-Boltzmann collision operator represents a still open problem in plasma physics. Eq. (3.15) does not constitute a closed equation. It has to be combined with the electrostatic version of Maxwell's equations which give additional connections between the electromagnetic fields, i.e., the potentials that determine them, and the ion distribution function. At first sight, Eq. (3.15) might look much more complicated than Eq. (3.3) but reducing the number of dimensions of the phase space and averaging out irrelevant fast particle dynamics proves to be of immense computational advantage despite the additional terms.

3.2 Effects of damped modes on plasma turbulence

In the description of Navier-Stokes turbulence in the previous chapter we focused almost entirely on the nonlinear effects while essentially neglecting the linear terms. The form of the latter was simple with a straightforward relation to the energy spectrum. Neglecting the nonlinear term and Fourier transforming the Navier-Stokes equations both with respect to space and time, one arrives at

$$\omega = -ik^2\nu, \quad (3.17)$$

where ω denotes the frequency arising as a conjugate variable to time. Since both k and ν are real variables, ω is purely imaginary, i.e., it possesses only growth rate, in this case negative, and no real frequency.¹ Thus, the linear version of the Navier-Stokes equations produces structures that only grow or decay with no oscillatory behaviour, i.e., they are not waves in the usual sense.

For the typical problems arising in plasma physics, however, the linearised version of the governing equations takes a much more complex form. Even the simple case of electrostatic Langmuir waves in a homogeneous electron plasma displays an immense variety of physical

¹In this representation the real space variable is proportional to $e^{-i\omega t} = e^{-i\Re(\omega)t}e^{\Im(\omega)t}$. Hence, the real part of ω gives the oscillatory frequency of the perturbation and the imaginary part - its growth rate.

phenomena which produced a lot of discussions in the plasma physics community.[60, 61, 62] First, the linear dispersion relations emerging in plasma physics allow for not just one but instead countably infinitely many eigenvalues at each wave vector \mathbf{k} . In addition, the eigenmodes produced by such a linear analysis have not only a growth rate but also an oscillation frequency. The latter results from the fact that the linear operators, the spectra of which we are computing, are not self-adjoint making their eigenvalues complex entities, in general.

Perhaps the most important difference between normal fluids and plasmas from the point of view of nonlinear dynamics is that plasmas represent an active medium. While in the case of the Navier-Stokes equations energy input is provided by an external force or by imposing specific boundary conditions, in plasmas linear instabilities can arise at certain wave numbers, e.g., in the presence of a temperature gradient, which injects energy into the system. In the case of a single ion species with adiabatic electrons in a slab magnetic geometry there exists at most one instability at a given \mathbf{k} . Due to the multiple solutions allowed by the linear dispersion relation, however, this instability coexists with infinitely many damped modes at the same wave vector. Thus, it is not *a priori* clear how the flow of energy will look like in spectral space. One of the possibilities is that the energy produced at low wave numbers, where instabilities arise, will be transferred via nonlinear mode coupling to higher wave numbers, where only damped modes exist, and dissipated. This view represents a complete analogy to fluid dynamics and is often highly favoured in the plasma physics community. However, according to another paradigm the damped eigenmodes at large scales play an essential role. Recent research [63] supports this notion showing that energy dissipation actually peaks at similar spatial scales where also energy injection reaches its maximum. (See Fig. 1 in Ref. [63].) This strengthens the idea that the main energy channel results from the nonlinear coupling of the unstable modes with damped ones at similar wave numbers. The main difficulty for determining the importance of different term for the energy dissipation in plasmas comes from the fact that the dynamics takes place in a six-dimensional phase space. The governing equations determine the time evolution of the particle distribution function where both velocities and spatial coordinates are independent variables. It is, however, an important point that in plasmas free energy is dissipated only by the collision operator, which acts in velocity space. Since the form of the collision term involves derivatives with respect to velocity, it becomes effective when the distribution function develops small structures in velocity space. On the other hand, nonlinear phase mixing [64] couples scales in both velocity and real space to each other and relates small structures in velocity space to small structures in real space. Such a connection reveals an additional way for the energy flow in real space. The role of different dissipation mechanisms was recently investigated in Ref. [65]. It was concluded that there are different saturation mechanisms in gyrokinetic turbulence with the collision frequency ν being the parameter determining the strength of each mechanism. At large ν , free energy dissipation takes place predominantly at large scales, both in real and velocity space, indicating possible excitation of damped eigenmodes at phase space scales comparable to those of the driving instabilities. At very small ν , however, the development of small

structures in velocity space, which correspond to small structures in real space according to nonlinear phase mixing, becomes necessary which leads to a dissipation picture that is to some extent similar to the one in fluid turbulence where energy is dissipated at small spatial scales. Nevertheless, nonlinear gyrokinetic simulations show unambiguously that the understanding of the complicated linear physics of the problem at hand, i.e., accurate reproduction of the eigenmodes, is important for obtaining the correct nonlinear dynamics in certain collisionality regimes.

3.3 Role of velocity hyperdiffusion

In this section we shall consider a simplified model often used in plasma physics for the theoretical study of plasmas in the interior of fusion devices with magnetic confinement. It follows as a systematic approximation of the gyrokinetic model, mentioned earlier. The results presented here were derived in the first part of the PhD project of the author and are published together with some of his previous work in Ref. [66]. The limit we consider in this section is called the drift-kinetic approximation and presents a simplified case of the gyrokinetic theory. One assumes that, similarly to the temperature and density gradients, the electrostatic potential varies only on scales large compared to the gyroradius but remains nearly constant over distances of the order of ρ_i . The resulting drift-kinetic equation does not contain finite Larmor-radius effects but we, nevertheless, keep one velocity dimension. Hence, in terms of approximation the drift-kinetic limit lies between the gyrokinetic theory and magnetohydrodynamics. Here we also assume a constant magnetic field \mathbf{B} , i.e., no magnetic curvature, which is oriented along the z -axis: $\mathbf{B} = B\mathbf{e}_z$. This geometrical configuration is known in the literature as slab geometry. Additionally, only the $\mathbf{E} \times \mathbf{B}$ -drift shall be considered, where \mathbf{E} denotes the self-generated electric field in the plasma. We treat the system as being in local thermal equilibrium where, however, temperature and density vary in x -direction. The thermal velocity of the ions is redefined as $v_{\text{th},i} = \sqrt{k_B T_i(x_0)/m_i}$, i.e., without the factor of 2 compared to Section 3.1, and x_0 represents a reference position along the x -axis. The gyration of the ions around the fixed magnetic field lines sets a typical timescale of the problem which is given by the inverse of the gyrofrequency $\omega_g = eB/m_i$ (we consider a case with singly-charged ions) and the thermal ion gyroradius equals $\rho_i = v_{\text{th},i}/\omega_g$. An essential aspect of the drift-kinetic approximation is the assumption that the dependence of the full particle distribution function on the perpendicular velocity, $v_\perp = \sqrt{v_x^2 + v_y^2}$, is of a Gaussian type allowing us to integrate over it. The reduced (integrated over v_\perp) ion equilibrium distribution function shall be denoted as $f_{i0}(x, v_\parallel)$ and the small perturbation as $g_{i1}(\mathbf{r}, v_\parallel, t)$ where for the ease of notation we have used small case letters for the spatial coordinate and in the spirit of the drift-kinetic limit shall not distinguish between gyro-centre and particle position. f_{i0} has the form of a local Maxwellian with respect to the parallel velocity. Thus, we neglect terms of the order g_{i1}^2 or higher and obtain a linearised equation for the time evolution of g_{i1} . The distribution functions are normalised over $n_{i0}(x_0)/v_{\text{th},i}$ with n_{i0} denoting the

equilibrium ion density. Further, dimensional quantities are redefined as $\varphi := \varphi/(k_B T_i/e)$, $v_{\parallel} := v_{\parallel}/v_{th,i}$, $T_i := T_i/T_i(x_0)$, $n_{i0} := n_{i0}/n_{i0}(x_0)$, $x, y := x, y/\rho_i$ and $z := z/R$, where φ denotes the electrostatic potential and R - a macroscopic scale characterising the variation of temperature and density in x -direction. The linearised equations governing the time evolution of g_{i1} read

$$\frac{1}{\rho_*} \frac{\partial g_{i1}}{\partial t} + v_{\parallel} \frac{\partial g_{i1}}{\partial z} - \frac{\partial \varphi}{\partial y} \frac{\partial f_{i0}}{\partial v_{\parallel}} - \frac{\partial \varphi}{\partial z} \frac{\partial f_{i0}}{\partial x} = \tilde{\nu} \frac{\partial^n g_{i1}}{\partial v_{\parallel}^n}; \quad (3.18a)$$

$$\varphi = \tau \frac{T_e(x)}{n_{i0}(x)} \int_{-\infty}^{\infty} g_{i1}(\mathbf{r}, v_{\parallel}, t) dv_{\parallel}, \quad (3.18b)$$

where $\rho_* := \rho_i/R$, $\tau := T_e(x_0)/T_i(x_0)$ and $\tilde{\nu}$ stands for the collision frequency normalised over the gyrofrequency. The right-hand side in Eq. (3.18a) represents collisional effects modelled via a so-called hyperdiffusion term with n being an even integer. It is indeed a very minimal model for collisions but due to its simplicity it finds large use in numerical simulations.[67] We emphasise again that the goal of this section is to investigate the behaviour of the eigenmodes in the system given by Eqs. (3.18) in the limit $\tilde{\nu} \rightarrow 0$. The interest in such an analysis arises from the fact that linear modes, both unstable and damped, can influence the nonlinear dynamics of the system. Thus, a dissipation model producing erroneous frequencies and growth rates deviating strongly from the correct physical values has the potential to alter significantly various nonlinear effects. At this point, one should elaborate on what the correct physical eigenvalues are. It has been the subject of intense discussion that the eigenvalues of the collisionless equation [61], i.e., right-hand side equals zero, are qualitatively different from the solutions arising by solving the collisionless initial value problem for the electric potential.[60] The latter corresponds closer to the physical situation since they determine the behaviour of the electrostatic potential and, thereby, the electric field, which are the quantities that are usually measured experimentally. Nevertheless, it has been shown analytically [68] that including collisional effects via the so-called Lenard-Bernstein collision operator [69] produces the same eigenvalues as the collisionless Landau solutions in the limit of vanishing $\tilde{\nu}$. This is illustrated in Fig. (3.2) for two different frequencies. In the case of a smaller collision frequency the corresponding eigenmodes match the collisionless Landau solutions much better than for a higher $\tilde{\nu}$. As we shall prove in this section, a similar result applies also when modelling collisional effects with a hyperdiffusion term. Other, more simplified models for collisional effects, like the Krook term [70], however, do not reproduce the Landau solutions as $\tilde{\nu} \rightarrow 0$. Since the hyperdiffusion term on the right-hand side of Eq. (3.18a) is chosen mainly on the basis of its simple form and numerical implementation, it is important to verify that it leads to the correct physical result. Note that the collision frequency is indeed very small in the core of magnetically confined fusion plasmas which makes the analysis of the mathematical limit $\tilde{\nu} \rightarrow 0$ for the eigenmodes of the system in Eq. (3.18) physically relevant.

The time evolution equation (3.18a) is insufficient and has to be supplemented with Eq. (3.18b) which derives from the Poisson's equation and accounts for the adiabatic re-

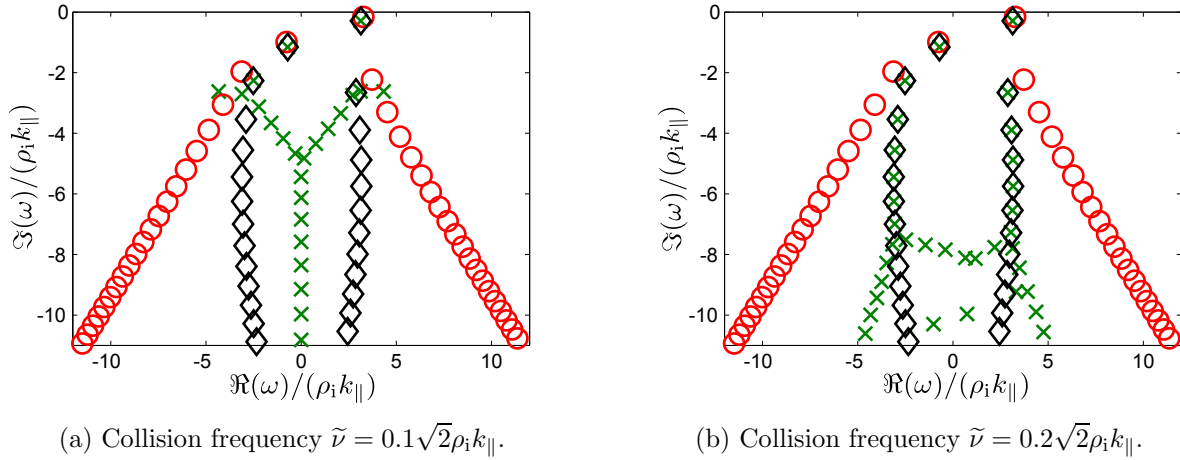


Figure 3.2: A comparison between the collisionless (red circles) and collisional (black diamonds) Landau solutions for two different collision frequencies in the case of the Lenard-Bernstein collision operator. The numerical solutions (green crosses) are obtained with the aid of the Hermite representation of velocity space. (The corresponding wave numbers are $k_y \rho_i$ and $k_{\parallel} R = 0.03$).

sponse of the electrons relating the electrostatic potential to the ion distribution function. The above equations are local in x since this coordinate enters only as a parameter. Thus, without loss of generality, one can set $x = x_0$ which in Fourier space is equivalent to setting $k_x = 0$. Regarding the temperature and density variation, we shall use the so-called local gradient approximation which we already referred to in the previous section. It gives very good results if the domain under consideration has a rather limited extent in the direction in which temperature and density vary. In such a configuration the latter quantities can be approximately treated as constant but, in the same time, their variation is taken into account by assuming that

$$\frac{1}{T_{i0}} \frac{dT_{i0}}{dx} =: -\frac{1}{L_T} = \text{const} \quad \text{and} \quad \frac{1}{n_{i0}} \frac{dn_{i0}}{dx} =: -\frac{1}{L_d} = \text{const} \quad (3.19)$$

with L_T and L_d denoting the temperature and density gradient lengths, respectively, and normalised over the macroscopic scale R . The quantities ω_{iT} and ω_{in} in Eq. (3.15) are inversely proportional to L_T and L_d , respectively. Further, we Fourier transform Eqs. (3.18) with respect to y and z , while also assuming that the perturbation g_{i1} follows a time variation as $e^{-i\omega t}$ where ω can, in general, be complex, i.e., we allow for nonzero growth rates. Defining further for convenience

$$\Omega := \frac{\omega}{\sqrt{2}k_{\parallel}\rho_*}; \quad \nu := \frac{\tilde{\nu}}{\sqrt{2}k_{\parallel}\rho_*}; \quad \kappa := \frac{k_y}{\sqrt{2}k_{\parallel}}; \quad u := \frac{v_{\parallel}}{\sqrt{2}}; \\ g(u) := f_{i1}(\dots, v_{\parallel}, \dots) \quad \text{and} \quad g_0(u) := \sqrt{2}f_{i0}(v_{\parallel}) \quad (3.20)$$

and taking into account that the equilibrium ion distribution function is given by $f_{i0}(v_{\parallel}) = \exp(-v_{\parallel}^2/2)/\sqrt{2\pi}$, we arrive at

$$\Omega g = ug + \frac{\tau}{\sqrt{\pi}} \left(\frac{\kappa}{L_T} u^2 + u + \frac{\kappa}{L_d} - \frac{\kappa}{2L_T} \right) e^{-u^2} \int_{-\infty}^{\infty} g(u') du' - i\nu \left(i^n \frac{\partial^n g}{\partial u^n} \right). \quad (3.21)$$

The above integro-differential equation incorporates both equation in Eqs. (3.18) determines not only the form of the unknown perturbation g but, as will become clear later, it admits solutions only for specific values of the complex frequency Ω . Thus, solving Eq. (3.21) one obtains a set of pairs (Ω_j, g_{Ω_j}) representing the eigenvalues and the corresponding eigenfunctions of the problem. We approach the problem by performing a Fourier transformation with respect to velocity defined as

$$G(p) := \frac{1}{\sqrt{2\pi}} \int_{-\infty}^{\infty} g(u) e^{ipu} du \Rightarrow g(u) = \frac{1}{2\pi} \int_{-\infty}^{\infty} G(p) e^{-ipu} dp, \quad (3.22)$$

where p denotes the variable conjugate to the velocity u . With the aid of this transformation the integral part in Eq. (3.21) yields $G(0)$ which at this point is simply a number. Thus, the integro-differential equation turns into a first-order ordinary differential equation, i.e.,

$$\frac{dG}{dp} + (\nu p^n - i\Omega)G(p) = \tau G(0) \left(i \frac{\kappa}{4L_T} p^2 + \frac{1}{2}p - i \frac{\kappa}{L_d} \right) e^{-p^2/4}. \quad (3.23)$$

the general solution of which has the form

$$G(p) = C \exp\left(-\frac{\nu}{n+1} p^{n+1} + i\Omega p\right) + \tau G(0) \exp\left(-\frac{\nu}{n+1} p^{n+1} + i\Omega p\right) \times \\ \times \int_a^p \left(i \frac{\kappa}{4L_T} x^2 + \frac{1}{2}x - i \frac{\kappa}{L_d} \right) \exp\left(\frac{\nu}{n+1} x^{n+1} - \frac{1}{4}x^2 - i\Omega x\right) dx, \quad (3.24)$$

with C and a being merely constants of integration. At first glance, the above result might seem incorrect since the solution of a first-order ordinary differential equation should depend only on one free parameter. However, the two constants are not independent of each other and both will be determined by the consistency condition that $G(p)$ is an absolutely integrable function, i.e., $G \in L^1(\mathbb{R})$, which will legitimate the Fourier transform with respect to u . Since $G(p)$, as given by Eq. (3.24), is evidently a C^∞ -function, it only remains to examine its decay at infinity.

First, $C = 0$ since otherwise the factor $\exp(-\nu p^{n+1}/(n+1))$ diverges when $p \rightarrow -\infty$ (n even), i.e., the functions belonging to the kernel of the differential operator on the right-hand side of Eq. (3.23) are not integrable. Additionally, $a = -\infty$.² This choice is unique,

²Otherwise we get an additive part that belongs to the kernel of the operator and G is, therefore, not integrable.

since Eq. (3.23) has at most one solution which does not lie in the kernel of the operator. Now, with $C = 0$ and $a = -\infty$, it remains to examine the behaviour of the residual part when $p \rightarrow \pm\infty$. Clearly, $G(p)$ tends to $(ip^2/(4L_T) + p/2 - i\kappa/L_d)e^{-p^2/4}$ when $p \rightarrow -\infty$, i.e., G approaches zero faster than any polynomial in this limit. The other extreme is more problematic, since for $n \geq 2$, as in our case, the integral in Eq. (3.24) diverges. On the other hand, the prefactor goes rapidly to zero which will prove to be sufficient. First, let us constrain $G(p)$ from above as

$$\frac{|G(p)|}{\tau|G(0)|} \leq e^{-\frac{\nu p^{n+1}}{(n+1)} - \Im(\Omega)p} \int_{-\infty}^p \left| i\frac{\kappa}{4L_T}x^2 + \frac{1}{2}x - i\frac{\kappa}{L_d} \right| e^{\frac{\nu x^{n+1}}{(n+1)} + \Im(\Omega)x - x^2/4} dx =: f(p). \quad (3.25)$$

The function $f(p)$ introduced above is positive definite and it suffices to determine its behaviour at $p \rightarrow \infty$ since it controls that of $G(p)$. Taking its derivative with respect to p leads to

$$\frac{df}{dp} = (-\nu p^n - \Im(\Omega))f(p) + \left| i\frac{\kappa}{4L_T}p^2 + \frac{1}{2}p - i\frac{\kappa}{L_d} \right| e^{-p^2/4}. \quad (3.26)$$

If we assume that at large p the second term dominates, then $f(p)$, and also $G(p)$, falls more rapidly than any polynomial, i.e., it is integrable. In the case that the first term dominates, we are left with the relation

$$\lim_{p \rightarrow \infty} \frac{df}{dp} = -\nu \lim_{p \rightarrow \infty} p^n f(p), \quad (3.27)$$

which, combined with the positive definiteness of f , means that $f(p)$ decreases strictly monotonically with p when its argument is large enough. Hence, we are left with two possibilities: either $f(p)$ tends to zero or to some positive constant when $p \rightarrow \infty$. Taking into account that the positive definiteness of f relies on $f' \rightarrow 0$, yields that $f(p) \rightarrow 0$ faster than p^n goes to infinity at large p . Thus, $G(p)$ is in indeed absolutely integrable.

The dispersion relation arises from the solution of Eq. (3.24) by using the self-consistency condition that both side should be equal also for $p = 0$ which allows us to eliminate the arbitrary constant $G(0)$ and leads to

$$1 - \tau \int_{-\infty}^0 \left(i\frac{\kappa}{4L_T}x^2 + \frac{1}{2}x - i\frac{\kappa}{L_d} \right) \exp\left(\frac{\nu}{n+1}x^{n+1} - i\Omega x - \frac{x^2}{4} \right) dx = 0. \quad (3.28)$$

The roots of the above equation are the values for Ω for which the solution of Eq. (3.23) is self-consistent, i.e., is absolutely integrable and admits a Fourier transform. To the best of our knowledge, the above integral cannot be reformulated in terms of elementary functions or any of the well-known special functions. Since we are interested in the behaviour of the dispersion relation for vanishing collision frequency ν , one might be tempted to expand the part of the exponential containing ν in terms of Taylor series around $\nu = 0$ and then

simply interchange integration and summation. However, in this case such a term-by-term integration cannot be justified mathematically. Instead we write

$$\exp\left(\frac{\nu}{n+1}x^{n+1}\right) = 1 + \frac{\nu}{n+1}x^{n+1} + \int_0^\nu \frac{x^{2(n+1)}}{(n+1)^2}(\nu-t) \exp\left(\frac{t}{n+1}x^{n+1}\right) dt, \quad (3.29)$$

where the last term is the residual. Defining for convenience $q(x)$ as the polynomial part in the integrand in Eq. (3.28) and D as the absolute value of the difference between the full integral in the dispersion relation and its reduced version where only the first two terms in Eq. (3.29) are taken into account, one can write that

$$D \leq \int_{-\infty}^0 |q(x)| \frac{x^{2(n+1)}}{(n+1)^2} \int_0^\nu (\nu-t) \exp\left(\frac{t}{n+1}x^{n+1}\right) dt |e^{-i\Omega x - x^2/4}| dx. \quad (3.30)$$

We need to constrain the inner integral by an expression of a polynomial type with respect to ν which will give us its order. Bearing in mind that n is even and $x \leq 0$, one sees immediately that

$$\int_0^\nu (\nu-t) \exp\left(\frac{t}{n+1}x^{n+1}\right) dt \leq \int_0^\nu (\nu-t) dt = \frac{1}{2}\nu^2. \quad (3.31)$$

Hence, the upper bound for the difference D between the exact integral and its linear approximation is of the same order and given by

$$D \leq \frac{1}{2}\nu^2 \int_{-\infty}^0 |q(x)| \frac{x^{2(n+1)}}{(n+1)^2} e^{-x^2/4 + \Im(\Omega)x} dx =: \nu^2 C_n(\Omega), \quad (3.32)$$

where the constant $C_n(\Omega)$ depends on n and Ω and is finite for every finite value of the latter. Note that the upper bound for D is indeed only local in the complex Ω plane, since C_n depends on Ω and in a way that $C_n(\Omega) \rightarrow \infty$ when $\Im(\Omega) \rightarrow -\infty$. Nevertheless, this is not a problem from a physical point of view since this area of the complex plane is populated by highly damped modes which have hardly any physical significance. Qualitatively, this implies that the error one introduces by considering only the first two terms of the expansion in Eq. (3.29) is small in the upper half of the complex Ω plane, where the unstable and the least damped linear modes are situated, and increases when $\Im(\Omega)$ decreases as can be seen in Fig. 3.2 for the Lenard-Bernstein collision operator. Thus, by taking into account only linear terms with respect to ν when approximating the integrand in Eq. (3.28), we arrive at

$$\begin{aligned} & 1 + \frac{1}{\tau} + \frac{\kappa}{L_T} \Omega + Z(\Omega) \left(\frac{\kappa}{L_T} \Omega^2 + \Omega + \frac{\kappa}{L_d} - \frac{\kappa}{2L_T} \right) + \\ & + i^{n+1} \frac{\nu}{n+1} \frac{d^{n+1}}{d\Omega^{n+1}} \left[\frac{\kappa}{L_T} \Omega + Z(\Omega) \left(\frac{\kappa}{L_T} \Omega^2 + \Omega + \frac{\kappa}{L_d} - \frac{\kappa}{2L_T} \right) \right] + O(\nu^2) = 0, \end{aligned} \quad (3.33)$$

where Z denotes the plasma dispersion function and we have made use of the relation

$$\int_{-\infty}^0 x^r e^{-x^2/4 - i\Omega x} dx = i^r \frac{d^r}{d\Omega^r} \int_{-\infty}^0 e^{-x^2/4 - i\Omega x} dx = -i^{r+1} \frac{d^r Z(\Omega)}{d\Omega^r}, \quad (3.34)$$

which applies for every $r \in \mathbb{N}_0$ and can be easily verified via mathematical induction. The definition of the plasma dispersion function and the explicit derivation of Eq. (3.34) are given in detail in Appendix A. By taking the limit $\nu \rightarrow 0$ Eq. (3.33) reduces to the well-known collisionless plasma dispersion relation for slab ITG modes. Thus, the hyperdiffusion operator in velocity space indeed captures properly the linear physics of the system. Since the use of such type of operators is wide spread in numerical simulations in plasma physics, the above analysis strengthens the theoretical support for this numerical practice. The treatment presented here follows the Van Kampen type of analysis, i.e., solving the eigenvalue equation for the linearised problem after a Fourier transformation with respect to space and assuming that fluctuations of the particle distribution function vary in time as $e^{-i\omega t}$. One could also follow the Landau approach by solving the initial value problem by means of a Laplace transform with respect to time. While in the collisionless case, as well as with simple collision operators as the Krook term, the two approaches lead to fundamentally different results, one should note that in the case of velocity hyperdiffusion, as well as in the case of the Lenard-Bernstein collision operator, they both give the same result, i.e., in this case the Landau solutions coincide with the eigenvalues of the system. Additionally, note that velocity hyperdiffusion terms also successfully capture important physical properties characteristic for genuine collision operators. They conserve particle number, momentum (which is violated by the Lenard-Bernstein operator) and, for $n > 2$ also energy.

3.4 Conclusion

In the current chapter we presented brief introduction to the problem of plasma turbulence in the framework of the gyrokinetic theory described in Section 3.1. There we motivated the equations governing the dynamics of strongly magnetised plasmas. This has a conceptual importance for the work presented in this thesis, since the main motivation for it derives from observations in the numerical solution of the gyrokinetic equation as discussed in Section 2.4. Section 3.2 clarified the role of linear effects on plasma turbulence. While in the classical Navier-Stokes model the features of the linearised equations are completely erased by the onset of turbulence, the analysis of the dynamics of magnetised plasmas shows that some characteristics of the linear solutions persist even in the nonlinear dynamics. Furthermore, for some regimes with respect to the value of the collision frequency, damped linear eigenmodes play an essential role for the damping mechanisms, determining the scales on which the latter are active. Thus, successful modelling of the turbulent dynamics requires in-depth understanding of the linear eigenmodes of the system, both unstable and damped.

Deriving the correct linear dispersion relation in the limit $\nu \rightarrow 0$ was done in Section 3.3 for a simple collision operator of a hyperdiffusion form which is, however, often used in numerical simulations. Our mathematical analysis showed that in the limit of vanishing collision frequency the linear eigenmodes approach the collisionless Landau solutions instead of the eigenmodes corresponding to the collisionless case. This result was already established for the special case of the Lenard-Bernstein operator. However, it was important to verify it analytically also for a collision operator of the hyperdiffusion type, since the latter is often adopted as a model for collisional effects in plasmas. Furthermore, for a nonzero collision frequency the corresponding eigenmodes match the collisional Landau solutions.

Chapter 4

Modified Kuramoto-Sivashinsky model

In our discussions so far we focused mainly on turbulence as originating from solutions of the Navier-Stokes equations in three or two dimensions at high Reynolds numbers. According to some definitions, only the first case can be referred to as ‘turbulence’. As specified in the introduction, however, we shall not advocate this rather restrictive view. Instead, in this work turbulence will be considered as a general description for a spatio-temporal chaos in an open system which is driven out of equilibrium. An additional and necessary feature for this chaotic behaviour to be called turbulence is that it arises due to nonlinear interactions of a huge number of degrees of freedom. The latter requirement shall distinguish turbulence from the field of chaotic systems where chaos is attributed to only few degrees of freedom.

One of the most simple models for spatio-temporal chaos is the Kuramoto-Sivashinsky equation which was originally put forward for describing the turbulence in magnetised plasmas.[71, 72] Unlike the gyrokinetic equation, discussed earlier, for which one relies heavily on numerical simulations to gain insight into the physical phenomena, this one-dimensional model provides a simple tool for analysing the nonlinear saturation of trapped electron modes. The equation did not become widespread in plasma physics because in roughly the same time the more realistic two-dimensional Hasegawa-Mima model was introduced which compared favourably to the experimental data at that time.[73, 74] The same one-dimensional equation was written down independently by Kuramoto [75] for the purpose of studying phase turbulence in reaction-diffusion processes of the Belousov-Zhabotinsky type. Later, Sivashinsky [76, 77] introduced a higher-dimensional version of the same model for the analysis of flame front propagation. In general, the equation describes spatially-extended systems driven out of thermodynamic equilibrium by large-scale instabilities. A saturation in the statistical sense is reached via nonlinear coupling and short-wavelength damping. With respect to the latter two features, it resembles the Burgers’ equation [12, 13] but does not need an external energy injection mechanism in order to reach a statistically stationary regime. Further, the Kuramoto-Sivashinsky equation

respects the translational, parity and Galilean symmetries and in its original form reads

$$\frac{\partial u}{\partial t} = -u \frac{\partial u}{\partial x} - \mu \frac{\partial^2 u}{\partial x^2} - \nu \frac{\partial^4 u}{\partial x^4}, \quad (4.1)$$

where $u(x, t)$ is a one-dimensional scalar field, here referred to as velocity, defined over the one-dimensional spatial coordinate x and time t . The positive parameters μ and ν determine the rates of energy injection and dissipation. For Eq. (4.1) to be complete it has to be supplemented with suitable boundary and initial conditions. In the reminder of this chapter we shall consider a finite-size domain $\Omega = [0, L]$ with periodic boundary conditions and the initial velocity field shall be a smooth function $u(x, t = 0) = u_0(x)$. In one spatial dimension the Cauchy problem of Eq. (4.1) is well posed both for the periodic and infinite domains [78, 79], i.e., there exists a unique solution and it depends continuously on the initial data $u_0(x)$. Note, however, that Eq. (4.1) is non-integrable since it does not pass the Painlevé test [80], i.e., a general analytical solution, although unique, cannot be constructed explicitly. In particular, the Kuramoto-Sivashinsky equation possesses a compact global finite-dimensional attractor.[81, 82, 83] Thus, the dynamics of the system is determined by a finite number of modes (not necessary Fourier), although this number can be very large. An even stronger result presents the existence of a finite-dimensional inertial manifold for Eq. (4.1) which contains the global attractor. The solutions of Eq. (4.1) enter the inertial manifold at an exponential rate.[84] Thus, the long-time behaviour of every solution is determined by the properties of the inertial manifold and is equivalent to that of a finite-dimensional dynamical system.

For the purpose of numerical computations, Eq. (4.1) has to be normalised. Thus, we need to set characteristic units of length and time. As a typical length we shall take some distance L_0 of the spatial domain. The coefficient μ plays the role of negative diffusivity and has the units of m^2/s . With its help a natural time scale can be constructed as L_0^2/μ . Thus, going to normalised units involves the substitution $L \rightarrow L_0 L$, $x \rightarrow L_0 x$, $t \rightarrow t L_0^2/\mu$, $u \rightarrow \mu u/L_0$ and $\nu \rightarrow L_0^2 \mu \nu$, where the quantities of the right are non-dimensional. The normalised equation has the same form as above with simply setting $\mu = 1$.

The individual terms on the right-hand side of Eq. (4.1) possess a straightforward physical interpretation. Due to the second derivative, the system is unstable with respect to fluctuations exhibiting large-scale variations, i.e., such fluctuations grow. On the other hand, the term involving a fourth-order spatial derivative acts in a stabilising way on small-scale fluctuations. Thus, the second contribution on the right-hand side of Eq. (4.1) injects energy into the system, while the last term acts as an energy sink. Without the nonlinearity the total energy of the system would grow without bounds. The mathematical results described in the previous paragraph, however, provide an upper bound for $\|u\|_{L^2}$. Hence, the nonlinear term induces an energy transfer mechanism from large to small scales, i.e., in the case of the Kuramoto-Sivashinsky equation, as well as its modified form that we will study in the this chapter, there is a forward energy flow as in incompressible three-dimensional Navier-Stokes turbulence. Note that as in the incompressible Navier-Stokes model, the nonlinear term is also quadratic and redistributes energy in a conservative manner. Multiplying the normalised version of Eq. (4.1) by u and integrating over space gives

$$\frac{dE}{dt} = \frac{1}{L} \int_{\Omega} \left(\frac{\partial u}{\partial x} \right)^2 dx - \nu \frac{1}{L} \int_{\Omega} \left(\frac{\partial^2 u}{\partial x^2} \right)^2 dx, \quad (4.2)$$

where $E(t)$ denotes the total energy of the system and is defined as the integral of $u^2/2$ over the spatial domain Ω and normalised over the interval length L .¹ The first term on the right-hand side of Eq. (4.2) gives the energy injection rate, while the second one quantifies the energy dissipation rate. In the statistically stationary regime, the time-average of the left-hand side of Eq. (4.2) vanishes meaning that the solution adjusts such that on average energy injection equals energy dissipation. The above picture resembles in many ways the situation in three-dimensional Navier-Stokes turbulence where, however, energy is injected by external forces and not by means of intrinsic instabilities. Nonetheless, the physics described by the equations differs considerably. While in Navier-Stokes the dominating pattern represents whirls whose stretching in the third dimension provides the mechanism for energy transfer to small scales, the Kuramoto-Sivashinsky equation, as the Burgers' equation, favours the formation of shocks. This is due to the absence of the incompressibility constraint² and provides the way for directly connecting the large scales with the small ones.

4.1 Spectral formulation

Supplementing Eq. (4.1) with periodic boundary conditions suggest the representation of the velocity field $u(x, t)$ in terms of Fourier series with respect to the spatial variable x . Mathematically, the decomposition of $u(x, t)$ reads

$$u(x, t) = \sum_k \hat{u}(k, t) e^{ikx}. \quad (4.3)$$

Strictly speaking, the wave number k takes only discrete values given by $k = n(2\pi/L)$ where $n \in \mathbb{Z}$ and a sum over k represents a shorthand notation for a sum over n from $n = -\infty$ to $n = +\infty$. The transformation from real to Fourier space is bijective and the Fourier coefficients can be computed as

$$\hat{u}(k, t) = \frac{1}{L} \int_0^L u(x, t) e^{-ikx} dx. \quad (4.4)$$

The physical constraint that u takes only real values implies the symmetry that $\overline{\hat{u}(k, t)} = \hat{u}(-k, t)$ where the overbar denotes complex conjugation. Thus, only half of the Fourier

¹This represents the same abuse of notation as with Navier-Stokes, since for u being a velocity field $\int u^2 dx / (2L)$ has the units of energy divided by mass. For the case of constant density, however, $\int u^2 dx / (2L)$ is proportional to the energy of the system and one can refer to it effectively as energy.

²Demanding that $\partial u / \partial x = 0$ would lead to a trivial solution that is constant both in space and time.

modes represent real degrees of freedom for the system and it is enough to keep track of the modes corresponding only to $n \in \mathbb{N}_0$. Applying the Fourier series representation to the (normalised) Kuramoto-Sivashinsky equation, one arrives at

$$\frac{\partial \hat{u}(k, t)}{\partial t} = -\frac{i}{2}k \sum_p \hat{u}(k-p, t)\hat{u}(p, t) + (k^2 - \nu k^4)\hat{u}(k, t), \quad (4.5)$$

which gives the temporal evolution of the coefficient $\hat{u}(k, t)$. The latter can be viewed as an infinite system of coupled ordinary differential equations. The convolution sum on the right-hand side arises from the multiplicative form of the nonlinearity and represents the coupling of the different Fourier modes. At this point the physical picture, discussed previously, becomes much more transparent. Without the nonlinear contribution the time evolution of the Fourier modes becomes trivial, namely $\hat{u}(k, t) = \hat{u}(k, t=0)e^{(k^2 - \nu k^4)t}$. Thus, the growth/damping rate γ of each coefficient can be defined as $\gamma = k^2 - \nu k^4$. At wave numbers $k < 1/\sqrt{\nu}$ the growth rate is positive, i.e., at large scales the system is linearly unstable. For $k > 1/\sqrt{\nu}$, however, $\gamma < 0$, meaning that small-scale fluctuations are linearly suppressed. In analogy to the Navier-Stokes case, we shall define the energy of mode k to be $E(k, t) := |\hat{u}(k, t)|^2/2$. Multiplying Eq. (4.5) by $\overline{\hat{u}(k, t)}$ and adding to the resulting equation its complex conjugate, one can write the evolution equation for $E(k, t)$ as

$$\frac{\partial E(k, t)}{\partial t} = G(k, t) + T(k, t) + D(k, t), \quad (4.6)$$

where G , T and D denote the energy injection, transfer and dissipation terms, respectively. In Fourier space they are given by

$$G(k, t) = 2k^2 E(k, t) \quad (4.7a)$$

$$T(k, t) = \frac{1}{2}k \Im(\overline{\hat{u}(k, t)} \mathcal{F}\{u^2\}(k, t)) \quad (4.7b)$$

$$D(k, t) = -2k^4 E(k, t) \quad (4.7c)$$

and the spectral energy balance given by Eq. (4.6) is completely analogous to the one derived in classical fluid turbulence and in the framework of the gyrokinetic theory for strongly magnetised plasmas. The results presented in this chapter were already published by the author of this thesis in Ref. [85]. In the case of a comparison, however, one should note that the definition of the mode energy in Ref. [85] is simply $|\hat{u}(k, t)|^2$, i.e., it differs by a factor of 2 from the definition used here.

As shown schematically in Fig. 2.3 (a), at large Reynolds numbers the Navier-Stokes model exhibits scale-separation between energy injection and dissipation which represents its most essential feature providing the basis for the Kolmogorov theory. A numerical computation of the three terms in Eqs. (4.7) for two different values of the parameter ν is displayed in Figs. 4.1 (a) and (b). The result has been obtained after the system has reached the statistically stationary state where we have performed a time-average denoted by $\langle \cdot \rangle_\tau$. The subscript τ denotes the time period over which we average. Thus, the contribution of the

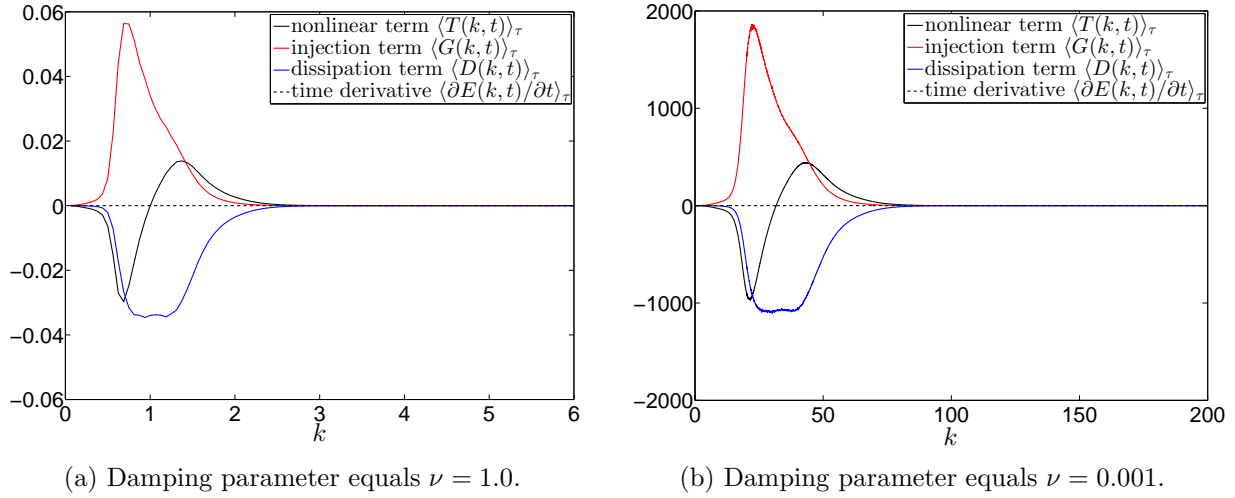


Figure 4.1: Numerical computation of the different terms in Eq. (4.6) for different values of the parameter ν . We have performed a time-average over the statistically-stationary state. The dashed line represents the time-average of the right-hand side and its negligible size compared to the other terms verifies numerically the attaining of statistical stationarity.

right-hand side (dashed line) is approximately zero, implying that G , T and D have to balance each other at every wave number. In Fig. 4.1 (a) it is evident that the physical picture is fundamentally different from classical Navier-Stokes turbulence, since here the spectral ranges, over which the injection and dissipation terms are active, overlap. Hence, there is no intermediate range of scales with vanishing nonlinearity $\langle T(k) \rangle_\tau$ and constant but non-zero energy flux as in Fig. 2.3 (a). The situation is much more similar to that in gyrokinetics, as displayed in Fig. 2.6, where the nonlinear term transitions gradually from a sink (negative contribution) at large spatial scales to a source (positive contribution) at small scales. The scale-separation in classical turbulence, of course, does not exist for a large viscosity but arises only in the limit of infinite Reynolds numbers, corresponding in this case to $\nu \rightarrow 0$. In order to insure that the overlapping is not simply a large- ν effect, we have performed the same computation also for $\nu = 0.001$, i.e., with 10^3 times smaller damping parameter compared to Fig. 4.1 (a). The result is displayed in Fig. 4.1 (b). As can be seen there, the form of the different terms remains unchanged and, despite the dramatic decrease of the damping factor, no scale separation arises. Thus, the fact that both energy injection and dissipation are active at the same scales is inherent to the system under consideration and not a nonzero- ν effect. The only change produced by the variation of ν is a mere rescaling of the individual terms. From the functional form $\gamma(k)$ given above one can easily derive that the instability with the maximal growth rate is located at the wave number $k_{\max} = 1/\sqrt{2\nu}$. Thus, for $\nu = 1$ we have that $k_{\max} \approx 0.7$ which corresponds approximately to the position of the peak of the energy injection term $\langle G(k) \rangle_\tau$ (red curve) in Fig. 4.1 (a). Respectively, for $\nu = 10^{-3}$ the energy injection reaches its maximum at $k \approx 0.7\sqrt{10^{-3}} \approx 22.1$. The lower value of the damping coefficient naturally

leads to a higher energy level at which the injection and dissipation terms reach a statistical balance which explains the vertical scaling between Fig. 4.1 (a) and (b). The reason why there is a scale separation in classical Navier-Stokes turbulence but not for the Kuramoto-Sivashinsky equation, lies in the fact that in the case of the former the injection mechanism is decoupled from the dissipation. There energy is injected into the fluid by external forces and is, ideally, concentrated at small wave numbers. Decreasing viscosity moves the dissipation term in Fig. 2.3 (a) further to the right (smaller scales) but does not influence the energy injection. The latter is due to an external force and remains localised at the same small wave numbers being virtually independent of viscosity. In the case of the Kuramoto-Sivashinsky equation, however, the mechanism of energy injection is intrinsic to the system. The spectral regions where both injection and dissipation are dominant is controlled by the growth rate $\gamma = k^2 - \nu k^4$ and are separated by the wave number k_0 for which $\gamma = 0$, i.e., by $k_0 = 1/\sqrt{\nu}$. Thus, by decreasing the damping parameter ν , one shifts not only the dissipation to smaller scales but also extends the unstable area in Fourier space. This interconnection between energy injection and dissipation is a general feature of active systems and prevents the straightforward application of ideas from fluid turbulence.

4.2 Modification of the linear part

At large wave numbers the damping rate in the original version of the Kuramoto-Sivashinsky equation is proportional to k^4 , i.e., it is variable with respect to the spatial scale. In Eq. (4.5) we shall modify the form of the linear terms as

$$k^2 - \nu k^4 \longrightarrow \frac{k^2 - \nu k^4}{1 + b k^4}, \quad (4.8)$$

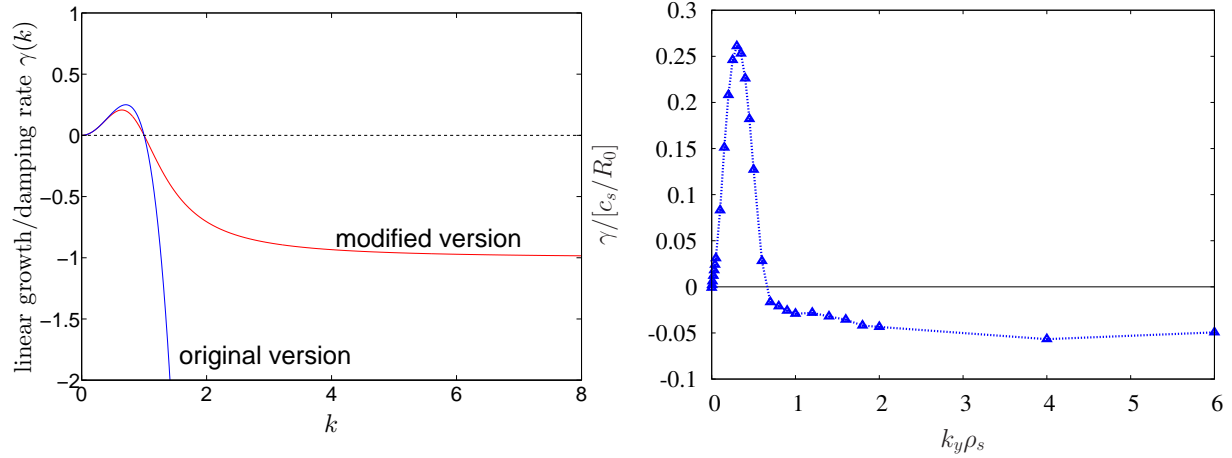
where b is a positive constant representing an additional parameter of the system. The Kuramoto-Sivashinsky equation modified in this way reads

$$\frac{\partial \hat{u}(k, t)}{\partial t} = -\frac{i}{2} k \sum_p \hat{u}(k-p, t) \hat{u}(p, t) + \frac{k^2 - \nu k^4}{1 + b k^4} \hat{u}(k, t), \quad (4.9)$$

Hence, the nature of the nonlinear mode-to-mode coupling was left unchanged by the modification. However, now the linear damping rate does not grow without bounds in the high-wave-number limit, but instead tends to the constant value of ν/b which is set externally. All the numerical results reported here were obtained with $\nu = 1$, unless otherwise stated. Thus, the value of b alone controls the damping rate at high wave numbers. The difference in the form of the linear terms is shown schematically in Fig. 4.2 (a). At small k the value of the denominator $1 + b k^4$ is close to one and the modified form yields nearly the original linear growth rate.³ However, there is a considerable qualitative difference at small scales. Thus, in the modified version of the Kuramoto-Sivashinsky equation

³The exact deviation depends on the value of the parameter b . For the typical values to be used later in this chapter the deviation in the unstable k -range is even smaller than the one seen in Fig. 4.2 (a).

both the large-scale energy injection mechanism and the nonlinear interaction are left unchanged, while the energy dissipation part is qualitatively altered. The motivation for such



(a) Modified form (red) of the linear terms in the Kuramoto-Sivashinsky equation compared to their original version (blue).

(b) Linear growth/damping rate of the ITG instability in the gyrokinetic model. (courtesy of Dr. Tobias Görler)

Figure 4.2: Comparison between the linear growth/damping rates for the Kuramoto-Sivashinsky equation (original and modified version) and for the gyrokinetic model.

a modification comes from the gyrokinetic theory of magnetised plasmas. Neglecting the nonlinear terms in Eq. (3.15) leads to a similar dispersion relation as in Eq. (3.33) which, however, does not rely on the drift-kinetic approximation and incorporates the effect of curved magnetic field lines. As already discussed, in such a setting there are countably infinitely many linear modes at every \mathbf{k} . At most one of those modes can become unstable in a certain part of wave number space. Determining the growth rate of this instability for different k_y -values⁴ yields Fig. 4.2 (b). [86] Therefore, in the gyrokinetic theory large-scale fluctuations are usually unstable, while small-scale fluctuations are damped. However, in contrast to the Navier-Stokes equations or the original Kuramoto-Sivashinsky equation, the amount of damping does not increase indefinitely when the spatial scale decreases, but tends to finite constant. This qualitative feature we model by introducing the modification given by Eq. (4.8). Furthermore, this is one of the simplest realisations of a controlled deviation from the classical fluid theories. Note additionally, that, although the real-space representation of the modified linear term is mathematically rather intricate, its action on the function u is well defined for $u \in C^4(\Omega) \cap L^2(\Omega)$, the class of functions for which also the original Kuramoto-Sivashinsky equation is well-defined. That is to say, it does not require additional regularity of the field u .

⁴One should view k_y here essentially as a synonym for $k_\perp = \sqrt{k_x^2 + k_y^2}$, since k_x is fixed.

4.3 Numerical implementation

For the purpose of this work, Eqs. (4.5) and (4.9) are solved numerically by using the exponential time differencing scheme for stiff PDEs combined with a fourth order Runge-Kutta algorithm as developed in Ref. [87] and improved in Ref. [88]. The spatial derivatives are handled via the pseudo-spectral approach which is advantageous due to the speed of modern algorithms for discrete fast Fourier transform and the imposed periodic boundary conditions. Thus, the derivatives are computed in Fourier space, while the evaluation of the nonlinear term takes place in real space. Since the nonlinearity is quadratic with respect to u , we apply the so-called 3/2-rule in order to avoid aliasing errors. It requires that the highest 1/3 of the Fourier modes are set to zero at every time step. The numerical method reproduces correctly the development of shock structures in the solution of Eq. (4.5) as displayed in Fig. 4.3 (a)-(d) where the first three plots trace the early-time evolution of the initial condition. Starting with a slowly varying wave-like profile, large-scale fluctuations, as seen on the left, soon become unstable developing steep slopes, i.e., shocks, as expected from the analysis of the linear terms in the equation. Without terms containing spatial derivatives such shocks would lead to the formation of finite-time singularities as in the case of the inviscid Burger's equation. In the long-time limit the solution to the Kuramoto-Sivashinsky equation represents a train of shock-like structures spread over the whole spatial domain as shown in Fig. 4.3 (d). The solution of the modified version as given in Eq. (4.9) exhibits under identical initial conditions the same short-time behaviour and in the long-time limit reveals qualitatively the same structures as those in Fig. 4.3 (d).

If the small spatial scales are well-resolved, i.e., the highest k -mode is high enough, the numerical solution reaches a statistically steady state. The same applies also for the modified version given by Eq. (4.9), since it also possesses an infinite number of damped modes at large wave numbers. A comparison between the temporal evolution of the total energy of the system for Eqs. (4.5) and (4.9) is given in Fig. 4.4. For the same initial condition incorporating few small- k components, the two curves are almost identical at small t . This results from the fact that at early times the dynamics is governed by the unstable modes (the positive part of the curves in Fig. 4.2 (a)) which have nearly identical growth rates for small b . Thus, in the beginning there is a linear phase of exponential energy increase. Since the nonlinear term is quadratic with respect to the velocity field, it grows faster than the linear terms and at a certain level starts influencing the dynamics by transferring energy to linearly damped modes and which allows the energy dissipation to balance the injection at large scales. Eventually, a statistically steady state is reached, as seen in Fig. 4.4, which persists indefinitely. The average total energy displays only a very small deviation between the two cases since the modification we introduced practically does not influence the low- k part of the energy spectrum where most of the energy is concentrated. The change in the form of $E(k)$ becomes noticeable only at large wave numbers which, however, contain only a small portion of the total energy of the system.

Similarly as in the Navier-Stokes case, the solution of the Kuramoto-Sivashinsky equation exhibits fluctuations at different spatial scales. The intensity of those fluctuations as a

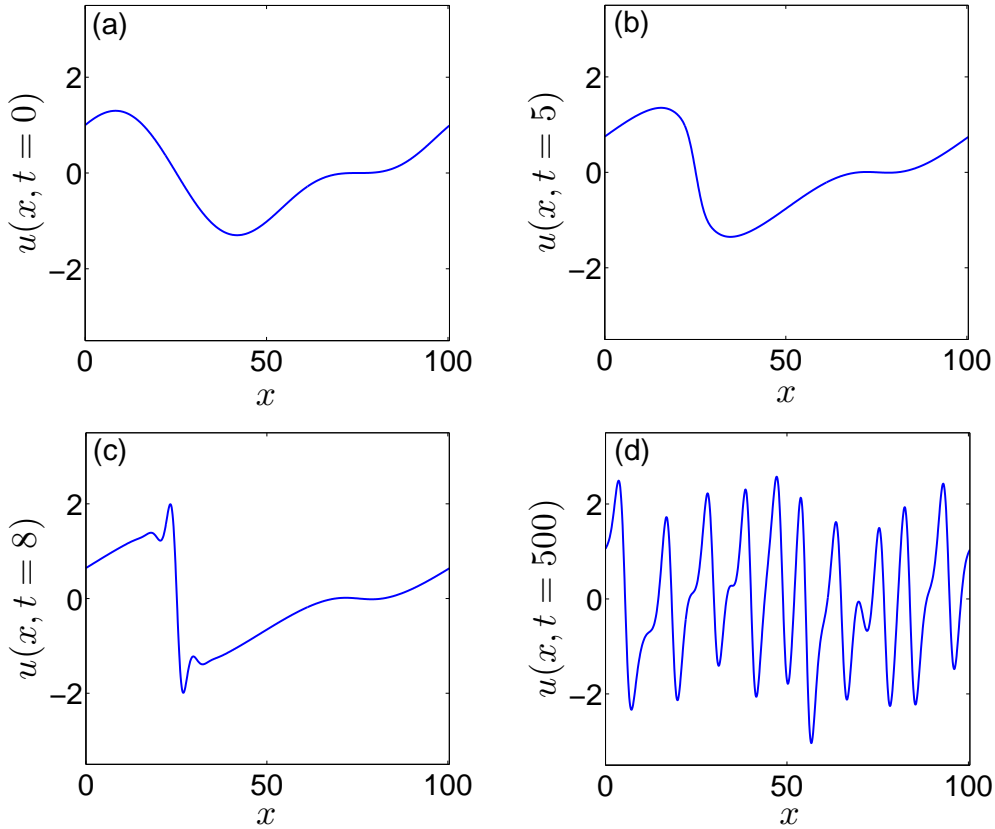


Figure 4.3: Development of shocks from in a real-space solution the original Kuramoto-Sivashinsky equation. We start with a slowly-varying wave-like solution (a). Due to the nonlinearity it quickly develops shock-like structures. The terms involving spatial derivatives prevent the forming of discontinuities and control the thickness of the shocks.

function of the scale represents a key feature of the system. Since, as discussed in Section 2.2, one often works in Fourier space, the fluctuations at different scales are quantitatively characterised by the energy spectrum. The computation of the latter constitutes one of the main goals of the theoretical approaches used to study equations of such type. As pointed out in the introduction to this chapter, for a smooth initial condition the Kuramoto-Sivashinsky equation possesses a smooth and unique solution which is global in time. Additionally, the solution is known to be analytic on the real line and in a strip around it and several conjectures regarding the dependence of this strip on the system length have been made and also supported numerically.[89] Thus, according to the von Neumann argument [39] the Fourier transform of the solution should decay exponentially at large wave numbers. If our numerical tool solves Eq. (4.1) correctly, it should reproduce the exponential decay at $k \rightarrow \infty$. Indeed, solving the original Kuramoto-Sivashinsky equation numerically, one obtains for the energy spectrum the result shown in Fig. 4.5, where we have averaged over the statistically stationary state. With the semi-logarithmic

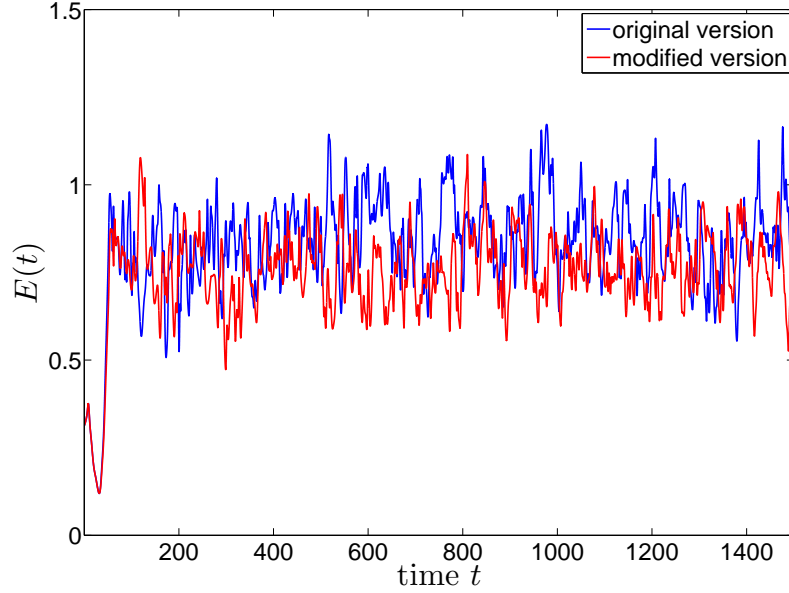


Figure 4.4: Time evolution of the total energy for the original (blue) and modified (red) version of the Kuramoto-Sivashinsky equation.

representation used in the figure an exponential decay translates into a straight line. Hence, our numerical solution conforms to this qualitative prediction at large k . The exponential fall-off is limited only by the machine precision producing the small flat part on the very right in Fig. 4.5.

4.4 Energy transfer between scales

Similarly as in the case of ordinary Navier-Stokes turbulence or plasma turbulence, one is interested not in the specific solution $u(x, t)$ or its Fourier transform but rather in energy-like quantities and their distribution in spectral space. The modified version of the balance equation for the energy of mode k reads

$$\frac{\partial E(k, t)}{\partial t} = \sum_p T(k, p, t) + 2 \frac{k^2 - \nu k^4}{1 + b k^4} E(k, t). \quad (4.10)$$

The term $T(k, p, t)$ on the right-hand side, which arises due to the nonlinear mode-to-mode interaction, is defined mathematically as

$$T(k, p, t) := \frac{1}{2} k \Im(\overline{\hat{u}(k, t)} \hat{u}(k - p, t) \hat{u}(p, t)) \quad (4.11)$$

and we shall refer to it as the nonlinear energy transfer function. In physical terms, $T(k, p, t)$ gives the rate of change of energy of the mode k due to its interaction with

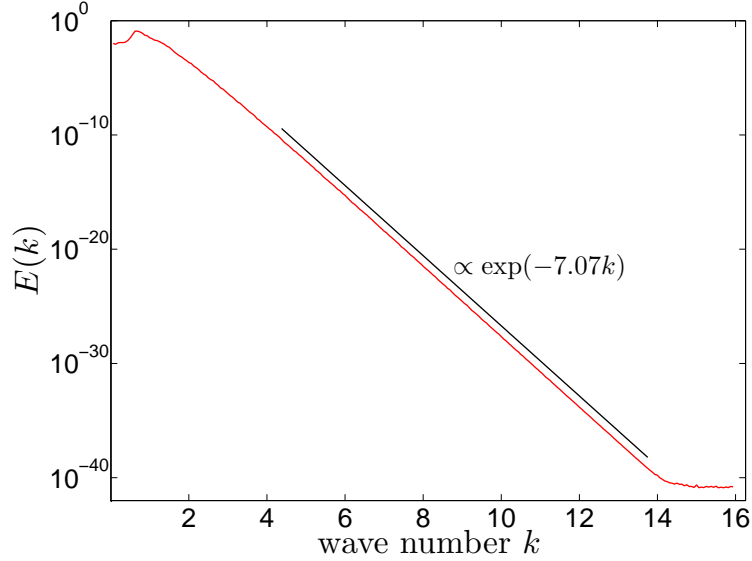


Figure 4.5: Semilogarithmic plot of the energy spectrum of the original Kuramoto-Sivashinsky equation. A comparison with an exponential decay is given.

the mode p via all other possible modes. If $T(k, p, t)$ is positive, then the mode k gains energy from the mode p and, on the contrary, a negative $T(k, p, t)$ means that the mode k loses energy to mode p . The conservative nature of the nonlinear interactions, as already discussed in connection with the original Kuramoto-Sivashinsky equation, implies that

$$\sum_k \sum_p T(k, p, t) = 0, \quad (4.12)$$

i.e., $T(k, p, t)$ only redistributes energy among the different modes without injecting or extracting it in/from the system. Based on the definition in Eq. (4.11) one can conclude that

$$T(0, p) = T(k, 0) = T(k, k) = 0. \quad (4.13)$$

where we have suppressed the time argument for brevity. While the fact that $T(0, p) = 0$ is immediately clear, the last two relations can be easily derived when one considers that in those cases $T(k, 0) = T(k, k) = k|\hat{u}(k)|^2\Im(\hat{u}(0))/2$. Recalling that $\hat{u}(k, t) = \hat{u}(-k, t)$, one sees that $\Im(\hat{u}(0)) = 0$. Additionally, the interaction term exhibits the symmetries that

$$T(-k, p, t) = T(k, -p, t) \text{ and} \quad (4.14a)$$

$$T(-k, -p, t) = T(k, p, t). \quad (4.14b)$$

Expressing $k - p$ as a distinct mode q , it becomes evident that Eq. (4.11) represents a three-mode coupling via the term $\Im(\hat{u}(-k, t)\hat{u}(q, t)\hat{u}(p, t))$. Thus, energy is not transferred directly from one wave number to another but requires a mediator. Additionally, not all

three-wave interactions are possible but only those for which the modes k , p and q fulfil the requirement that

$$k + p + q = 0, \quad (4.15)$$

which in the multi-dimensional case is referred to as the triangle condition, since in that case Eq. (4.15) transforms into a vector equation requiring that the three modes form a triangle in Fourier space. Let us focus for a moment purely on the nonlinear interactions by neglecting the linear terms in Eq. (4.9).⁵ Discarding all the modes but k , p and q , one can easily derive that the nonlinear terms cancel each other such that

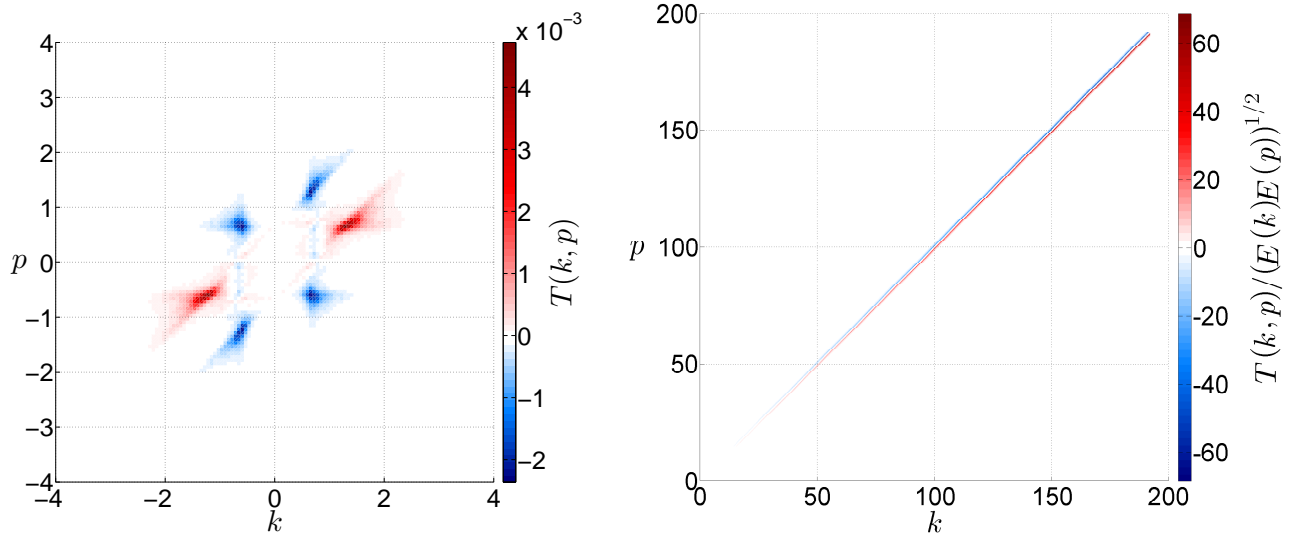
$$\frac{\partial \mathcal{E}(k, t)}{\partial t} + \frac{\partial \mathcal{E}(p, t)}{\partial t} + \frac{\partial \mathcal{E}(q, t)}{\partial t} = 0, \quad (4.16)$$

where \mathcal{E} stands for the energy of a single mode in this truncated system. Thus, the nonlinear energy transfer among the three coupled wave numbers is indeed conservative. While Eq. (4.10) represents the time-resolved energy balance for each mode, this usually involves a lot of redundant information, since we are not interested in all the changes in $E(k, t)$ on short time scales. As we saw in Fig. 4.4, the nonlinear interactions lead to a statistically stationary state where there are still changes in energy on small time scales, but on large time scales the energy of the system remains the same. This picture applies not only for the whole system but also to the energy of each mode individually. Thus, for studying the global-in-time properties one needs to apply some type of averaging procedure over the quasi-stationary state in order to eliminate the rapid fluctuations in time. Assuming ergodicity, one can employ time averaging, denoted here by $\langle \cdot \rangle_\tau$, on Eq. (4.10) which zeros out the time derivative on the right-hand side and yields

$$\sum_p \langle T(k, p, t) \rangle_\tau + 2 \frac{k^2 - \nu k^4}{1 + b k^4} E(k) = 0, \quad (4.17)$$

where $E(k)$ is a shorthand notation for $\langle E(k, t) \rangle_\tau$. Thus, in order to derive the stationary form of the energy spectrum, one needs to examine the structure of the first term on the left-hand side. A numerical computation of $\langle T(k, p, t) \rangle_\tau$, denoted hereafter simply by $T(k, p)$ for brevity, is shown in Fig. 4.6. Since the form of $T(k, p)$ changes qualitatively when going from larger to smaller scales, we display separately both cases. The time-average has been performed over the statistically-stationary regime. Fig. 4.6 (a) reveals the low-wave-number part of the nonlinear coupling. The structure of $T(k, p)$ in this region is rather complex involving the interaction of many different couples (k, p) . The positive and negative contributions have qualitatively different form, resulting from the lack of antisymmetry of $T(k, p)$. There are more negative entries which, however, have a smaller amplitude than the positive ones. Thus, summing over the whole plane equals zero, confirming the globally conservative character of the nonlinear interactions. We see that along the axes $k = 0$ and $p = 0$, as well as along the diagonal $k = p$, the coupling

⁵Since we have modified only the linear terms in Eq. (4.5), the following conclusion applies also to the original Kuramoto-Sivashinsky equation.



(a) The low-wave-number region of $\langle T(k, p, t) \rangle_\tau$. The symmetry of the nonlinear coupling is immediately evident. From the upper two quadrants one can reconstruct the lower two.

(b) High-wave-number part of $\langle T(k, p, t) \rangle_\tau$. In order to make the structure visible, we have normalised it by taking into account the energy of the modes k and p .

Figure 4.6: Numerical computation of the mode-to-mode coupling $\langle T(k, p, t) \rangle_\tau$ averaged over the statistically-stationary state.

is zero in accordance with Eq. (4.13). Additionally, our numerical tool has successfully reproduced the analytical symmetry of $T(k, p)$ as given by Eqs. (4.14). Indeed, the first quadrant represents a mirror image of the fourth, while the second can be mapped one-to-one on the third. Thus, only the information of one half of the (k, p) -plane, e.g., when $p > 0$, is needed in order to reproduce the whole function $T(k, p)$. Fig. 4.6 (b) shows the nonlinear coupling at large wave numbers where we have restricted the plot to the second quadrant of the (k, p) -plane, since this is where the important features are located. In this part of the spectral space $T(k, p)$ decays very fast with the distance from the origin. This is due to the fact that it involves three velocity fields $\hat{u}(k)$, $\hat{u}(p)$ and $\hat{u}(k - p)$. Away from the origin the amplitude of the first two decreases rapidly⁶, meaning that the prefactor k cannot compensate for the decay. In order to make the structure visible we have normalised $T(k, p)$ over the term $\sqrt{E(k)E(p)}$ which does not influence the symmetry but compensates the decrease away from the origin. Thus, structures which were not visible in the non-normalised case due to the larger amplitude of the entries around the origin, are now apparent as a result of the normalisation. We see that at large wave numbers $T(k, p)$

⁶Recall that the amplitude of the Fourier-transformed velocity field is proportional to the square root of the energy spectrum, $\sqrt{E(k)}$. For the original Kuramoto-Sivashinsky equation the latter decays exponentially at large k . In the modified case, the decay is not exponential but polynomial, as we shall see later, however, still very rapid. Due to the condition of finite energy alone, $E(k)$ has to decrease faster than k^{-1} .

is approximately antisymmetric with respect to the interchange of k and p , at least around the diagonal. This property does not follow strictly from the mathematical formulation of $T(k, p)$ given in Eq. (4.11), since we have that

$$T(p, k) = -\frac{p}{k}T(k, p). \quad (4.18)$$

However, when $k \approx p$ their ratio is close to one and, therefore, $T(p, k) \approx -T(k, p)$. The main goal in this chapter is to model $T(k)$, obtained after summation of $T(k, p)$ over p , as a function of the wave number k and the energy spectrum $E(k)$. Hence, we shall take k constant and large which corresponds to plotting a slice of Fig. 4.6 (b) parallel to the p -axis, and determine in more detail the contribution from different modes p . Such a slice is displayed in Fig. 4.7 where we have taken $k = 50$ and normalised $T(k, p)$ only over the energy of that mode. The reason for the change of normalisation is to have a factor which is constant with respect to p in order not to influence the form of the curve. It is evident that the most prominent structures are around $p = k$, which is expected based on Fig. 4.6 (b). Away from this point the values are negligibly small and, therefore, we have not displayed them here. The norm of T gives the strength of the interaction between the mode $k = 50$ and the corresponding p . A very similar structure can be observed for all large wave numbers k . Hence, the strongest coupling is between modes for which $k \approx p$ where, however, there is no coupling when $k = p$, as expected based on Eq. (4.13). The nonlinear mode-to-mode interaction is most substantial at $p = 49.4375$ and $p = 50.5625$. Since we consider a one-dimensional equation, we can immediately determine the third mode participating in the three-wave coupling, namely $q = k - p = 0.5625$ and $q = -0.5625$. The mediator mode q remains the same even if we vary k and consider the analogous curve at $k = 100$, $k = 150$ or $k = 200$, i.e., in the whole large- k part of the spectral plane in Fig. 4.6 (b). The result in Fig. 4.7 corresponds to parameter values of $b = 0.03$ and $\nu = 1.0$, while the normalised system length measures $L = 32\pi$, meaning that the distance between adjacent modes is $\Delta k = 0.0625$ and the linearly most unstable mode is located at $k = 0.6875$. Correspondingly, the energy spectrum attains its maximum at $k = 0.625$ which is very close to the linearly most unstable mode. Thus, at large k we have the following picture for the important nonlinear interactions. Two large wave numbers, say k and p , interact with each other and the coupling is mediated by a very small wave number q that lies in the spectral region where the (linear) energy injection is most intensive and the energy spectrum reaches its maximum. Looking at Fig. 4.7 we see that in this range there is a positive contribution where $p \lesssim k$ and negative for $p \gtrsim k$. The physical interpretation of this implies that the mode $k = 50$ gains energy from slightly smaller wave numbers (mostly from $p = 49.4375$) and loses it via the interaction with slightly larger ones (mostly to $p = 50.5625$). Hence, the modified version of the Kuramoto-Sivashinsky equation, as well as its original form, exhibits a forward flow of energy from large to small scales. We don't have a cascade as in classical three-dimensional Navier-Stokes turbulence at large Reynolds numbers, since the corresponding energy flux, i.e., the integral $-\int_0^k T(k')dk'$, is not constant. Based on these results one concludes that, for this modification of the Kuramoto-Sivashinsky equation, energy flows rather locally between

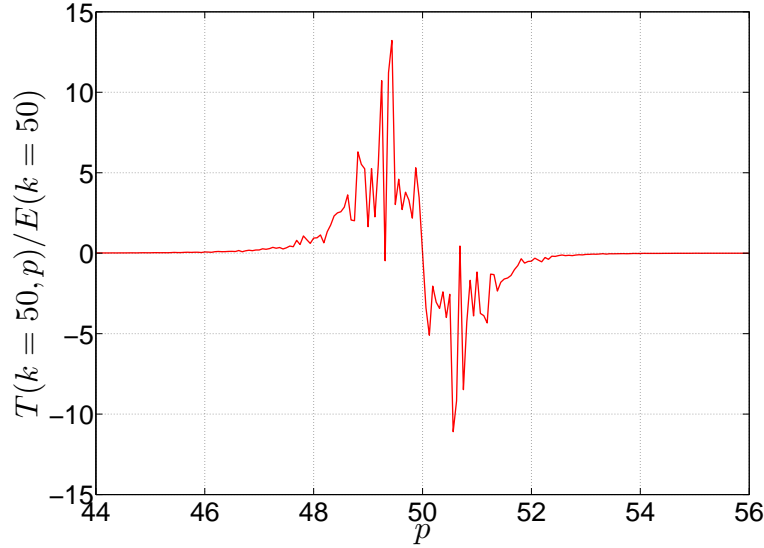


Figure 4.7: Numerical computation of $T(k, p)$ as a function of p with k fixed at $k = 50$. The result is normalised over the energy of the mode $k = 50$ and obtained with the modified version of the Kuramoto-Sivashinsky equation when $b = 0.03$ and $\nu = 1.0$. The structure is qualitatively antisymmetric around the point $p = k$. The quantitative deviation from exact antisymmetry is necessary for the compensation of the linear term in Eq. (4.17).

modes of very similar amplitude but this flow is due to extremely non-local interactions. A closer examination of Fig. 4.7 reveals that the function is not exactly antisymmetric around $p = k$, but the positive part has a slightly larger amplitude than the negative one. This feature can be easily understood by looking at Eq. (4.17). The summation over p in the first term is equivalent to integration of the curve in Fig. 4.7 over p which gives us (with the corresponding sign) the area enclosed by it. At large k the second term in Eq. (4.17) is negative and approximately given by $-2(\nu/b)E(k)$. Thus, in order to compensate for it, the integral over the red curve has to be positive and equal nearly $2\nu/b$. This requires that the area enclosed by the positive part of the curve is larger than the one enclosed by its negative part. Combining this condition with the requirement of approximate antisymmetry as in Eq. (4.18), it follows that the structures on the left from the $p = k$ line should have the same form but a slightly larger amplitude than those on the right.

In order to obtain a better qualitative understanding for the nonlinear interactions we shall make use of the so-called scale disparity parameter S , which was already mentioned in Section 2.4. It represents a commonly used metric to study the locality of wave-number interactions in homogeneous and isotropic Navier-Stokes turbulence. In the multi-dimensional case, setting the length of two of the modes, say \mathbf{k} and \mathbf{p} , does not determine the length of the third one, \mathbf{q} . The geometrical interpretation of this is straightforward, since fixing the length of two of the sides of a triangle leaves the third one undetermined which can

vary freely between zero and their sum, i.e., $0 < |\mathbf{q}| < |\mathbf{k}| + |\mathbf{p}|$. Thus, in the standard turbulence literature S is a function of three variables: $S = S(|\mathbf{k}|, |\mathbf{p}|, |\mathbf{q}|)$. For a one-dimensional system, however, the length of the first two modes, k and p , together with their relative sign, determine unambiguously the length of the third one. Thus, here the scale disparity parameter is a function of only two variables and, following Ref. [90], we define it as

$$S(k, p) = \frac{\max\{|k|, |p|, |k - p|\}}{\min\{|k|, |p|, |k - p|\}}, \quad (4.19)$$

where \max and \min denote, respectively, the maximal and minimal values in the set of three interacting wave numbers. From the structure of $S(k, p)$ it is clear that small values of S correspond to local interactions where all modes in the triad are nearly the same, while large values of S resemble triads with great disproportion between the largest and the smallest mode, i.e., nonlocal interactions. Although the border line is rather ambiguous, we shall follow the turbulence literature and refer to interactions with $S < 20$ as local and vice versa.[91] One should note, however, that the scale disparity parameter alone does not give any information about the structure of the velocity field \hat{u} , since it involves only the interacting wave numbers and not the corresponding field. S merely groups different triads and substitutes the two-dimensional parameter space $\{k, p\}$, on which, in our case, triads ‘live’, with a single positive real number that goes from 1 to infinity.⁷ In order to gain insight into the interactions one has to express physical quantities like the nonlinear transfer as a function of S . Note that the singularity of S corresponds to cases in which one of the interacting modes is zero, i.e., $k = 0, p = 0$ or $k = p$. In those cases, however, the transfer function $T(k, p, t)$ vanishes. We incorporate S into the analysis by defining

$$T(k, S_n) = \sum_{p|2^n \leq S < 2^{n+1}} T(k, p), \quad (4.20)$$

where $T(k, S_n)$ denotes the contribution from nonlinear interactions that correspond to a disparity parameter S in the range $2^n \leq S < 2^{n+1}$ where $n \in \mathbb{N}_0$. As common in classical turbulence, we have divided the disparity range in intervals such that the length of every following interval is two times greater than that of the previous one. In Navier-Stokes turbulence the most important nonlinear interactions in the inertial range are local, i.e., arise from couplings with $S < 20$, meaning that $T(k, S_n)$ attains its maximum for $n < 5$ at a given k . The same observation is made also for the turbulent dynamics produced by the driven Burgers equation both in the inertial and dissipation ranges.[90] Our numerical analysis revealed that this type of behaviour carries over to the original Kuramoto-Sivashinsky equation at large wave numbers⁸ which is a new result and, to the best of our knowledge, has never been reported before. The modified version of the Kuramoto-Sivashinsky equation, however, displays a completely different behaviour. The numerical result for its disparity-filtered transfer function $T(k, S_n)$ is shown in Fig. 4.8 for

⁷The derivation of the result that $S \in [1, \infty)$ is shown in detail in Appendix B.

⁸Note that, as observed in Fig. 4.1, the original Kuramoto-Sivashinsky equation does not have an inertial range. Same applies also for its modified version.

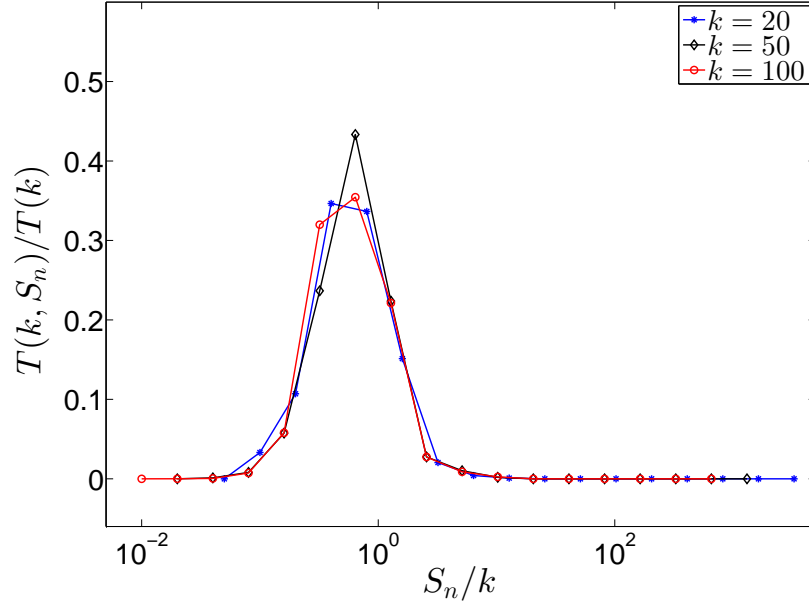


Figure 4.8: Net energy transfer into mode k as a function of the disparity parameter S_n characterising the corresponding three-wave couplings. We have normalised $T(k, S_n)$ over the total transfer $T(k)$ into mode k , while the x -axis is given by the ratio S_n/k in order to further emphasise the structure of $T(k, S_n)$.

three large values of k , where we have normalised it to the total transfer into the mode k . This takes into account the decreasing amplitude of $T(k, S_n)$ when k increases and facilitates comparison between the disparity structures at different wave numbers, since

$$\sum_{n=0}^{\infty} \frac{T(k, S_n)}{T(k)} = 1 \quad (4.21)$$

for all k . As can be seen in Fig. 4.8, the function $T(k, S_n)$ obtains its maximum when $S_n/k \sim 1$ for large k . The three cases presented in the figure are exemplary for the large-wave-number region. Thus, at small scales the greatest contribution derives from triads with large values of the disparity parameter S , i.e., from highly nonlocal interactions. This confirms the physical picture deduced from Fig. 4.7 that at high k energy is transferred by the coupling of two large and similar modes with a very small one that lies in the region of energy injection. This small-wave-number mode controls the interaction and acts as a kind of catalyst.

4.5 Closure approximation and energy spectrum

In this section we shall study further the nonlinear interactions and develop a simple closure valid at small scales in order to close the energy balance equation and solve for the energy

spectrum in the limit $k \rightarrow \infty$. The form of Eq. (4.11) displays a symmetry between the interchange $p \leftrightarrow k - p$. Thus, the main contribution at large k comes from two types of triads: $k \approx p$ and $k - p$ small or $k \approx k - p$ and p small.⁹ Both cases exhibit the same nonlocality, i.e., two very large modes couple via a very small one as discussed before. Here we shall consider only the first case and take account of the contribution of the second one by simply multiplying the result by two. We shall define for convenience $q := p - k$ and express the nonlinear transfer as

$$T(k) = \frac{1}{2}k \sum_q P(k, q), \quad (4.22)$$

where $P(k, q)$ denotes the triple correlation function, i.e., $P(k, q) := \overline{\langle \hat{u}(k, t) \hat{u}(q, t) \hat{u}(k+q) \rangle}_\tau$. In order to find a closure approximation for $P(k, q)$ we shall first study its scaling with k . A numerical computation of the triple correlation is shown in Fig. 4.9 for three different large values of k . We have normalised $P(k, q)$ to the energy $E(k)$ of the mode k . The

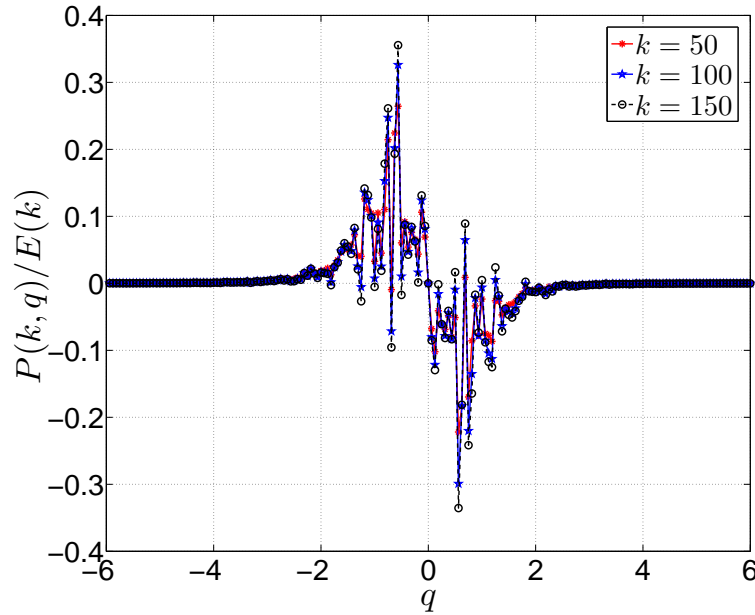


Figure 4.9: Triple correlation $P(k, q) = \overline{\langle \hat{u}(k, t) \hat{u}(q, t) \hat{u}(k+q) \rangle}_\tau$ as a function of q at three different large wave numbers k . The result is normalised over the energy $E(k)$. The three curves display a significant similarity indicating that the functional dependence of $P(k, q)$ on k follows closely that of the energy spectrum.

three curves display not only the same form but also roughly the same magnitude with the only difference being that at small scales the correlation function fluctuates more strongly

⁹In Fig. 4.6 (b) only the contribution of the first case can be seen, since we have normalised over $\sqrt{E(k)E(p)}$. If we would have normalised over $\sqrt{E(k)E(k-p)}$ the result would have been a clockwise rotation of Fig. 4.6 (b) by 45° with reversion of the colours.

suggesting that at such values of k the time period τ over which the time averaging is performed should be increased. This result demonstrates that at large wave numbers the triple correlation scales in the same way as the energy spectrum, meaning that it can be written as

$$P(k, q) \sim E(k)h(q), \quad (4.23)$$

where h is function only of q . The above relation represents an important consequence that gives us a rough form of the triple correlation. Furthermore, since the nonlinear transfer term arises after integration of $P(k, q)$ over q , it is essential to model correctly the small asymmetry between the positive and negative contribution to $P(k, q)$. Recall that this agrees with the decrease of the energy spectrum as k increases. The latter is due to the damping term in Eq. (4.17) which, at large wave numbers, is proportional to $E(k)$ and independent of k . As observed in the previous section, the positions of the maximum and minimum, located at $q = q_{\max}$ and $q = q_{\min}$, respectively, correspond to a coupling to a mode of a small magnitude, denoted hereafter as k_d , in the drive range, i.e., $q_{\max} = -k_d$ and $q_{\min} = k_d$. In order to quantify further the features of the triple correlation function $P(k, q)$ we measure the ratio between the amplitudes of its maximum, $\max(P(k, q)) = P(k, q_{\max})$, and minimum, $|\min(P(k, q))| = |P(k, q_{\min})|$, as a function of k . Investigating the numerical data shows that at large k this ratio scales roughly as the ratio between the energy spectrum at $k - k_d$ and $k + k_d$ which are the positions of the maximum and minimum, respectively, i.e.,

$$\frac{P(k, q = -k_d)}{|\min(P(k, q = k_d))|} \approx \frac{E(k - k_d)}{E(k + k_d)}. \quad (4.24)$$

The above relation suggests that one can model the triple correlation as

$$f_P(k, q) = -qE(k - k_d)\psi_{-\xi}(q) - qE(k + k_d)\psi_{\xi}(q), \quad (4.25)$$

where $f_P(k, q)$ is a continuous function of k and q which approximates $P(k, q)$. $\psi_{-\xi}(q)$ is a very localised non-negative function that is centred at and symmetric around $q = \xi$. The later depends on k_d and is of the same order, i.e., $\xi \sim k_d$. Thus, we model $P(k, q)$ by approximating it by the sum of two localised functions, one at $q < 0$ and the other one at $q > 0$. If they decay fast enough, their mutual influence will be negligible. The model in Eq. (4.25) does not incorporate the fluctuations observed in Fig. 4.9. However, this is not necessary, since they are not independent but the variations of the positive part of the q -axis follow exactly those of the negative q -axis. The different prefactors contain the energy spectrum at the corresponding maxima giving a different weight to the localised functions and insuring the small asymmetry around $q = 0$. The factor q guarantees that $f_P(k, 0) = 0$ for all k which takes into account the analytical constraint that $T(k, p) = 0$ when $k = p$. Although Eq. (4.25) is not strictly proportional to $E(k)$, it, nevertheless, agrees with Eq. (4.23), since we consider it at $k \gg k_d$, i.e., $k \pm k_d \approx k$. Thus, $f_P(k, q)$ scales with k in roughly the same way as demanded by Eq. (4.23). Since $f_P(k, q)$ is a continuous function, one has to exchange the summation over q in Eq. (4.22)

with integration which is justified when the distance between adjacent modes in spectral space is small enough, i.e., $\Delta k \ll 1$. Hence, one can write that

$$\sum_q P(k, q) \approx \frac{1}{\Delta k} \int_{-\infty}^{\infty} f_P(k, q) dq = -\frac{\Phi(\xi)}{\Delta k} (E(k + k_d) - E(k - k_d)), \quad (4.26)$$

where $\Phi(\xi)$ denotes the integral over $q\psi_\xi(q)$. Taking into account that the function $\psi_\xi(q)$ is per construction symmetric around $q = \xi$, we have that the area enclosed by it is

$$\Phi(\xi) := \int_{-\infty}^{\infty} q\psi_\xi(q) dq = - \int_{-\infty}^{\infty} q\psi_{-\xi}(q) dq = -\Phi(-\xi), \quad (4.27)$$

which leads to Eq. (4.26). Further, using that $k_d \ll k$, we can approximate the difference between the value of the energy spectrum at the slightly different positions as

$$E(k - k_d) - E(k + k_d) = 2k_d \left(\frac{E(k - k_d) - E(k + k_d)}{2k_d} \right) \approx 2k_d \frac{dE(k)}{dk}, \quad (4.28)$$

which relates the integral over $f_P(k, q)$ to the first derivative of the energy spectrum. Combined, the above results provide an approximation for the transfer $T(k)$ in terms of the wave number k , the energy spectrum $E(k)$ or functions of it. Thus, we have arrived at a closure for the energy balance equation. Substituting the above relations in Eq. (4.17), we arrive at

$$-\frac{1}{\lambda} k \frac{dE}{dk} + 2 \frac{k^2 - \nu k^4}{1 + bk^4} E(k) = 0, \quad (4.29)$$

where λ is positive and defined as

$$\lambda := \frac{\Delta k}{2k_d \Phi(\xi)}. \quad (4.30)$$

The above definition deviates by a factor of two from the one derived solely on the basis of Eqs. (4.28) and (4.26). This is due to the fact that, as explained in the beginning of this section, at large k the transfer function $T(k)$ arises from two main contributions of $T(k, p)$ - the first one around $p \approx k$ and the second one around $k - p \approx k$. They are both identical and our model for $P(k, q)$ takes into account only the first one. Since the two contributions are the same, one should multiply the result in Eq. (4.26) by two. The factor λ is constant with respect to k and has the physical units of time. Hence, at large k the ratio $1/\lambda$ can be interpreted as the characteristic frequency of the energy transfer into the mode k . Its analogue in the theory of classical Navier-Stokes turbulence would be the eddy-turn over time in the inertial range. Eq. (4.29) represents a closed first-order ordinary differential equation for the energy spectrum $E(k)$. It can be readily solved and yields

$$E(k) = \tilde{E}_0 \exp\left(\frac{\lambda}{\sqrt{b}} \arctan(\sqrt{b}k^2) - \frac{\lambda\nu}{2b} \ln(1 + bk^4)\right), \quad (4.31)$$

where \tilde{E}_0 is a constant of integration. Taking into account that for a positive argument x

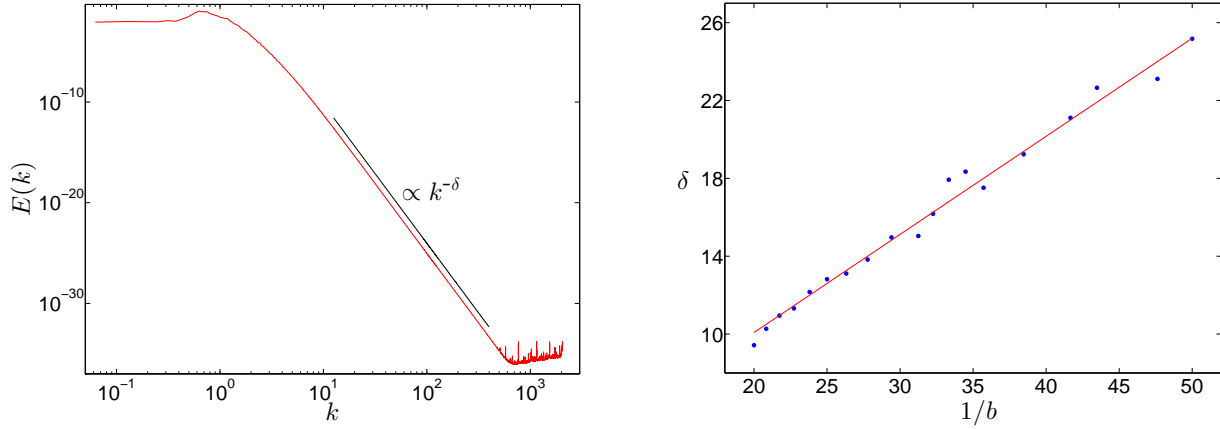
$$\arctan\left(\frac{1}{x}\right) = \frac{\pi}{2} - \arctan(x) \quad (4.32)$$

and that $\arctan(x) \rightarrow 0$ when $x \rightarrow 0$, we see that the first term in the exponent in Eq. (4.31) is bounded from above by $\pi/2$. The second term, however, increases monotonically without bound when its argument increases. Thus, in the limit of large wave numbers the dominant contribution in the exponent in the solution given by Eq. (4.31) comes from the logarithmic term. Accordingly, for large k one can write that

$$E(k) = E_0 k^{-2\lambda\nu/b}, \quad (4.33)$$

where E_0 is a constant that can depend on b . One can also arrive directly at this simplified form by approximating the second term in Eq. (4.29) as $-2\nu/bE(k)$ which is justified at large k . The first conclusion from the expression in Eq. (4.33) is that at large k the energy spectrum of the modified Kuramoto-Sivashinsky equation behaves fundamentally different from that of its original version. While in the latter case $E(k)$ decays exponentially in the limit $k \rightarrow \infty$, the modified version displays an energy spectrum of the form of a power-law. The correctness of this result derived from our closure approximation can be investigated numerically. Such a numerical computation of Eq. (4.9) is displayed in Fig. 4.10 (a) where the new damping parameter equals $b = 0.03$. While the form of the energy spectrum at small wave numbers is practically the same as for the original Kuramoto-Sivashinsky equation, the large- k region demonstrates a fundamental difference. For large wave numbers the numerical computation of $E(k)$ reveals indeed a power-law form as predicted by Eq. (4.33).¹⁰ The same form we observed consistently, regardless of the value of b . The range in spectral space where the spectrum exhibits a power-law form, however, depends on the particular values of the damping parameters ν and b . A straight line in the double-logarithmic representation of $E(k)$ is observed only when k is large enough such that the damping frequency of the modified term becomes nearly constant as shown in Fig. 4.2 (a). The result in Eq. (4.33) combined with Eq. (4.17) gives a greater insight into the dynamics of the system than merely the asymptotic form the the energy spectrum. The linear term in the energy balance equation in Fourier space reduces to $-2\nu/bE(k)$ at large wave numbers. The prefactor ν/b has the physical units of frequency. In analogy to the classical theory of turbulence it can be considered as the characteristic damping frequency at the scale $\sim 1/k$. Thus, the physical interpretation of the modification we introduced is that we changed fundamentally the damping time scales. While in the original Kuramoto-Sivashinsky equation the dissipation processes have a characteristic frequency that grows with wave number as νk^4 , in its modified version the dissipation mechanism exhibits a constant time scale given by $b/(2\nu) =: \omega_L$. On the

¹⁰Note that in the double logarithmic representation used in the figure, a power law corresponds to a straight line. In Fig. 4.5, however, only the vertical axis is logarithmic, while the scaling of the horizontal axis is linear. Thus, there a straight line represents an exponential fall-off.



(a) Double-logarithmic representation of the energy spectrum $E(k)$, red line. The result is obtained with $b = 0.03$. The black line corresponds to the closest power law.

(b) Slope of the energy spectrum (computed by a power-law fit to the large- k part of $E(k)$) as a function of $1/b$. We see a clear linear dependence as predicted by Eq. (4.33).

Figure 4.10: Numerical verification of the power-law features of the energy spectrum as given in Eq. (4.33).

other hand, λ gives us the time scale of the nonlinear interactions in analogy to the eddy-turn-over time in classical turbulence theory, although in one-dimensional systems the mechanisms for nonlinear energy transfer are fundamentally different compared to those in the Navier-Stokes model. As evident from Eq. (4.30) the characteristic nonlinear frequency $\omega_{NL} := 1/\lambda$ does not depend on the particular spatial scale under consideration as soon as k is large enough. Moreover, it is a function of k_d , both directly and through $\Phi(\xi)$, which represents a mode in the energy-injection range and can be associated with the modest unstable wave number. The latter is set by the system parameters and does not vary with k . Thus, the modified version of the Kuramoto-Sivashinsky equation displays the important property that the ratio ω_{NL}/ω_L between the characteristic nonlinear and linear frequencies is scale-independent at high k . Through the modification of the linear terms we create a spectral range in which $\omega_{NL}/\omega_L = \text{const}$ and in this range the energy spectrum develops a power-law form. Furthermore, the steepness of this power-law is not universal, but depends on different the system parameters, both linear and nonlinear. In addition, the slope of this power law is directly controlled by the frequency ratio, i.e., one can rewrite Eq. (4.33) as $E(k) = E_0 k^{\omega_L/\omega_{NL}}$. A numerical verification of this feature is shown in Fig. 4.10 (b). We have performed simulations with different values of b and the value of the spectral slope has been computed by fitting a power-law to its high- k end. The results obtained in this way are presented by blue dots. The quantity δ denotes the absolute value of the exponent in Eq. (4.33) and is given by $\delta = 2\lambda\nu/b$. Evidently, our closure approximation predicts a slope δ which depends linearly on $1/b$ with no free term. A fit of such form (the red line) is also shown in Fig. 4.10 (b) together with the numerical data. We see a good agreement between the numerical results and our closure

approximation for a considerable range of values for $1/b$. The upper and lower limits along the $1/b$ -axis are set by the numerical constraints. If the parameter b is too small, then the damping frequency reaches its plateau regime at high k and large damping rates, meaning that also the $E(k)$ will exhibit a power-law form when the values of the mode energy are already close to the machine precision making a reliable fit in that range very difficult. On the other hand, a too large value for b implies a small damping rate and a slow decay of the energy spectrum. Thus, one needs a much larger number of Fourier modes in order to avoid numerical bottleneck effects meaning that numerical simulations will become too computationally expensive and impractical.

4.6 Conclusion

In the present chapter we considered a modified form of the one-dimensional Kuramoto-Sivashinsky equation. The latter presents one of the simplest examples of a continuous system displaying spatio-temporal chaos where energy injection is due to internal instabilities. The modification we made to the equation of motion was motivated by the analysis of turbulence in magnetised plasmas and retains the chaotic nature of the solution. It does not influence the large-scale instabilities driving the system but modifies fundamentally the structure of the damping terms at small scales. As a consequence, the characteristic damping frequency becomes scale-invariant in analogy to the solution provided by the dispersion relation for magnetised plasmas. Our numerical investigations revealed that at large wave numbers non-local interactions dominate the energy transfer. Thus, the triads realising the nonlinear coupling consist of two modes of very large magnitude while the third one is much smaller and located in the energy injection range. This finding differs fundamentally from the case involving the original version of the Kuramoto-Sivashinsky equation. Based on this results and examining the scaling properties of the triple correlation function, we constructed a closure scheme applicable at small scales. With the aid of it we were able to close the spectral energy balance equation and derive a first-order ordinary differential equation which determines the form of the energy spectrum at large wave numbers. The solution of this equation yields a power-law form that was verified numerically. Additionally, it displays the novel feature that, in contrast to the classical theory of Navier-Stokes turbulence, the slope of this power law is not universal but depends strongly on system parameters. As a further verification of our closure model we investigated the dependence of the slope on the linear damping. The numerical data agree well with our predictions strengthening further the conclusions from our analysis.

As already discussed in Chapter 1 and Chapter 2 the case of a power-law spectrum with a non-universal exponent is not merely a peculiar special case but arises in various physical systems where there is no true inertial range present and both driving and dissipation mechanisms are active at multiple scales. Such a case present, in particular, magnetised laboratory plasmas.[92] An additional example provides kinetic Alfvén-wave turbulence which is theorised to occur in the solar wind. There the characteristic frequency of the

nonlinear transfer scales as $k_{\perp}^{4/3}$ at spatial scales smaller than the ion gyroradius. The linear frequency in this case will be given by the Landau damping rates of kinetic Alfvén waves which arise as solutions of the corresponding linear dispersion relation analogous to the drift-kinetic case as discussed in Chapter 3. In general, the Landau damping rates may exhibit a rather complex dependence on the scale k_{\perp} controlled by the ion-to-electron temperature ratio or the ratio between magnetic and thermal pressure.[93] For some parameter regimes and in some k_{\perp} -ranges the ratio between linear and nonlinear frequencies seems to be roughly scale-independent which might induce energy spectra of nonuniversal power-law form.

Chapter 5

Turbulence in living fluids

As already discussed in the introduction of this work, turbulence represents a fundamental and ubiquitous phenomenon in Nature that manifest itself in a wide range of systems: from biophysics, via atmospheric dynamics to astrophysics. Traditionally, turbulence is considered in the framework of the Navier-Stokes equations which provides a practical simplification of the problem capturing the essence of the turbulent behaviour without any additional complications. Nevertheless, realistic situations often involve systems which deviate considerably from the simple passive fluids considered by the Navier-Stokes model. Thus, one of the goals of present-day turbulence research is to incorporate systems exhibiting internal drive and/or dissipation on multiple, often overlapping, spatial scales. This includes various types of complex fluids, plasmas, as well as active systems. An interesting example for the last type comes from the field of biophysics where dense bacterial suspensions can produce a so-called 'low-Reynolds-number turbulence'. The latter has been recently observed experimentally and a continuum model has been put forward in order to quantitatively describe the observations.[94, 95, 96] The model incorporates the Navier-Stokes equations as a special case while including additional terms of the most general form that is admitted by the symmetry of the problem. This includes, in particular, Swift-Hohenberg terms which provide linear drive/dissipation mechanisms and a nonlinearity of the Toner-Tu type as in the theory of flocking behaviour which models the tendency of bacteria to align parallel to each other. In this chapter we present the first systematic study of the turbulence generated by this model. Our analytical and numerical analysis reveals a power law form of the energy spectrum at small wave numbers. However, the value of the slope is different from the one reported in Ref. [94]. Furthermore, it also depends on the size of the simulation domain in a way that leads to convergence of the slope when the real-space domain is arbitrarily large. This converged value, however, depends continuously on system parameters, including the ones controlling the linear terms.

The classical theory of two- and three-dimensional turbulence as presented in Chapter 2 has had some considerable successes providing important physical insights into the spatial structure of turbulent velocity fields. One of its basic achievements represents the

prediction for the basic form¹ of the turbulent energy spectrum and velocity correlations of higher order, in general. This, however, applies only in the framework of the Navier-Stokes equations in the limit of an infinitely large Reynolds number and is based on the assumption of scale separation as discussed in Sec. 2.2 and displayed in Fig. 2.3 (a). In spite of its pedagogical value, the assumption of scale separation is highly unrealistic and there exist many turbulent systems of practical interest where the scales of energy injection and dissipation are rather extended and may even overlap. An example of such a system, which the remainder of this chapter is devoted to, present dense bacterial suspensions. Under certain conditions they exhibit a spatio-temporal chaos with a large number of degrees of freedom which adheres to our definition of turbulence. A novel characteristic of such bacterial suspensions is that the turbulent behaviour is manifested already at small Reynolds numbers. Such a feature challenges the orthodox theory of turbulence and requires a detailed theoretical analysis. The Navier-Stokes model yields a power-law form for the energy spectrum in the spectral range where both energy injection and dissipation are negligible. As discussed in Section 2.4, this result has established the view that an energy spectrum of such type is inseparably intertwined with the dominating role of the nonlinear transfer and the negligibility of linear effects. Thus, the conception prevails that, if turbulent motion produces spectral power laws, their slope should be universal with respect to parameters of the system. Nevertheless, many turbulent models exhibit power laws in their energy spectrum on spatial scales where the effect of linear terms, both injective and dissipative, is comparable with that of the nonlinearity. As we shown in the the previous chapter and in a previous publication of the author of this thesis [85], an appropriately modified version of the Kuramoto-Sivashinsky equation also belongs to the group of such models. Furthermore, not only that a power law exists on dissipation dominated scales but its slope depends on a linear parameter.

The present chapter is devoted to the analytical and numerical study of a continuum model proposed in Refs. [94, 95, 96] to qualitatively explain the collective dynamics of dense bacterial suspensions. As explained in more detail in Ref. [94], the bacterial motion in a thin two dimensional layer can exhibit many qualitatively different phases. For large concentrations and certain ranges in parameter space, one observes a highly disordered state of the bacterial motion characterised by spatio-temporal chaos. Since it also possesses a large number of degrees of freedom, we shall refer to it as turbulence. The model involves a coarse-grained version of the bacterial flow that is described as fluid by a continuous velocity field $\mathbf{v}(\mathbf{x}, t)$ that obeys an equation of motion given by

$$\frac{\partial \mathbf{v}}{\partial t} + \lambda_0(\mathbf{v} \cdot \nabla)\mathbf{v} = -\frac{1}{\rho}\nabla p - (\alpha + \beta|\mathbf{v}|^2)\mathbf{v} - \Gamma_0\Delta\mathbf{v} - \Gamma_2\Delta^2\mathbf{v}, \quad (5.1)$$

where ρ and p denote the density and pressure of the fluid, respectively. λ_0 , α , Γ_0 and Γ_2 are physical parameters, constant in space and time, which are determined by the particular bacterial type and the experimental setting. Eq. (5.1) is supplemented by the

¹We neglect here the corrections of the slope due to intermittency, the theoretical computation of which presents still an open problem.

incompressibility condition $\nabla \cdot \mathbf{v} = 0$, which provides a good approximation for dense bacterial suspensions. Similarly to the Navier-Stokes model, the equation of motion includes an advective nonlinearity, $(\mathbf{v} \cdot \nabla)\mathbf{v}$, and a pressure term, ∇p . From a mathematical point of view, the latter plays the role of a Lagrange multiplier necessary for satisfying the incompressibility constraint. There are, however, also additional terms both linear and nonlinear that will be analysed in detail later. At this point we shall only note that they provide intrinsic drive mechanisms as well as means for energy dissipation. Disregarding the pressure term and setting α and β to zero, Eq. (5.1) provides a straightforward (incompressible) multi-dimensional generalisation of the Kuramoto-Sivashinsky equation, the one-dimensional version of which we reviewed in the beginning of the previous chapter. Note that the equation given in Ref. [94] contains the additional term $\lambda_1 \nabla |\mathbf{v}|^2$ on the right-hand side. Since it represents merely the gradient of a scalar function, it can be absorbed by the pressure term without any effect on the dynamics of $\mathbf{v}(\mathbf{x}, t)$. Additionally, our definition of Γ_0 is such that positive values correspond to linear instabilities. For normalising Eq. (5.1) appropriately, we need only to specify a velocity and a length scale, v_0 and ℓ respectively. This will naturally induce a time scale for the system dynamics given by $\tau = \ell/v_0$. For setting the velocity scale we can use the parameters Γ_0 and Γ_2 that control the isotropic part of the linear energy injection and dissipation. Their physical units imply a velocity of $v_0 = \sqrt{\Gamma_0^3/\Gamma_2}$. An intrinsic length scale of the system is determined by considering the spectral form of the linear terms, discussed in detail in Section 5.1, which sets the growth rate of each Fourier mode. The linear dispersion relation attains its maximum at $k_{\max} = \sqrt{\Gamma_0/(2\Gamma_2)}$ indicating that the instability is most prominent at the spatial scale of π/k_{\max} . Resolving the physical processes properly requires that the size of the simulation domain is much larger than π/k_{\max} . Thus, it is convenient to define as a normalisation length scale $\ell = 5\pi/k_{\max} = 5\pi\sqrt{2\Gamma_2/\Gamma_0}$. Accordingly, the dimensional physical quantities and operators are mapped to their dimensionless counterparts as

$$v \rightarrow v/v_0 ; t \rightarrow t/\tau ; p \rightarrow \frac{p}{v_0^2 \rho} ; \alpha \rightarrow \alpha/\tau ; \quad (5.2)$$

$$\beta \rightarrow \frac{\beta}{\ell v_0} ; \Gamma_0 \rightarrow \Gamma_0 \ell v_0 ; \Gamma_2 \rightarrow \Gamma_2 \ell^3 v_0 \text{ and } \nabla \rightarrow \frac{1}{\ell} \nabla. \quad (5.3)$$

As a consequence of the definition of v_0 and ℓ , the values of the parameters Γ_0 and Γ_2 are set automatically to $\Gamma_0 = 1/(5\sqrt{2}\pi) \approx 0.045$ and $\Gamma_2 = \Gamma_0^3 \approx 9 \cdot 10^{-5}$. The normalisation units chosen here are nearly the same as those used in Ref. [94] which will facilitate comparison. Unless otherwise stated, all the numerical results presented in this work were performed with a value for the non-dimensional form of the parameter β set to $\beta = 0.5$. The normalised equation is almost identical to the original one with the only difference being that the density is also incorporated into the pressure, i.e.,

$$\frac{\partial \mathbf{v}}{\partial t} + \lambda_0 (\mathbf{v} \cdot \nabla) \mathbf{v} + \nabla p = -(\alpha + \beta |\mathbf{v}|^2) \mathbf{v} - \Gamma_0 \Delta \mathbf{v} - \Gamma_2 \Delta^2 \mathbf{v}. \quad (5.4)$$

A numerical solution of the above equation is shown in Fig. 5.1. We have visualised the structures in the dynamics by displaying the vorticity field instead of the velocity. The

relation between the two quantities was given already in Section 2.3. This represents a common choice for displaying dynamics of two-dimensional continuous systems since in such a setting the vorticity is merely a (pseudo) scalar quantity and not a vector field as the velocity. Analogously to the Kuramoto-Sivashinsky equation, for positive Eq. (5.4) parameters

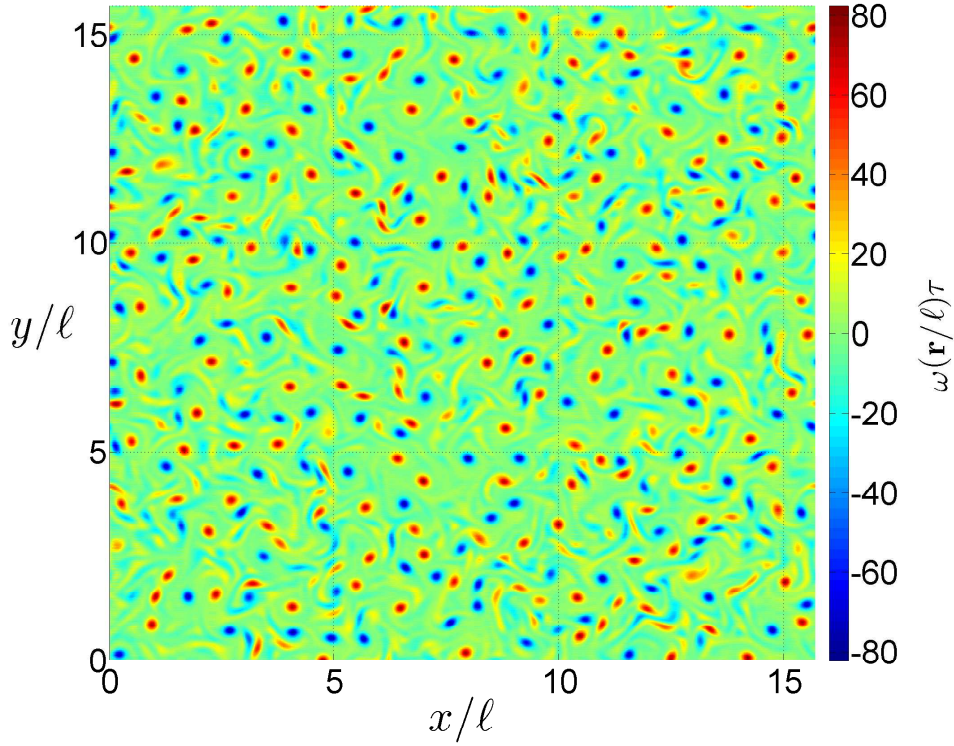


Figure 5.1: A snapshot of the vorticity distribution as produced by a numerical simulation of Eq. (5.4). The apparent disorder in the vorticity distribution supports our referring of the dynamics as turbulent. The same chaotic behaviour can be observed also in time.

Γ_0 and Γ_2 possesses a band of linearly unstable modes at low wave numbers. Thus, the system is unstable with respect to large-scale fluctuations. On the other hand, modes corresponding to large wave numbers, i.e., small-scale fluctuations, are linearly damped. We shall refer to the terms controlled by the parameters Γ_0 and Γ_2 as Swift-Hohenberg terms, since they were first introduced in models of nonlinear dynamics constructed by Swift and Hohenberg.[97] In the case of active systems, as the bacterial suspensions discussed in this chapter, they model energy injection by means of stress-induced instabilities.[98] In contrast to the Kuramoto-Sivashinsky case, in a two-dimensional system the $\Delta^2 \mathbf{v}$ -term is a very ineffective energy sink due to the mostly inverse flow of kinetic energy. Thus, a statistically stationary state is reached mostly by means of nonlinear energy dissipation via the cubic nonlinearity $|\mathbf{v}|^2 \mathbf{v}$. The first two terms on the right-hand side of Eq. (5.4) were originally introduced by Toner and Tu in order to model flocking behaviour in groups of variety of living organisms, e.g., schools of fish or herds.[99, 100] Thus, the dynamics of the

system arise from the interplay between the mechanism of energy injection, redistribution and dissipation. As we shall see later, the second effect is mostly due to the Navier-Stokes nonlinearity which couples different spatial scales. Hence, Eq. (5.4) incorporates all essential features of meso-scale turbulence which constitute the basic ingredients of more complex hydrodynamic models of active matter.[101] The fact that the above continuum model comprises the most important aspects of active turbulence and in the same time is rather minimal and computationally feasible makes it a useful test bed for studying active systems. In particular, one can address the universality of low-Reynolds-number meso-scale turbulence and establish important similarities and differences with respect to classical turbulence at large Reynolds numbers. Additionally, there are still many open questions regarding the basic features of the energy flow between scales.

5.1 Fourier representation

Similarly as with the Navier-Stokes equations, Eq. (5.4) is mathematically too complex to be solved analytically, neither exactly nor in any reasonable approximation that preserves the turbulent character of the fluid motion we want to study. Hence, we solve Eq.(5.4) numerically by using the pseudo-spectral approach discussed in Sec. 2.2. In analogy to the modified Kuramoto-Sivashinsky equation, the time evolution has been obtained by means of the exponential time differencing scheme first developed in Ref. [87] and later improved in Ref. [88]. The incompressibility condition has been accounted for by the form of the tensor $D_{ij}(\mathbf{k})$ given in Sec. 2.2. We solve the equation on the domain $\Omega = [0, L_x] \times [0, L_y]$ with $L_x = L_y = L$ and supplement it by periodic boundary conditions which, in most of the cases, present a requirement for the use of the pseudo-spectral method. The particular choice of an initial condition does not play any role, as long as it involves few long-wavelength modes. The intrinsic instabilities and nonlinear interactions establish fairly quickly a quasi-stationary state that is independent of the specific form of the initial velocity field. Note, additionally, that the 3/2-rule used in Navier-Stokes simulations for removing aliasing errors is insufficient here. The reason for this derives from the cubic nonlinearity involved in Eq. (5.4) which demands that the maximal wave number present in the numerical simulation is 2 times larger than the largest physically relevant mode, instead of merely 1.5 times as in the case of a quadratic nonlinearity. Since the supplementary modes are on the outer side of the spectral domain, for a two-dimensional problem a factor of 2 more wave numbers in each direction adds four times more modes that need to be calculated at each time step. Thus, a numerical solution of Eq. (5.4) in two spatial dimensions requires nearly a 85% greater computational effort than solving the two-dimensional Navier-Stokes equations.

We decompose the velocity field in Fourier series as

$$\mathbf{v}(\mathbf{r}, t) = \sum_{\mathbf{k}} \hat{\mathbf{v}}(\mathbf{k}, t) e^{i\mathbf{k} \cdot \mathbf{r}}, \quad (5.5)$$

where the variable conjugate to the real-space position \mathbf{r} is the wave-number vector $\mathbf{k} = (k_x, k_y)$. Due to the periodic boundary conditions and the finite size of the simulation domain, its components can attain only discrete values which are related to the system size in each direction by $k_{x,y} = n_{x,y}2\pi/L_{x,y}$ with $n_x, n_y \in \mathbb{N}_0$ and independent of each other. In accordance with the above definition, the Fourier coefficients are computed as

$$\hat{\mathbf{v}}(\mathbf{k}, t) = \frac{1}{L_x L_y} \int_0^{L_y} \int_0^{L_x} \mathbf{v}(\mathbf{r}, t) e^{-i\mathbf{k} \cdot \mathbf{r}} dx dy. \quad (5.6)$$

Correspondingly, the wave vector \mathbf{k} is normalised over k_ℓ defined as the inverse of the characteristic length scale, i.e., $k_\ell = 1/\ell$. In analogy to Navier-Stokes turbulence the energy of the mode \mathbf{k} shall be defined as

$$E(\mathbf{k}) := \frac{1}{2} \langle |\hat{\mathbf{v}}(\mathbf{k}, t)|^2 \rangle, \quad (5.7)$$

where the brackets $\langle \cdot \rangle$ denote an appropriate ensemble average. In the statistically stationary state and under the assumption of ergodicity one can substitute it by a time average over a large time period. Strictly speaking, $E(\mathbf{k})$ does not have the unit of energy, but for fluids of constant density it is proportional to the mode energy and it is convenient to refer to it in this way.

The one-dimensional energy spectrum obtained by solving Eq. (5.4) numerically is displayed in Fig. 5.2 for different sizes of the simulation domain. The box size and number of points representing the real-space domain that correspond to the red curve are nearly the same as those used in Ref. [94]. It is evident that the minimal wave number (set by the size L) is comparatively large and close to the peak of the spectrum. Hence, there are only very few points on the left from the peak and they are highly insufficient to accurately identify a power law much less the correct value of its slope. The upper black line in Fig. 5.2 corresponds to a slope of $5/3$, i.e., $E(k) \propto k^{5/3}$, as reported in Ref. [94]. Our simulations do not reproduce this slope. Note that we have plotted the one-dimensional energy spectrum. The latter is calculated from its original two-dimensional form, i.e., $E(\mathbf{k}) = E(k_x, k_y)$, by grouping together modes with similar $|\mathbf{k}|$. Namely, we construct circular bands around the origin $\mathbf{k} = 0$, sum the energy of all the modes in the particular band and assign to it the corresponding wave number k . However, there are different ways to choose the wave number representing the specific band which are all equally justifiable. At large k the small variations of the value of the wave number introduced by this ambiguity are negligible but for small k their effect can be quite noticeable. Thus, if the power law at large scales extends only over few points, its slope can be very sensitive to such numerical details. The use of a larger simulation domain allows for a smaller k_{\min} while in the same time leaving physical features as position of the peak of the energy spectrum virtually invariant. As we see by the blue line in Fig. 5.2, this allows for a much clearer power law encompassing more than one order of magnitude along the k -axis. Additionally, it extends over many points and its slope can be determined with essentially no ambiguity. However, making solely the

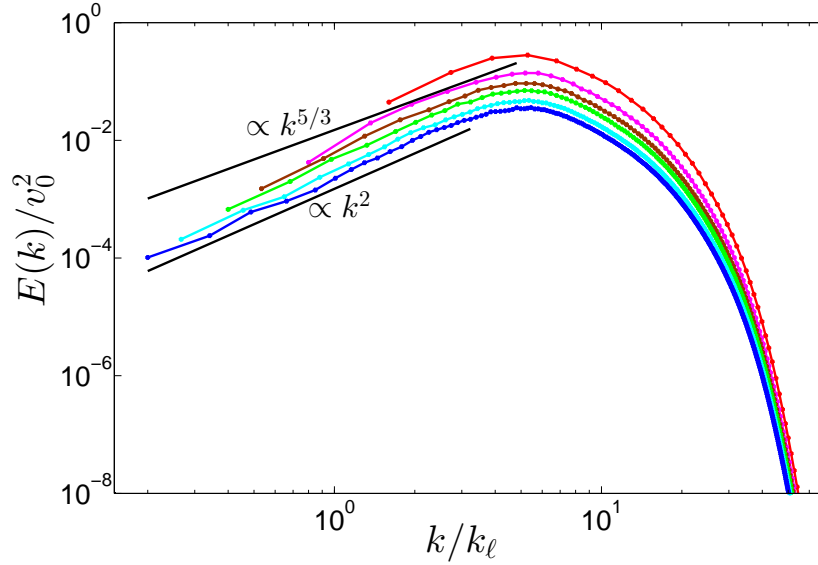


Figure 5.2: Energy spectrum for different sizes of the simulation domain: red - $L = 1.25\pi\ell$; magenta - $L = 2.5\pi\ell$; brown - $L = 3.75\pi\ell$; green - $L = 5.0\pi\ell$; cyan - $L = 7.5\pi\ell$ and blue - $L = 10.0\pi\ell$. All simulations were performed with the same real-space resolution (point density). For obtaining a clear power law form for the energy spectrum at small k the size of the simulation domain needs to be relatively large.

box size larger results in a worse spatial resolution. Thus, for all the curves in Fig. 5.2 the number of points in each direction was increased in the same way as L which kept the resolution constant. By means of extensive computer simulation we found that for small L the slope of the power law was sensitive to the size of the simulation domain. When the latter is large enough the slope converges to a certain value and does no longer depend on such a numerical parameter. The converged value, however, is not universal, but depends on various physical system parameters as we shall see later in this chapter. In order to eliminate such numerical artifacts, all the numerical results reported in this work were obtained with a box size of $L = 10.0\pi\ell$ and an effective resolution of $N_x \times N_y = 1024 \times 1024$. The latter implies the computation of 2048×2048 Fourier modes including dealiasing. Most the results presented in this chapter are new and will be published in a condensed form in a future publication.[102]

Before we try to understand why the energy spectrum looks the way it does at large scales, it is necessary to gain a deeper insight into the dynamics of the system. For this purpose we shall analyse the different terms in Eq. (5.4) in Fourier space. In analogy to the mathematical steps we conducted with the Navier-Stokes equations in Section 2.2 and the Kuramoto-Sivashinsky equation in Chapter 4, we derive for the spectral energy balance

resulting from Eq. (5.4)

$$\begin{aligned} \frac{\partial E(\mathbf{k})}{\partial t} = & -2\alpha E(\mathbf{k}) - \beta \Re \left(\sum_{i,j,l} \sum_{\mathbf{p},\mathbf{q}} D_{ij}(\mathbf{k}) \langle \hat{v}_i(-\mathbf{k}) \hat{v}_l(\mathbf{k} - \mathbf{p} - \mathbf{q}) \hat{v}_l(\mathbf{q}) \hat{v}_j(\mathbf{p}) \rangle \right) + \\ & + \lambda_0 \Re \left(\sum_{i,j,l} \sum_{\mathbf{p}} M_{ijl}(\mathbf{k}) \langle \hat{v}_i(-\mathbf{k}) \hat{v}_l(\mathbf{k} - \mathbf{p}) \hat{v}_j(\mathbf{p}) \rangle \right) + 2\Gamma_0 k^2 E(\mathbf{k}) - 2\Gamma_2 k^4 E(\mathbf{k}), \quad (5.8) \end{aligned}$$

where we have suppressed the time argument for simplicity and the tensors $D_{ij}(\mathbf{k})$ and $M_{ijl}(\mathbf{k})$ have the form defined in Eq. (2.12). In the statistically stationary state the ensemble average can be substituted with a time average and the time derivative on the left-hand side gives zero. Thus, in this case the terms on the right-hand side have to balance each other out. Looking at Eq. (5.8), it is straightforward to determine the effect of the linear terms proportional to $E(\mathbf{k})$. The first term can both inject or dissipate energy into the system in dependence on the sign of α . For $\alpha > 0$, large-scale friction drains energy from the fluid, while in the case of $\alpha < 0$, on the other hand, we have the opposite effect - energy injection with a rate proportional to the mode energy. Since we defined the constants Γ_0 and Γ_2 to be both positive, the corresponding terms behave in the same way as in the case of the Kuramoto-Sivashinsky equation. The Γ_0 -contribution excites long-wavelength fluctuations, i.e., large-scale structures, and, in analogy to the viscosity term in the Navier-Stokes equations, it tends to restore isotropy and homogeneity in the system. This plays an important role here, since an energy injecting α -term will tend to align all the bacteria in one direction and, thereby, create a global ordered state with strong anisotropy. Most of the considerations we have made so far and the analysis performed in the reminder of this chapter depend essentially on the assumption of homogeneous and isotropic turbulence. For them to be correct, the effect of the Γ_0 -term has to dominate over that of the anisotropic energy-injection mechanism. The last linear term is proportional to Γ_2 and also has a counterpart in the Kuramoto-Sivashinsky equation. It dissipates energy from the system and its effect is most prominent on smaller scales. The Γ_2 -contribution resembles the hyperdiffusion term that is often included in the Navier-Stokes equations for numerical reasons to substitute real viscosity effects. The effect of nonlinear terms in Eq. (5.8) cannot be easily predicted based only on their structure in Fourier space. For the Navier-Stokes nonlinearity, i.e., the λ_0 -term, we can use the intuition based on the study of the two-dimensional version of the Navier-Stokes equations. Due to the two-dimensional setting of the bacterial suspensions we consider, the constraint of enstrophy conservation in the inviscid limit (here $\alpha = 0$, $\beta = 0$, $\Gamma_0 = 0$ and $\Gamma_2 = 0$) still holds. Thus, one can expect a form of an inverse energy cascade as predicted by F rtoft and Kraichnan. Eq. (5.8) displays an important feature of the β -term. While the Navier-Stokes term couples modes in triads such that they form a triangle in spectral space, a cubic nonlinearity induces a four-mode interaction in the energy balance equation. The condition posed on the interacting Fourier modes demands that their wave vectors sum up to zero, i.e., they form a tetragon in spectral space. For a quantitative analysis one needs to approach the nonlinear terms in Eq. (5.8) numerically. The result from such a numerical

simulation for a particular parameter set is shown in Fig. 5.3. Instead of performing an ensemble average, which is computationally very cumbersome, we have obtained the time average of the terms in a statistically stationary state. As a result, the time derivative of $E(\mathbf{k})$ on the left-hand side averages out as can be seen by the solid black line in the figure. A positive value of a curve means that the corresponding term injects energy into

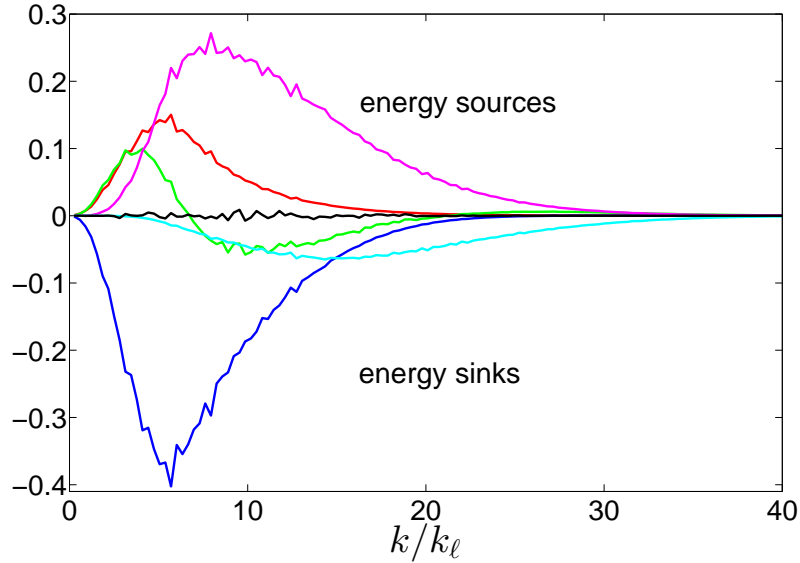


Figure 5.3: Time average of the different terms in Eq. (5.8) ($\alpha = -1$) after a statistically stationary state has been reached. The colour coding is: red - Ekman term, green - Navier-Stokes nonlinearity, dark blue - cubic interaction, magenta - k^2 -injection, light blue - k^4 -dissipation, black - right-hand side. A positive contribution corresponds to energy injection and a negative one - to energy dissipation.

the system at those wave numbers, while a negative value denotes energy dissipation. As predicted by their analytic forms, in this case ($\alpha = -1$) both the α - and Γ_0 -terms (red and magenta lines, respectively) act as energy sources, while the k^4 -term (light blue) is negative over the entire spectral range. On the other hand, the Navier-Stokes nonlinearity (green) exhibits a different behaviour depending on the spatial scale under consideration. It takes energy from the relatively large wave numbers and transfers it mainly² to larger scales. Thus, there is indeed an inverse flow of energy from large to small wave numbers as expected based on the two-dimensional setting. Strictly speaking, one cannot talk about a cascade as in the Navier-Stokes model at large Reynolds numbers. A cascade implies a constant energy flux due to nonlinear interactions. As a consequence, the nonlinear term in the balance equation gives zero, since it is the spectral derivative of the energy flux as discussed in Section 2.2. In Fig. 5.3, however, there exist no spectral range where the net effect of the Navier-Stokes nonlinearity is zero. Accordingly, there is no true inverse energy

²The Navier-Stokes nonlinearity has a positive contribution also at very large k which, however, is hardly visible in Fig. 5.3. This area is not essential for the present work, since we focus only on the large scales.

cascade in the classical sense but, nevertheless, an inverse flow of energy with non-constant flux. This variance of the flux is to be expected, since at all scales there are additional active terms, both linear and nonlinear, which constantly add and remove energy from a given mode. Another important term at large and intermediate scales presents the cubic nonlinearity the contribution of which is denoted in Fig. 5.3 by a dark-blue line. The effect of this nonlinearity is almost exclusively dissipative.³ Its action is essential for reaching a statistically stationary state when $\alpha < 0$. In that case, without the cubic interaction there will be only energy injective terms at large scales with no means of dissipation. Thus, in a system of finite extend energy will steadily accumulate at the lowest wave numbers as explained in Sec. 2.3 for the two-dimensional Navier-Stokes model. For $\alpha = 0$ the cubic term is necessary for reaching a statistically stationary state, since the k^2 -injection will provide significant energy input.[103] Furthermore, our numerical studies showed that even in the case of large-scale friction, i.e., $\alpha > 0$, Eq. (5.4) with $\beta = 0$ cannot always reach statistically stationary state. For a given Γ_0 there needs to be some minimal amount of friction, i.e., $\alpha = \alpha_{\min}$, in order to compensate both the linear energy injection and the energy flux to larger scales due to the Navier-Stokes nonlinearity. If $\beta > 0$, however, energy saturation is guaranteed. As evident from Fig. 5.3, at large scales the effect of the cubic interaction follows closely the form of the Ekman term. In Sec. 5.3 we shall derive an approximation for the cubic term that will manifest this observation and in the same time preserves its nonlinear character such that its contribution scales roughly as \hat{v}^4 . Thus, increasing the energy content of the large scales will strongly amplify the cubic dissipation mechanism such that a statistically stationary state can be reached.

5.2 Spectral shell decomposition

In this section we shall introduce new tools for a more detailed study of the energy transfer between different spatial scales. We divide the spectral space into circular bands, i.e., shells, S_J , $J = 1, 2, 3, \dots$, centred around the origin $\mathbf{k} = 0$. Mathematically, one has $S_J = \{\mathbf{k} | k \in (k_{J-1}, k_J]\}$, where $k_0 = 0$.⁴ The grouping of the Fourier modes in shells is common in the turbulence literature where the borders of the latter are usually chosen such that $k_J/k_{J-1} = \text{const}$. For the analysis of the low-wave-number region, however, such a condition is rather problematic, since it does not allow for many spectral shells over the range where there exists a spectral power law as seen in Fig. 5.2. Thus, we construct shells of equal width which shall not influence our results. Independent of this, the contribution of a given shell is singled out by the projection operator P_J defined by the action on an arbitrary function

³At very small scales the cubic nonlinearity can have a small positive contribution. Nevertheless, for such wave numbers its effect is much smaller than that of the other terms, e.g., Navier-Stokes nonlinearity, linear injection or dissipation.

⁴We write the indices denoting the shell number with capital Latin letters in order to distinguish them from the indices designating the Cartesian components of a vector.

$f(\mathbf{r})$ as

$$(P_J f)(\mathbf{r}) := \sum_{\mathbf{k} \in S_J} \hat{f}(\mathbf{k}) e^{i\mathbf{k} \cdot \mathbf{r}} =: \langle f(\mathbf{r}) \rangle_J. \quad (5.9)$$

By virtue of the above definition one can easily verify that P_J is idempotent and, thereby, a projection operator. Additionally, P_J is self-adjoint with respect to the natural scalar product in L^2 and commutes with spatial and temporal derivatives. The energy of a given shell can be constructed as

$$E_J := \frac{1}{2} \frac{1}{V} \int_{\Omega} |\langle \mathbf{v} \rangle_J|^2 d\Omega = \frac{1}{2} \sum_{\mathbf{k} \in S_J} |\hat{\mathbf{v}}(\mathbf{k})|^2, \quad (5.10)$$

where $V = L_x L_y$ denotes the volume of Ω and $d\Omega = dx dy$ - an infinitesimal volume element. Since projection operators corresponding to different shells are orthogonal to each other, i.e., $P_J P_I = 0$ for $J \neq I$, we have that

$$E_0 = \sum_J E_J \quad \text{when } J \in \mathbb{S}, \quad (5.11)$$

where E_0 stands for the total energy of the system and \mathbb{S} represents a set of mutually disjunctive shells covering the whole spectral space. Applying P_J on Eq. (5.4), multiplying the result by $\langle \mathbf{v} \rangle_J$ and integrating over Ω , one derives an equation for the time evolution of the energy of each shell which reads

$$\begin{aligned} \frac{\partial E_J}{\partial t} = & -2\alpha E_J - \frac{\lambda_0}{V} \int_{\Omega} \langle \mathbf{v} \rangle_J \cdot \langle (\mathbf{v} \cdot \nabla) \mathbf{v} \rangle_J d\Omega - \frac{\beta}{V} \int_{\Omega} \langle \mathbf{v} \rangle_J \cdot \langle |\mathbf{v}|^2 \mathbf{v} \rangle_J d\Omega - \\ & - \Gamma_0 \frac{1}{V} \int_{\Omega} \langle \mathbf{v} \rangle_J \cdot \nabla \langle \mathbf{v} \rangle_J d\Omega - \Gamma_2 \frac{1}{V} \int_{\Omega} \langle \mathbf{v} \rangle_J \cdot \Delta^2 \langle \mathbf{v} \rangle_J d\Omega. \end{aligned} \quad (5.12)$$

As a result of the periodic boundary conditions and the incompressibility constraint the contribution from the pressure term vanishes, i.e.,

$$\int_{\Omega} \langle \mathbf{v} \rangle_J \cdot \nabla \langle p \rangle_J d\Omega = \langle p \rangle_J \langle \mathbf{v} \rangle_J \cdot d\boldsymbol{\sigma} \Big|_{\partial\Omega} - \int_{\Omega} \langle p \rangle_J \langle \nabla \cdot \mathbf{v} \rangle_J d\Omega = 0, \quad (5.13)$$

where $d\boldsymbol{\sigma}$ denotes an oriented infinitesimally small element from the boundary of Ω (which corresponds to a line for a two-dimensional Ω) the direction of which points outwards. Both terms on the right-hand side vanish separately - the first one because of the periodic boundary conditions, while the second one yields zero due to the incompressibility constraint. Analogously, for the linear terms involving spatial derivatives integration by parts leads to

$$\int_{\Omega} \langle \mathbf{v} \rangle_J \cdot \Delta \langle \mathbf{v} \rangle_J d\Omega = - \int_{\Omega} \sum_{i=x,y} |\nabla \langle v_i \rangle_J|^2 d\Omega = - \int_{\Omega} |\nabla \langle \mathbf{v} \rangle_J|^2 d\Omega = - \sum_{\mathbf{k} \in S_J} k^2 |\hat{\mathbf{v}}(\mathbf{k})|^2 \quad (5.14)$$

$$\int_{\Omega} \langle \mathbf{v} \rangle_J \cdot \Delta^2 \langle \mathbf{v} \rangle_J d\Omega = \int_{\Omega} |\Delta \langle \mathbf{v} \rangle_J|^2 d\Omega = \sum_{\mathbf{k} \in S_J} k^4 |\hat{\mathbf{v}}(\mathbf{k})|^2 \quad (5.15)$$

where we have used the norm-preserving property of the Fourier transform. Thus, we see that the linear terms are very local, i.e., the rate of change of the energy of a given shell depends only on properties of that shell. With the nonlinear terms, however, the situation is more complicated. In order to gain further physical insight, we shall decompose the velocity field as

$$\mathbf{v} = \sum_I \langle \mathbf{v} \rangle_I = \sum_I P_I \mathbf{v} \quad (5.16)$$

where $I \in \mathbb{S}$. Substituting for brevity the integral over Ω with the L^2 scalar product $\langle \cdot, \cdot \rangle$ and using the self-adjointness of the projection operator P_J we can write for the second term on the right-hand side in Eq. (5.12)

$$\lambda_0 \langle P_J \mathbf{v}, P_J ((\mathbf{v} \cdot \nabla) \mathbf{v}) \rangle = \lambda_0 \langle P_J \mathbf{v}, (\mathbf{v} \cdot \nabla) \mathbf{v} \rangle = \sum_I \lambda_0 \langle P_J \mathbf{v}, (\mathbf{v} \cdot \nabla) P_I \mathbf{v} \rangle =: \sum_I T_{JI}^{NS}. \quad (5.17)$$

Hence, the Navier-Stokes nonlinearity changes the energy balance of shell J by coupling it to all the other shells. A coupling induced by a quadratic nonlinearity, of course, involves three interacting modes. Similarly, in the scalar product above the velocity field \mathbf{v} appears three times. For obtaining T_{JI}^{NS} we have decomposed only two of the velocity fields into their shell components. Thus, T_{JI}^{NS} is to be interpreted as the interaction between shells S_J and S_I via all possible other shells, i.e., we sum implicitly over the third leg of the triad. Additionally, as shown in detail in Appendix C, in incompressible fluids the Navier-Stokes shell-to-shell coupling is antisymmetric, i.e., $T_{JI}^{NS} = -T_{IJ}^{NS}$. Such a symmetry property implies that the coupling between S_J and S_I moves energy from one to the other in a conservative manner. As a consequence, all the diagonal terms in the matrix \mathbf{T}^{NS} are zero, meaning that the Navier-Stokes nonlinearity does not introduce any self-interaction of shells.

The same methods of decomposition we can apply also to the third term on the right-hand side in Eq. (5.12) and obtain

$$\beta \langle P_J \mathbf{v}, P_J |\mathbf{v}|^2 \mathbf{v} \rangle = \beta \langle P_J \mathbf{v}, |\mathbf{v}|^2 \mathbf{v} \rangle = \sum_I \beta \langle P_J \mathbf{v}, |\mathbf{v}|^2 P_I \mathbf{v} \rangle =: \sum_I T_{JI}^C. \quad (5.18)$$

Thus, the cubic nonlinearity also introduces a shell-to-shell coupling defined above as T_{JI}^C . From Eq. (5.18) it is immediately evident that the interaction term T_{JI}^C is symmetric with respect to interchanging the two shells, i.e., $T_{JI}^C = T_{IJ}^C$, implying that the matrix \mathbf{T}^C is symmetric. Recall that every second-rank tensor can be uniquely decomposed in a symmetric and antisymmetric part. Taking this into account, \mathbf{T}^C cannot be viewed as a transfer term in the usual sense. It describes processes that behave fundamentally different from the notion of transfer and rather orthogonal to it. T_{IJ}^C couples two shells, say S_I and S_J , in such a way that the same amount of energy is produced/dissipated in/from both shells. The resulting energy excess/loss does not come/flow from/to other shells. This manifests again the non-conservative nature of the cubic interaction.

For the sake of completeness, we express the nonlinear shell coupling also in Fourier space

in terms of $\widehat{\mathbf{v}}(\mathbf{k})$ as

$$T_{IJ}^{NS} = -\lambda_0 \sum_{\mathbf{k}} \langle \widehat{\mathbf{v}}(\mathbf{k}) \rangle_J \cdot \mathcal{F}\{(\mathbf{v} \cdot \nabla) \langle \mathbf{v} \rangle_I\}(\mathbf{k}), \quad (5.19)$$

$$T_{IJ}^C = -\beta \sum_{\mathbf{k}} \langle \widehat{\mathbf{v}}(\mathbf{k}) \rangle_J \cdot \mathcal{F}\{|\mathbf{v}|^2 \langle \mathbf{v} \rangle_I\}(\mathbf{k}), \quad (5.20)$$

where \mathcal{F} denotes the Fourier transform. Thus, written with T_{IJ}^{NS} and T_{IJ}^C the energy balance equation for each shell reads

$$\frac{\partial E_J}{\partial t} = -2\alpha E_J + \sum_I T_{IJ}^{NS} + \sum_I T_{IJ}^C + \Gamma_0 \sum_{\mathbf{k} \in S_J} k^2 |\widehat{\mathbf{v}}(\mathbf{k})|^2 - \Gamma_2 \sum_{\mathbf{k} \in S_J} k^4 |\widehat{\mathbf{v}}(\mathbf{k})|^2. \quad (5.21)$$

Ideally, each shell contains a large number of modes which participate in the interaction. Thus, computing quantities shell-wise acts as a kind of a smoothing procedure meaning that in the statistically stationary state the term $\partial E_J / \partial t$ on the left-hand side of Eq. (5.21) will be very close to zero even without time averaging.

In order to gain further insight into the structure of the nonlinear coupling terms, we compute numerically the elements T_{IJ}^{NS} and T_{IJ}^C and the result is shown in Fig. 5.4 (a) and (b), respectively. In Fig. 5.4 (a) one can readily see the antisymmetry of the Navier-Stokes transfer. Indeed, summation over all shells gives zero up to machine precision indicating that our numerical tool represents correctly the advective nonlinearity. The numerical computation of the latter displays four distinctive branches. Two of the branches next to the diagonal mark the flow of kinetic energy from smaller to larger wave numbers. In Fig. 5.4 such an ordering (positive contributions above the diagonal and negative entries below it) corresponds to a forward cascade. The fact that those contributions are located next to the diagonal means that the transfer is local. Here, we will generally speak of flow of energy instead of a cascade, since the latter implies a constant flux that is not the case for Eq. (5.4). The forward energy flow dominates the Navier-Stokes transfer at larger wave numbers (above $k = 15k_\ell$) and explains why at those scales the green curve in Fig. 5.3 becomes positive again. The other important structure exhibited by the Navier-Stokes coupling are the two side branches located further away from the diagonal. The inverted colours (the entries above the diagonal are negative while those below it - positive) imply a backward energy flow which is in accord with the positive contribution of the advective term at small wave numbers in Fig. 5.3 (green line). The position of the contributions leading to the inverse flow (far from the diagonal) indicates that it results from nonlocal interactions. In summary, the Navier-Stokes nonlinearity in the context of Eq. (5.4) implies local interactions at large wave numbers, leading to a forward energy flow, and non-local interactions at small wave numbers, inducing an inverse energy flow.

Fig. 5.4 (b) presents the numerical computation of the elements T_{IJ}^C of the cubic shell-to-shell coupling. The result confirms the symmetric form dictated by the analytical considerations. The vast majority of the entries at small or intermediate wave numbers are negative. Due to the large deviations in magnitude between the diagonal and the off-diagonal terms, in Fig. 5.4 (b) we show the common logarithm of their absolute value such

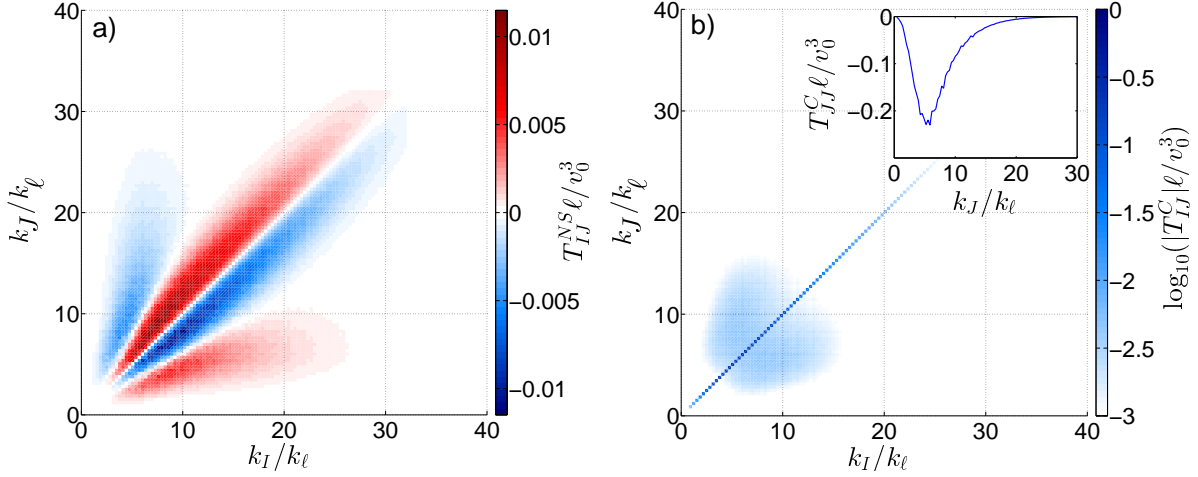


Figure 5.4: Numerical computation of the nonlinear interaction between shells as defined in Eq. (5.19). (a) Shell-to-shell transfer T_{IJ}^{NS} resulting from the Navier-Stokes nonlinearity. (b) Coupling term T_{IJ}^C due to the cubic interaction.

that the structure of the off-diagonal part is still visible. Although the other entries are not exactly zero, the main contribution comes from the diagonal terms which are often larger by nearly two orders of magnitude. Such a structure of the cubic interaction matrix \mathbf{T}^C closely resembles the one produced by linear terms. The latter correspond to a purely diagonal matrix where the off-diagonal contributions are exactly zero. This similarity of the cubic interaction with linear terms represents one of its most important features at moderate wave numbers and it should be captured by any successful approximation. The inset in Fig. 5.4 (b) shows only the diagonal terms T_{JJ}^C on a linear scale. The curve follows closely the form the dark-blue line in Fig. 5.3 which emphasises again the secondary role of the off-diagonal entries.

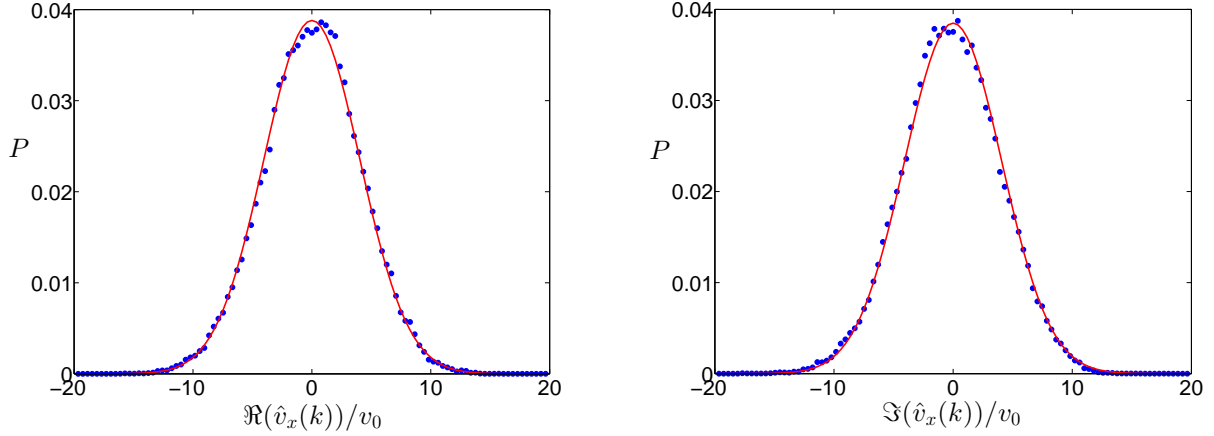
5.3 Quasi-normal approximation

Although the fundamental unknown quantity in Eq. (5.4) is the velocity field $\mathbf{v}(\mathbf{r}, t)$ as a function of space and time, from a practical point of view it contains too much unnecessary information like rapid fluctuations of velocity at a large number of spatial scales. A much more reasonable goal is the determination of statistical properties of the velocity field, e.g., velocity correlation functions of different orders or their Fourier representation. Similarly to the case of classical Navier-Stokes turbulence or the modified version of the Kuramoto-Sivashinsky equation as discussed in Chapter 4, the central quantity of interest here will be the one-dimensional energy spectrum $E(k)$ under the assumption of homogeneous and isotropic turbulence. In Section 5.1 we already derived an equation for the mode energy $E(\mathbf{k})$. However, Eq. (5.8) is insufficient in order to compute second-order velocity correlations since it involves correlations of higher order which are still unknown.

A natural step would be to use the Fourier representation of Eq. (5.4) in order to derive evolution equations for the nonlinear terms in Eq. (5.8). Such an approach is futile, since it leads to the same ‘hierarchy problem’ that we already discussed in Section 2.1 in the context of the Navier-Stokes model. In the case of Eq. (5.4), the system of coupled equations that arises in this way is even more intricate, since the evolution equation for the velocity field involves not only quadratic but also a cubic nonlinearity. Thus, an evolution equation for the structure function of order n will include not only correlations of order $n + 1$ but also $n + 2$. Accordingly, every equation of this infinite hierarchy, except the first two, will be coupled to four other equations instead of only two, complicating further the analysis. The usual way to deal with this problem is to make some simplifying assumptions that provide an additional relation between the coupled equations and, thereby, truncate the hierarchy. An important point for that matter is that the system under study is effectively two-dimensional and indeed exhibits a flux of energy towards large spatial scales which is a characteristic feature of such flows. An important observation in classical two-dimensional Navier-Stokes turbulence is that at large scales the statistics of the velocity-field fluctuations is very close to Gaussian. Nevertheless, Eq. (5.4) deviates from the pure Navier-Stokes model, hence, we first have to address this issue and verify it in this framework. Since we focus on the spectral representation of the correlation functions and Eq. (5.8) involves the Fourier transformed field $\hat{\mathbf{v}}(\mathbf{k}, t)$, we examine the probability distribution of its components. For this purpose, we fix the value of \mathbf{k} and analyse the time series of $\Re(\hat{v}_x(\mathbf{k}, t))$ and $\Im(\hat{v}_x(\mathbf{k}, t))$.⁵ Due to the turbulent motion of the fluid, \hat{v}_x will vary in such a way that some values will be assumed more often than others. This gives a probability distribution for \hat{v}_x . A numerical computation of the latter is shown in Figs. 5.5 (a) and (b) for the real and imaginary part of \hat{v}_x , respectively. The range over which the velocity field varied was divided in bins of equal length and the horizontal position of the blue dots (numerical result) in the figure correspond to the middle of the \hat{v}_x -cells, while their height shows how often the velocity field landed in the corresponding bin at the end of the time step. The simulation was performed with $\alpha = 1.0$ and we considered the velocity field at the wave number $\mathbf{k} = (0.6, 0.6)k_\ell$ which lies in the spectral range where we observe a power law in the energy spectrum. The red line represents the closest fit of a centred Gaussian distribution of the form $Ae^{-\hat{v}_x^2/\sigma^2}$, to the data set where A and σ are fit parameters. Evidently, our two-dimensional model for incompressible active turbulence inherits the feature of the two-dimensional Navier-Stokes equations to exhibit near-Gaussian statistics at large scales. Such a result suggests the application of the quasi-normal approximation developed in the framework of classical turbulence.[104] It was originally introduced by Millionshchikov in 1941 [105] and is known as the Millionshchikov hypothesis. According to this idea velocity correlations of odd orders, e.g., $\langle \hat{v}_i(-\mathbf{k})\hat{v}_l(\mathbf{k}-\mathbf{p})\hat{v}_j(\mathbf{p}) \rangle$, are not identically zero in contrast to a strictly Gaussian distribution.⁶ On the other hand, however, one

⁵Recall that the incompressibility condition $\mathbf{k} \cdot \hat{\mathbf{v}}(\mathbf{k}) = 0$ couples $\hat{v}_x(\mathbf{k})$ and $\hat{v}_y(\mathbf{k})$ such that we need to know the real and imaginary parts of only one of the components.

⁶The time average of the spectral form of the velocity correlations is equivalent to taking the expectation value. As is well known, the expectation value of a product of an odd number of mutually independent normally-distributed random variables is zero.



(a) Probability distribution of the real part of the component \hat{v}_x .

(b) Probability distribution of the imaginary part of the component \hat{v}_x .

Figure 5.5: Numerical computation (blue dots) of the probability distribution of the Fourier transformed velocity field $\hat{\mathbf{v}}$ at the wave number $\mathbf{k} = (0.6, 0.6)k_\ell$ compared to a Gaussian distribution (red line); $\alpha = 1.0$.

assumes that even-order correlations equal approximately the sum of products of all possible second-order correlations, which is a characteristic feature of mutually independent normally-distributed random variables. Such an approximation will allow us to approach directly the second term on the left-hand side in Eq. (5.8) which incorporates a fourth-order correlation. Quantitatively, the quasi-normal approximation yields in our case

$$\begin{aligned}
 \langle \hat{v}_i(-\mathbf{k}, t) \hat{v}_l(\mathbf{k} - \mathbf{p} - \mathbf{q}, t) \hat{v}_l(\mathbf{q}, t) \hat{v}_j(\mathbf{p}, t) \rangle = \\
 = \langle \hat{v}_i(-\mathbf{k}, t) \hat{v}_l(\mathbf{k} - \mathbf{p} - \mathbf{q}, t) \rangle \langle \hat{v}_l(\mathbf{q}, t) \hat{v}_j(\mathbf{p}, t) \rangle + \\
 + \langle \hat{v}_i(-\mathbf{k}, t) \hat{v}_l(\mathbf{q}, t) \rangle \langle \hat{v}_l(\mathbf{k} - \mathbf{p} - \mathbf{q}, t) \hat{v}_j(\mathbf{p}, t) \rangle + \\
 + \langle \hat{v}_i(-\mathbf{k}, t) \hat{v}_j(\mathbf{p}, t) \rangle \langle \hat{v}_l(\mathbf{k} - \mathbf{p} - \mathbf{q}, t) \hat{v}_l(\mathbf{q}, t) \rangle.
 \end{aligned} \tag{5.22}$$

This is an important step that truncates the infinite hierarchy of correlation functions arising via the nonlinear terms. Recall further that for homogeneous and isotropic turbulence the velocity correlation in spectral space are zero unless the wave numbers involved sum up to zero, as we discussed in Section 2.2. Thus, under the assumption of homogeneity and isotropy, the terms on the left-hand side of Eq. (5.22) can be simplified as

$$\begin{aligned}
 \langle \hat{v}_i(-\mathbf{k}, t) \hat{v}_l(\mathbf{k} - \mathbf{p} - \mathbf{q}, t) \rangle \langle \hat{v}_l(\mathbf{q}, t) \hat{v}_j(\mathbf{p}, t) \rangle &= D_{il}(\mathbf{k}) D_{jl}(\mathbf{p}) Q(k, t) Q(p, t) \delta_{\mathbf{q}, -\mathbf{p}} \\
 \langle \hat{v}_i(-\mathbf{k}, t) \hat{v}_l(\mathbf{q}, t) \rangle \langle \hat{v}_l(\mathbf{k} - \mathbf{p} - \mathbf{q}, t) \hat{v}_j(\mathbf{p}, t) \rangle &= D_{il}(\mathbf{k}) D_{jl}(\mathbf{p}) Q(k, t) Q(p, t) \delta_{\mathbf{q}, \mathbf{k}} \\
 \langle \hat{v}_i(-\mathbf{k}, t) \hat{v}_j(\mathbf{p}, t) \rangle \langle \hat{v}_l(\mathbf{k} - \mathbf{p} - \mathbf{q}, t) \hat{v}_l(\mathbf{q}, t) \rangle &= D_{ij}(\mathbf{k}) D_{ll}(\mathbf{q}) Q(k, t) Q(q, t) \delta_{\mathbf{p}, \mathbf{k}},
 \end{aligned} \tag{5.23}$$

where $\delta_{\mathbf{k}, \mathbf{p}}$ denotes the Kronecker delta for a vector argument, i.e., it equals 0 for $\mathbf{k} \neq \mathbf{p}$ and 1 when $\mathbf{k} = \mathbf{p}$. Additionally, instead of the energy spectrum we have used the equal-time

spectral correlation function $Q(k, t)$. Recall that for statistically isotropic systems we have $\langle \hat{v}_i(\mathbf{k}, t) \hat{v}_j(-\mathbf{k}, t) \rangle = D_{ij}(\mathbf{k})Q(k, t)$. Hence, with the aid of the quasi-normal approximation we can simplify the second term on the right-hand side in Eq. (5.8) as

$$\begin{aligned}
& \Re \left(\sum_{i,j,l} \sum_{\mathbf{p}, \mathbf{q}} D_{ij}(\mathbf{k}) \langle \hat{v}_i(-\mathbf{k}, t) \hat{v}_l(\mathbf{k} - \mathbf{p} - \mathbf{q}, t) \hat{v}_l(\mathbf{q}, t) \hat{v}_j(\mathbf{p}, t) \rangle \right) = \\
& = \sum_{i,j,l} \sum_{\mathbf{p}} D_{ij}(\mathbf{k}) D_{il}(\mathbf{k}) D_{jl}(\mathbf{p}) Q(k, t) Q(p, t) + \\
& + \sum_{i,j,l} \sum_{\mathbf{p}} D_{ij}(\mathbf{k}) D_{il}(\mathbf{k}) D_{jl}(\mathbf{p}) Q(k, t) Q(p, t) + \\
& + \sum_{i,j,l} \sum_{\mathbf{q}} D_{ij}(\mathbf{k}) D_{ij}(\mathbf{k}) D_{ll}(\mathbf{q}) Q(k, t) Q(q, t) = \\
& = 2Q(k, t) \sum_{\mathbf{p}} \left(N - 2 + \frac{(\mathbf{k} \cdot \mathbf{p})^2}{k^2 p^2} \right) Q(p, t) + (N - 1)^2 Q(k, t) \sum_{\mathbf{p}} Q(p, t),
\end{aligned} \tag{5.24}$$

where for the sake of generality we have left the number of spatial dimensions N arbitrary. In our case $N = 2$. For the derivation of the above equation we have used the relations

$$\sum_j D_{jj}(\mathbf{k}) = \text{tr}(D) = N - 1, \tag{5.25a}$$

$$\sum_i D_{ij}(\mathbf{k}) D_{il}(\mathbf{k}) = D_{jl}(\mathbf{k}), \tag{5.25b}$$

$$\sum_{ij} D_{ij}(\mathbf{k}) D_{ij}(\mathbf{k}) = N - 1, \tag{5.25c}$$

$$\sum_{j,l} D_{jl}(\mathbf{k}) D_{jl}(\mathbf{p}) = N - 2 + \frac{(\mathbf{k} \cdot \mathbf{p})^2}{k^2 p^2}. \tag{5.25d}$$

which follow directly from the definition of the tensor $D_{ij}(\mathbf{k})$ as shown in detail in Appendix D. As a next step we need to compute the sums over \mathbf{p} in the last part of Eq. (5.24) and relate them to energy-like quantities that are either global or local in the spectral domain. Taking into account that the total energy of the system, $E_0(t)$, is given by summing $\langle |\hat{v}_i(\mathbf{k}, t)|^2 \rangle / 2$ over all Fourier modes and Cartesian components, we derive

$$E_0(t) := \sum_{\mathbf{k}} \sum_i \frac{1}{2} \langle \hat{v}_i(\mathbf{k}, t) \hat{v}_i(-\mathbf{k}, t) \rangle = \frac{1}{2} \sum_{\mathbf{k}} \sum_i D_{ii}(\mathbf{k}) Q(k, t) = \frac{N - 1}{2} \sum_{\mathbf{k}} Q(k, t) \tag{5.26}$$

under the condition that $N > 1$. For the sake of generality, we have considered here $\langle \cdot \rangle$ as an ensemble average which contains also the case of turbulence with non-constant amplitude of the fluctuations. In the statistically stationary state, the ensemble average can be substituted by a time average and E_0 will not depend on time. This result shows

that the last term in Eq. (5.24) is proportional to E_0 . The other contribution contains the scalar product $\mathbf{k} \cdot \mathbf{p}$ and we will compute it in the limit $L \rightarrow \infty$, i.e., $k_{\min} \rightarrow 0$, in which the wave number becomes a continuous variable. Then one can substitute the sum over Fourier modes with integrals which will make the computation more convenient. Denoting the angle between \mathbf{k} and \mathbf{p} by θ and setting $d = 2$, we arrive at

$$\begin{aligned} \sum_{\mathbf{p}} \frac{(\mathbf{k} \cdot \mathbf{p})^2}{k^2 p^2} Q(p, t) &= \sum_{\mathbf{p}} \cos^2(\theta) Q(p, t) \approx \int_0^{2\pi} \int_0^\infty \cos^2(\theta) Q(p, t) p dp d\theta = \\ &= \frac{1}{2} 2\pi \int_0^\infty p Q(p, t) dp = \frac{1}{2} \int_0^{2\pi} \int_0^\infty Q(p, t) p dp d\phi = \frac{1}{2} \sum_{\mathbf{p}} Q(p, t) = E_0. \end{aligned} \quad (5.27)$$

Hence, the second contribution in the last line of Eq. (5.24) is also proportional to E_0 .⁷ Since the linear terms are expressed as functions of $E(\mathbf{k})$, we need to establish a relation between $E(\mathbf{k})$ and $Q(k)$. Note that, despite the vector notation of the argument, in the isotropic case after averaging, which is part of the definition of $E(\mathbf{k})$, it is a function only of k . Thus, for isotropic turbulence we derive

$$E(\mathbf{k}, t) = \frac{1}{2} \sum_j Q_{jj}(\mathbf{k}, t) = \frac{1}{2} Q(k, t) \sum_j D_{jj}(\mathbf{k}) = \frac{N-1}{2} Q(k, t), \quad (5.28)$$

which allows for a direct comparison between the linear terms in Eq. (5.8) and the last line in Eq. (5.24). Thus, in the framework of the quasi-normal approximation, Eq. (5.8) transforms into

$$\begin{aligned} \frac{\partial Q(k, t)}{\partial t} &= -2\alpha - 8\beta E_0(t)) Q(k, t) + \Gamma_0 k^2 Q(k, t) - \Gamma_2 k^4 Q(k, t) + \\ &+ 2\lambda_0 \Re \left(\sum_{i,j,l} \sum_{\mathbf{p}} M_{ijl}(\mathbf{k}) \langle \hat{v}_i(-\mathbf{k}, t) \hat{v}_l(\mathbf{k} - \mathbf{p}, t) \hat{v}_j(\mathbf{p}, t) \rangle \right), \end{aligned} \quad (5.29)$$

which provides a major simplification compared to the exact energy balance equation. Note that the closure problem is not solved yet, since the third-order correlation arising from the Navier-Stokes nonlinearity represents a still unknown function of the spectral density $Q(k, t)$. We shall deal with this issue in the next section.

The above results reveal an important feature of the cubic interaction. Under the assumption of quasi-Gaussianity the corresponding term in the energy balance equation, denoted hereafter by $T^C(k)$, adopts a very simple functional form which is directly proportional to the energy spectrum $E(k)$. Quantitatively, we have

$$T^C(k) \approx -8\beta E_0 E(k). \quad (5.30)$$

⁷Note that $Q(p, t)$ under the integral sign denotes a continuous function while $Q(p, t)$ in the summation is defined on a discrete grid, since the transition in the limit $L \rightarrow 0$ induces a change in the physical units. However, this does not play an essential role here and, therefore, we use the same letter in order to simplify notation.

Its form closely resembles that of the strictly linear terms in Eq. (5.8). This result resonates with our observation in Fig. 5.4 (b) where we found that the diagonal terms in the matrix \mathbf{T}^C are the dominant ones. Thus, the quasi-normal approximation seems to be consistent with the numerical results obtained so far. This is true at least at large spatial scales, i.e., for small k , which is also the spectral region we are interested in. There, the cubic interaction can be modelled as an Ekman term, the parameter in front of which, however, is not constant as in the case of true Ekman friction. Instead, the strength of this new quasi-Ekman term is proportional to the energy E_0 of the whole system. The prefactor E_0 manifests the nonlinear character of the term and serves as a self-regulation mechanism of the system ensuring that it reaches a statistically stationary state. In the beginning, when the total energy is small, the dissipation due to the cubic interaction is also small and, thus, energy grows with most of it contained at large scales due to the inverse energy flow. This increases E_0 and, thereby, also the amplitude of the cubic dissipation. Owing to the product $E_0 E(k)$, the latter scales as $|\widehat{\mathbf{v}}|^4$ and, hence, increases faster than both the linear terms, scaling as $|\widehat{\mathbf{v}}|^2$, and the Navier-Stokes contribution, scaling in the best case as $|\widehat{\mathbf{v}}|^{3/2}$. Thus, a statistically stationary state can always be reached.

As an additional test to the quasi-normal approximation one can compute $T^C(k)$ numerically and compare it to the energy spectrum $E(k)$. If the above assumptions are correct, it should hold that

$$\frac{T^C(k)}{8\beta E_0 E(k)} \approx -1, \quad (5.31)$$

where $T^C(k)$ represents the exact expression given in Eq. (5.8) and is computed independently from $E(k)$. Furthermore, E_0 is also computed numerically and independently. In this way we obtain the result displayed in Fig. 5.6 for $\alpha = 1.0$. We have removed the

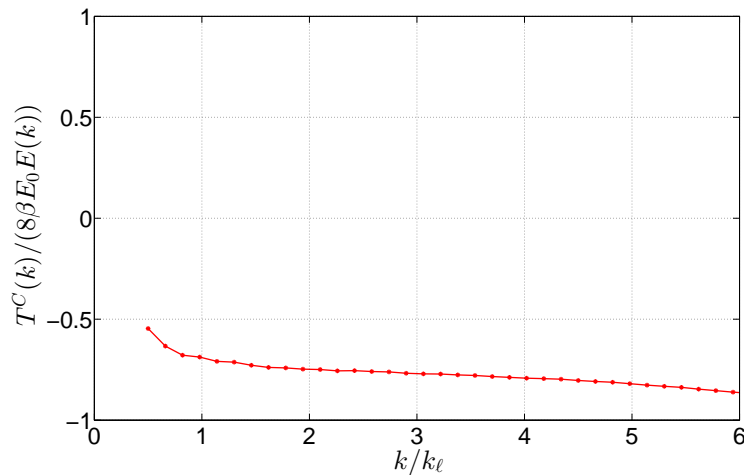


Figure 5.6: Comparison between the numerical result for the contribution of the cubic nonlinearity and its model bases on the quasi-normal approximation.

first couple of points at the lowest k , since at such large scales, comparable with the sys-

tem size, the condition of homogeneity and isotropy does not hold. Our result compares rather favourably to the approximation given in Eq. (5.31). The ratio between $T^C(k)$ and $8\beta E_0 E(k)$ is not exactly -1 but it remains relative constant and close to this value for a large range of wave numbers. It varies by less than 30% over more than one order of magnitude which indicates a rather weak dependence of the ratio on k . Although it does not saturate at exactly -1 , the important result of the quasi-normal approximation, that we will use later in Section 5.5, is its functional independence on k . The exact value of the constant and its small deviation from -1 will not influence the fundamental conclusions for the energy spectrum that we shall derive.

5.4 Navier-Stokes nonlinearity

In the previous section we chose the quasi-normal approximation in order to simplify one of the terms in the energy balance equation. The use of such an approach lent itself due to the particular form of the term arising from the cubic interaction. It already contains a product of four velocity fields and can be directly estimated with the aid of the Millionshchikov hypothesis. On the other hand, the Navier-Stokes nonlinearity results in a third-order velocity correlation. In order to resolve this problem with the quasi-normal approximation, one has to build an evolution equation for the triple correlation $\langle \hat{v}_i(-\mathbf{k})\hat{v}_l(\mathbf{k}-\mathbf{p})\hat{v}_j(\mathbf{p}) \rangle$. In this equation a quadratic nonlinearity will result in a fourth-order correlation on which one can apply the Millionshchikov hypothesis. The first problem that we encounter this way is the fact that cubic nonlinearities in the equation of motion for the velocity field, will result in fifth-order correlations in the equation for $Q_{ilj}(\mathbf{k}, \mathbf{k}-\mathbf{p}, \mathbf{p}, t)$. A possible way to avoid such a complication will be to substitute the cubic nonlinearity directly in the spectral equation of motion with a linear term based on the result in Eq. (5.30). However, this will introduce an additional source of error in the approximation of the Navier-Stokes-induced term. The second and more practical problem arising from such an iterative construction is that the resulting approximate system of equations can hardly be dealt with analytically. Such an approach usually leads to computational schemes which are executed numerically as an alternative to the exact equation of motion for the velocity field. We, on the other hand, aim for a simpler closed equation for the energy spectrum that can be solved analytically and is justified at least in the spectral range of small wave numbers which we are interested in. Hence, we shall take a more heuristic approach to the problem and borrow ideas from the field of classical turbulence. As discussed already in Section 2.2, the quantity of energy flux $\Pi(k)$ plays an important role for understanding the energy distribution in spectral space. Without loss of generality, we can express the energy flux arising from the Navier-Stokes term as proportional to the energy content of the corresponding scale. Taking into account that the energy of an eddy of size $\sim 1/k$ scales as $kE(k)$, one can write

$$\Pi^{NS}(k) \propto \zeta(k)kE(k). \quad (5.32)$$

Strictly speaking, the above relation does not present a closure for the energy balance equation, since the function $\zeta(k)$ is still unknown. It merely shifts the problem from finding $T^{NS}(k)$ to finding $\zeta(k)$ which will allow us to construct the flux $\Pi^{NS}(k)$ and then derive from it $T^{NS}(k)$, since they are related by Eq. (2.32). Nevertheless, the formulation given by Eq. (5.32) still represents a step towards developing a closure approximation, since it provides a physical interpretation for the unknown function. $\zeta(k)$ has the physical units of frequency and the notion behind it is that $1/\zeta(k)$ can be viewed as the characteristic distortion time of eddies of size $\sim 1/k$. This distortion couples the different spatial scales and provides the mean for energy transfer between them. Hence, one can regard $\zeta(k)$ as the typical frequency governing the Navier-Stokes energy flux at the scale $\sim 1/k$. In the classical theory of turbulence $\zeta(k)$ is given in the spectral ranges of the energy or enstrophy cascades by

$$\zeta(k) \sim \sqrt{\int_0^k p^2 E(p) dp}. \quad (5.33)$$

The above relation does not hold rigorously but is rather constructed on the basis of dimensionality considerations. Nevertheless, under the assumption of cascades, i.e., constant energy or enstrophy flux, it yields both the Kolmogorov and Kraichnan spectra including the logarithmic correction of the latter.[49] The physical motivation behind Eq. (5.33) relies on $\zeta(k)$ monotonically increasing with k in the cascade range. This implies that smaller scales exhibit higher characteristic frequencies than the larger ones. Hence, the effect of the smaller scales averages out on times comparable to the eddy-turn-over time of the scale $1/k$. On the other hand, the comparatively slower dynamics of the larger scales ensures that wave numbers smaller than k contribute to the average shear acting on scale $1/k$. Given that the energy spectrum decreases with k slower than k^{-2} , the integrand in Eq. (5.33) increases steadily with k and the main contribution comes from wave numbers at the upper end, i.e., $p \sim k$. Thus, in such cases the characteristic distortion time at the scale k will depend mostly on the slightly larger scales expressing the locality of the interactions. Indeed, it has been verified numerically that the energy transfer in the energy cascades both in the two- and three-dimensional Navier-Stokes model are local. On the other hand, the faster decrease of $E(k)$ in the enstrophy cascade for the two-dimensional Navier-Stokes equations means that the degree of locality there is much smaller which has also been demonstrated numerically. The recognition that for two-dimensional fluids the large scales can directly affect the small scales together with the form of the characteristic frequency as given in Eq. (5.33) has provided corrections of the Kraichnan spectrum for some extensions of the Navier-Stokes equations.[52]

Two-dimensional bacterial suspensions governed by the evolution equation Eq. (5.4), however, exhibit a qualitatively different type of energy transfer compared to the cascade ranges in the classical Navier-Stokes model. As already displayed in Fig. 5.3, there is no range of wave numbers in Fourier space where the term $T^{NS}(k)$ arising from the advective nonlinearity is close to zero and negligible compared to the other terms in the energy balance equation. Furthermore, we can compute numerically the corresponding energy flux

$\Pi^{NS}(k)$. The result is shown in Fig. 5.7 where we have divided it by $kE(k)$ for convenience.

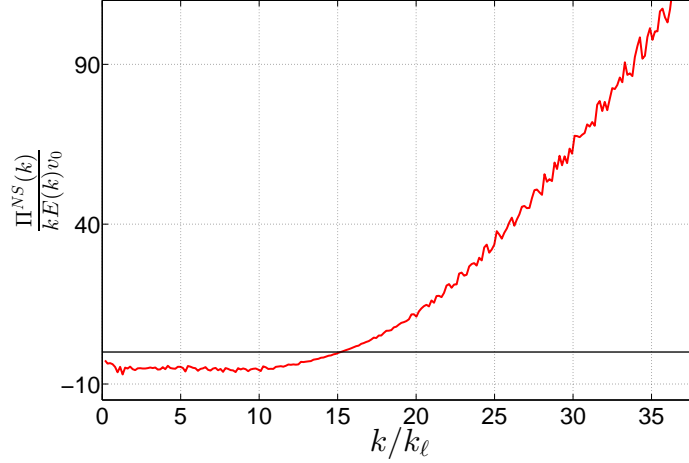


Figure 5.7: Numerical computation of the energy flux $\Pi^{NS}(k)$ normalised over the energy at the corresponding scale, i.e., $kE(k)$, as a function of the wave number.

Thus, the resulting curve provides a numerical computation of $\zeta(k)$ for our system. A negative value of the frequency corresponds to a negative flux and vice versa. For k up to $k \approx 15k_\ell$ the flux is negative, i.e., energy flows from smaller to larger scales, and for k larger than this value it becomes positive, i.e., energy flows from larger to smaller scales. The former manifests clearly the nature of two-dimensional fluids. Taking into account that at small k the energy spectrum in our case increases with k , say as $E(k) \propto k^r$ where $r > 0$, then Eq. (5.33) gives a characteristic frequency that goes as $\zeta(k) \propto k^{r+3}$. More generally, for any monotonically increasing $E(k)$ Eq. (5.33) yields in this range $\zeta(k)$ that grows faster than k^3 . Such a functional form disagrees with what we observe in Fig. 5.7 where $\zeta(k)$ remains relatively constant over a wide range of wave numbers at small k . The physical interpretation of this fact is that the large scales are synchronised and exhibit the same characteristic frequency. Such a synchronisation can result from nonlocal interactions as those indicated by the side branches in Fig. 5.4 (a). Another issue to be considered in our case is the energy distribution among scales. In classical Navier-Stokes turbulence, both two and three dimensional, the larger scales are always more energetic than the smaller ones. Apart from their characteristic frequency being low enough such that their action on the smaller scales does not average out over the corresponding eddy-turn-over time, being energetic enough represents a further condition necessary for the large scales to shear the smaller ones. In our case, however, the most energetic scales are those where energy injection peaks. This happens at scales smaller than the ones we want to investigate. Hence, in our bacterial system the large-scale flow structures do not possess the energetic potential to shear the smaller ones. We shall incorporate this observation in our analysis in a rather heuristic way by writing

$$\Pi^{NS}(k) = -\lambda_0 \zeta_0 k E(k) \quad (5.34)$$

for small k where $\zeta_0 = \text{const}$ in this range. This provides an observationally-motivated

closure expression for the Navier-Stokes nonlinearity that we will use in the next section.

5.5 Variable spectral exponent

In this section we shall use the insight gained so far into the turbulent dynamics produced by Eq. (5.4) in order to derive a quantitative expression of the energy spectrum of the velocity field $\mathbf{v}(\mathbf{r}, t)$. As a starting point of our analysis serves the expression for the spectral energy balance given by Eq. (5.8). In the statistically stationary state its left-hand side can be neglected compared to each of the major terms on the right. Hence, we can write that

$$-2\alpha E(k) + T^C(k) - \frac{d\Pi^{NS}}{dk} + 2\Gamma_0 k^2 E(k) - 2\Gamma_2 k^4 E(k) = 0, \quad (5.35)$$

where the cubic interaction is represented by the general term $T^C(k)$ and we have used the relation between the Navier-Stokes term $T^{NS}(k)$ and the corresponding energy flux. The above equation is in this form still exact but it incorporates unknown terms. Taking into account the result from the quasi-normal approximation, given quantitatively by Eq. (5.30), and the form of the energy flux at small scales as provided by Eq. (5.34), we arrive at

$$-2\alpha E(k) - 8\beta E_0 E(k) + \lambda_0 \zeta_0 \frac{d(kE(k))}{dk} + 2\Gamma_0 k^2 E(k) = 0, \quad (5.36)$$

which gives a closed expression for the energy spectrum in the form of a first-order ordinary differential equation. In Eq. (5.36) we have neglected the hyper-viscous term $2\Gamma_2 k^4 E(k)$, since its contribution is insignificant at small wave numbers, which is the spectral range we are interested in. The above differential equation is separable with respect to k and $E(k)$. Thus, its solution can be readily derived as

$$E(k) = C k^\delta \exp\left(-\frac{\Gamma_0}{\lambda_0 \zeta_0} k^2\right), \quad (5.37)$$

where C is merely a constant of integration. The exponent δ , that we introduced for brevity, is expressed in terms of the system parameters as

$$\delta = \frac{2\alpha + 8\beta E_0}{\lambda_0 \zeta_0} - 1. \quad (5.38)$$

Eqs. (5.37) and (5.38) represent the main results of this chapter. First, they confirm that for small wave numbers, i.e., in the limit $k \rightarrow 0$, the energy spectrum $E(k)$ exhibits a power-law of the form $E(k) \propto k^\delta$. Such an analytical result is consistent with the numerical observations made before, as well as with those made by other groups.[94] The other and more important feature given by Eqs. (5.37) and (5.38) is the fact that the power law is not universal. In contrast to what is given in Ref. [94], its slope depends both directly

and indirectly on various system parameters. The most sensitive dependence is the one on α which is the parameter controlling the large-scale friction. This result bears certain analogy to the model examined in Chapter 4 where the slope of the spectral power law also depends on linear parameters. Nevertheless, there are also some important differences. In the previous model we argued that the important condition to be met is that the ratio between the characteristic frequencies of the linear and nonlinear terms has to be scale-independent. The different frequencies alone can still vary with k . Here, however, the above results were derived under the explicit condition that the frequency ζ governing the Navier-Stokes energy transfer is constant at small wave numbers. A different form of ζ will change the differential equation given in Eq. (5.36) leading to a completely different result. Under the quasi-normal approximation for the cubic interaction, a constant ζ is the only form that leads to a power-law type of energy spectrum at small k such that the slope of the spectrum depends on α . The dependence on the linear parameter α is clearly observed in our numerical computations as displayed in Fig. 5.8 (a). Note also that the power-law form at small k is corrected by the factor $\exp(-\Gamma_0 k^2/(\lambda_0 \zeta_0))$ as the wave numbers grows. Its contribution for $k \rightarrow 0$ is negligible but at moderate k the correction provides a decreasing energy spectrum consistent with the physical requirement of a finite total energy. Nevertheless, the superexponential decrease of the energy spectrum at large k should not be taken seriously, since in that range many of the assumptions made so far do not apply. In the step from Eq. (5.35) to Eq. (5.36) we neglected the hyperviscous term $-\Gamma_2 k^4 E(k)$. It is easy to verify that such a term would produce a multiplicative correction to the energy spectrum in Eq. (5.37) of the form $\exp(\Gamma_2 k^4/(2\lambda_0 \zeta_0))$. At first glance, this looks like a failure of the simplifications we used since they lead to a superexponential divergence of the energy in the limit $k \rightarrow \infty$. However, in this limit the other assumptions we made are not valid neither. Most importantly, the hyperviscous term leads to an increasing contribution only in the case of an inverse energy flux. As seen in Fig. 5.7, this is true only at moderate wave numbers up to $k \approx 15k_\ell$. In the range of scales where the Γ_2 -term becomes important and even dominant the energy flow arising from the Navier-Stokes nonlinearity is positive, i.e., energy flows from larger to smaller scales. Additionally, at those scales the functional form of $\zeta(k)$ will not be constant, leading to a solution of a different form than simply Eq. (5.37) corrected by $\exp(\Gamma_2 k^4/(2\lambda_0 \zeta_0))$. Lastly, the quasi-normal approximation we made in Section 5.3 has to be reconsidered. Solving Eq. (5.4) numerically shows that at very small scales the cubic interaction leads to a positive contribution in the spectral energy balance equation. Thus, at large k the model developed in Section 5.3 has to be corrected.

Although not applicable at very small scales, the approximations developed so far yield very good results when k is small, which is also the part of the spectral space we are interested in. In this limit, the superexponential corrections of Eq. (5.37) can be neglected and $E(k) \propto k^\delta$ provides an useful approximation. Taking into account also the explicit dependence of the slope δ on the system parameters, one sees that, qualitatively, a stronger dissipation corresponds to a steeper power law and vice versa. As an example, we show in Fig. (5.8) (a) the energy spectrum produced by Eq. (5.4) for two different values of α . For comparison, the black lines represent pure power-laws with exponent shown above them.

The difference is unambiguous and is qualitatively consistent with Eq. (5.38). In the figure

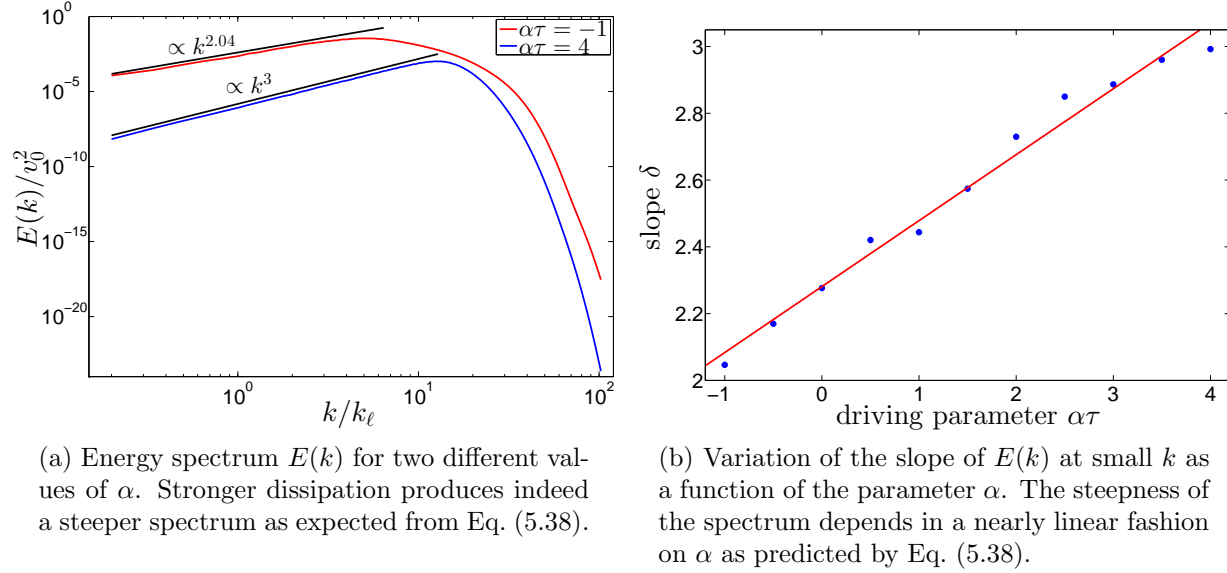


Figure 5.8: Numerical results for the energy spectrum produced by Eq. (5.4) for different system parameters.

the red line lies entirely above the blue one which comes from the fact that the former corresponds to a system where the Ekman term acts as an energy source, while in the other case it dissipates energy. Thus, the total energy of the system, i.e., the area under $E(k)$, is larger for $\alpha = -1$ than for $\alpha = 4$, which is to be expected, since in the first case there is an additional energy injection mechanism. For a more qualitative verification of our results we have performed numerical simulations of the turbulent flow for various values of the parameter α . It is important, however, that α is not too large such that there are still enough linearly unstable modes to drive the turbulence. This sets the upper bound for the parameter scan. On the other hand, α must not be too small (too negative) neither, otherwise the Toner-Tu term, modelling the flocking behaviour of bacteria will dominate and destroy the statistical isotropy of the flow. This condition sets the lower bound for the parameter scan. In each case we have performed a power-law fit over the left part of $E(k)$ and computed the value of the slope numerically. The results are shown in Fig. 5.8 (b) as blue dots. The data manifest a nearly linear dependence of the slope δ on the linear parameter α which agrees with Eq. (5.38) derived from our model. The red line represents the closest linear fit. The numerical data follow the linear form more closely in the area where α is small. This is due to the fact that in this parameter region the total energy of the system also scales linearly with α .

Further numerical simulations indicate that the slope of the energy spectrum exhibits qualitatively the same dependence also for variation of the parameter β , i.e., $E(k)$ is steeper at small k when β is larger, which is also in agreement with Eq. (5.38). Quantitatively, however, the dependence on β seems to be much weaker than that on α . The reason

for this might be that in Eq. (5.38) β appears in the combination βE_0 . Linear stability analysis of the fixed points of Eq. (5.4) show that for $\lambda_0 = \Gamma_0 = \Gamma_2 = 0$ and $\alpha < 0$ a global ordered state arises where the velocity field has a constant magnitude and direction. In this case the total system energy scales as $E_0 \propto \alpha/\beta$. If a similar scaling applies also in the turbulent case, the product βE_0 will depend only weakly on β .

5.6 Conclusion

In the present chapter we investigated, both analytically and numerically, a continuous model for the coarse-grained description of bacteria suspensions. In general, it can describe active fluids that are driven by internal instabilities. The intrinsic means of energy injection represent a distinctive feature not only of biological systems but can be found also in nonliving matter, as in plasmas. In contrast to classical Navier-Stokes turbulence which exhibits a large separation of scales between driving and dissipation ranges, the model studied here displays a very different behaviour. Both energy injection and dissipation terms are active on the same scales. Nevertheless, at these scales the system still displays an energy spectrum of the power-law type. Such an observation cannot be explained by the theory of classical turbulence where power laws in the energy spectrum are associated with a conservative energy/enstrophy cascade which is absent here.

A distinctive feature of the model studied here, compared to most of the known turbulent systems, constitutes an additional cubic nonlinearity which does not conserve neither energy nor enstrophy. In this chapter we analysed the impact of such a nonlinear term on the system. By splitting the set of Fourier modes in different circular shells we found that such a nonlinearity cannot be viewed as a transfer term in the usual sense. Instead, it couples different spatial scales in such a way that the same amount of energy is dissipated/created in both shells. Numerical computation showed that the effect of the cubic term is usually dissipative. Moreover, the shell-to-shell coupling matrix is dominated by the diagonal elements which resembles great similarity with linear terms. After verifying that at small wave numbers the statistics of the Fourier-transformed velocity field is close to Gaussian, we applied the quasi-normal approximation to the contribution arising from the cubic nonlinearity. As a result, it yielded a term that is very similar in form to the Ekman damping. However, the resulting prefactor is proportional to the total energy of the system which manifests again the nonlinear character of the term.

Similarly to most of the fluid models in physics, the model examined here involves also an advective nonlinearity of the Navier-Stokes type. Since we consider an incompressible system, it conserves energy globally and merely provides a mean for energy transfer between different scales. Due to the two-dimensional setting of the problem, the Navier-Stokes term is responsible for an inverse flow of energy at large scales, i.e., it transports energy from intermediate to large scales where it acts as an energy source. Numerical investigation showed that the characteristic frequency at wave number k (inversely proportional to the

turn-over time of an eddy of size $1/k$), defined in the same way as in classical Navier-Stokes turbulence, remains relatively constant with respect to k when the latter is small. This provided a heuristic closure for the corresponding term in the energy balance equation.

Besides the study of the general energetic properties of the fluid model given by Eq. (5.4), one of the main goals of this chapter was the understanding of the behaviour of the energy spectrum $E(k)$ at large scales. For this reason we derived the corresponding energy balance equation and developed closure approximations for the nonlinear terms in it. This resulted in a differential equation for $E(k)$ which was solved analytically allowing us to obtain the functional form of $E(k)$. Apart from finite-size effects that have to be taken into account, we found that the energy spectrum exhibits a power-law form in the limit of $k \rightarrow 0$. In contrast to the inertial ranges of classical Navier-Stokes turbulence, the steepness of this power law is not universal but, instead, depends on various system parameters, including linear ones. The dependence of the slope on the strength of the Ekman term (both in the injective and dissipative regime) was examined numerically and the result compared favourably to the analytical prediction. This property of a nonuniversal power-law spectrum should be observable in laboratory experiments and also apply to other active fluids. Overall, one can argue that the high-dimensional nonlinear dynamics in such systems defines a new class of turbulence which is distinct from the Navier-Stokes model.

Chapter 6

Summary and outlook

In beginning of the present work we gave a physical description of turbulence. The latter describes the chaotic and irregular motion of fluids and plasmas. It is an ubiquitous phenomenon in Nature and manifests itself in a variety of different situations in science and engineering. Despite more than a century-long research our understanding of turbulent flows remains to a high degree unsatisfactory and we still lack the analytical tools to make reliable quantitative predictions. The most prominent success in developing a systematic theory, which models turbulence, was made by Kolmogorov. However, it provides a rather heuristic approach and relies on assumptions, e.g., a statistically homogeneous and isotropic flow, which pose a strong restriction to the applicability of the theory in realistic situations. Besides the conditions of homogeneity and isotropy the classical theory of turbulence considers only cases where the mechanisms of energy injection are external and active at much larger scales compared to the dissipation. Many real-life turbulent systems, however, do not fulfil this restriction and their description presents a challenge to our fundamental understanding of turbulence. In many cases the energy injection, which gives rise to the turbulence and sustains the statistically steady state, is due to internal instabilities and not to external forces. One such example provide magnetised plasmas. The turbulence in such systems is driven by unstable linear eigenmodes which act as a source of free energy. In general, also the condition for a considerable scale separation between injection and dissipation is not fulfilled. Despite those considerable differences, however, the nonlinear plasma dynamics produces power-law spectra in the Fourier representation of many energy-like quantities. Such an observation presents a surprising similarity to the classical theory of turbulence. In contrast to the latter, however, the steepness of the power laws exhibited by magnetised plasmas is not universal but depends on particular linear properties of the system, e.g., the type of the driving instability. This remarkable feature provided the main motivation for the present work. Instead of analysing the full equations governing the plasma dynamics, we investigated, both analytically and numerically, simpler turbulent models which also display a lack of scale separation and nonuniversal spectral power laws.

In contrast to classical fluid turbulence, the nonlinear dynamics in plasmas preserves some of the linear features of the system. In addition, energy is injected by linear instabilities and in some parameter regimes damped modes control the range of scales at which dissipation is particularly active. This implies the importance of the linear physics for the complete understanding of the nonlinear dynamics and provides a motivation for the study of linear solutions. Thus, in Chapter 3 we considered a simplified setting in magnetised plasmas where we linearised the governing equations and investigated the corresponding eigenmodes. In particular, we examined the effect which a collision operator of the hyperdiffusion type has on the linear modes. This represents an important example since such collision operators are often used in numerical simulations. In the limit of vanishing collisionality, which is of immediate relevance for nuclear fusion approaches using magnetic confinement, we proved analytically that the frequency spectrum in the complex plane tends to the collisionless Landau solutions. The latter are of great physical importance since they predict the correct decay of the electrostatic potential as measured in experiments. On the other hand, there exist other collisional operators, e.g., the Krook model, which exhibit a completely different limit when the collisionality tends to zero. Hence, our result verifies that the collisional operators of the hyperdiffusion type, which are often used in numerical simulations due to their computational simplicity, reproduce correctly the linear physics.

In Chapter 4 we studied a one-dimensional nonlinear model exhibiting the spatio-temporal chaos characteristic for turbulence. It is based on the Kuramoto-Sivashinsky equation which, in similarity to the gyrokinetic theory of magnetised plasmas, possesses linear instabilities at large scales which inject energy into the system. Nonlinear interactions then transfer the energy conservatively to small scales where it is dissipated. The similarity between this one-dimensional model and the dynamics observed in plasma physics was further extended by modifying the equation such that the large scales remain virtually intact while the damping rate at high wave numbers tends to a constant value instead of increasing indefinitely as in the original formulation. Based on our analytical and numerical study of the model we managed to construct an approximation for the spectral energy balance equation that is valid at small scales. It predicted an energy spectrum in the form of a power law which we also observed in numerical simulations. With the aid of this approximation, we additionally concluded that the steepness of this power law is not universal but instead depends on the constant linear damping rate at small scales. Such a spectral nonuniversality suggests a connection to the observations made in plasma turbulence. An essential condition for this result was the scale-invariance of the ratio between the typical nonlinear frequency governing the energy transfer to small scales and the corresponding damping frequency. This frequency ratio determines the steepness of the spectral power law at high wave numbers. Such a scenario can be relevant for Alfvén-wave turbulence in the solar wind where for some parameter regimes and over some ranges the ratio between nonlinear and linear frequency can also be scale-independent. The investigation of the precise conditions under which Alfvén-wave turbulence can mimic the situation in the one-dimensional model studied here will be the subject of future work.

Chapter 5 presents the first systematic study of a continuum model which was originally put forward to describe the large-scale dynamics of dense bacterial suspensions. In general, it constitutes a two-dimensional active system which rests on the framework of the incompressible Navier-Stokes equations but extends it by including additional linear and nonlinear terms. Introducing linear instabilities provides the mean for intrinsic energy injection. Additionally, a third-order nonlinearity is used to mimic the flocking tendency of bacteria. As a result, in some parameter regimes the model exhibits turbulence although the corresponding Reynolds number is very small. Applying tools developed in the framework of the classical theory of turbulence, we analysed the flow of kinetic energy in Fourier space. In contrast to the incompressible Navier-Stokes model, here no inertial ranges in the usual sense exist. Despite this essential difference we observe power laws in the energy spectrum at large scales which again suggests that their occurrence in turbulent systems extends outside the range of validity of the Kolmogorov theory. The physical insights gained from the investigation of the scale-to-scale energy flow helped us to develop an approximation for the energy balance equation at small wave numbers. Its solution confirmed the existence of a power-law in the energy spectrum in this spectral range. Furthermore, our approximation predicted that the form of this power law is not universal and provided the functional dependence of its steepness on various system parameters. Investigating the continuum model with the aid of extensive numerical simulations we verified the functional dependence derived from our approximation. An essential role for our result played the fact that the dynamics studied is constrained to two dimensions. This enforces an inverse energy flow at large scales, which corresponds to the spectral range where the nonuniversal power law is observed. A natural continuation of our present analysis would be to consider the extension of the model at hand to three spatial dimensions where the constraint of inviscid vorticity conservation is not present. The analysis of this geometrical setup will be the subject of further research.

Appendix A

Relations involving the plasma dispersion function Z

For the definition of the plasma dispersion function used in Section 3.3 we follow Ref. [106] and write

$$Z(\Omega) := \frac{1}{\sqrt{\pi}} \int_{-\infty}^{+\infty} \frac{e^{-x^2}}{x - \Omega} dx, \quad (\text{A.1})$$

which is mathematically unambiguous when $\Im(\Omega) > 0$. In the other parts of the complex plane, i.e., when $\Im(\Omega) \leq 0$, we take the analytical continuation of the expression on the right-hand side in Eq. (A.1). More precisely, in the case of $\Omega \in \mathbb{R}$ we integrate along a contour which approaches the singularity at $x = \Omega$ from the left on the real line, then goes around it by a semi-circle of infinitesimally small radius from below and continues along the real line till $+\infty$. Thus, in the limit $\Im(\Omega) \rightarrow 0$ the integration contour has been deformed in a continuous way. For Ω in the lower part of the complex plane $Z(\Omega)$ is given by the integral in Eq. (A.1) plus the result from the integration along a closed circle of an infinitesimally small radius around the singularity. Thus, when Ω crosses the real line from above the integration contour is deformed continuously such that it always goes below Ω . One can also use the alternative definition

$$Z(\Omega) := 2ie^{-\Omega^2} \int_{-\infty}^{i\Omega} e^{-x^2} dx, \quad (\text{A.2})$$

which is valid for all $\Omega \in \mathbb{C}$ and relates the plasma dispersion function to the complex error function. The advantage of Eq. (A.2) is that the integrand does not involve any singularities and, hence, there is no need to distinguish between the different cases with respect to the sign of $\Im(\Omega)$. With the aid of the second definition one sees immediately that $Z(0) = i\sqrt{\pi}$ and that the complex derivative of Z is related to the function its self by

$$\frac{dZ(\Omega)}{d\Omega} = -2(1 + \Omega Z(\Omega)). \quad (\text{A.3})$$

In addition, Z possesses the symmetry properties that

$$\Re(Z(\Omega_r, \Omega_i)) = -\Re(Z(-\Omega_r, \Omega_i)), \quad (\text{A.4a})$$

$$\Im(Z(\Omega_r, \Omega_i)) = \Im(Z(-\Omega_r, \Omega_i)) \text{ and} \quad (\text{A.4b})$$

$$Z(\overline{\Omega}) = -\overline{Z(-\Omega)}, \quad (\text{A.4c})$$

where $\Omega = (\Omega_r, \Omega_i)$ with $\Omega_r, \Omega_i \in \mathbb{R}$ and the overbar denotes complex conjugation.

The first relation in Eq. (3.34) can be derived immediately by interchanging the differentiation with respect to Ω and integration with respect to x which can be justified, since both $\exp(-x^2/4 - i\Omega x)$ and all its derivatives $\partial^r \exp(-x^2/4 - i\Omega x)/\partial \Omega^r$ are continuous functions both with respect to x and Ω for $x \in (-\infty, 0]$ and all Ω . Additionally, for a given parameter set there is at most one instability with a growth rate Ω_i^{\max} . Thus, $|\exp(-x^2/4 - i\Omega x)|$ and $|\partial^r \exp(-x^2/4 - i\Omega x)/\partial \Omega^r|$ have upper bounds given by $\exp(-x^2/4 + \Omega_i^{\max})$ and $|x|^r \exp(-x^2/4 + \Omega_i^{\max})$, respectively, which are integrable over the interval $x \in (-\infty, 0]$. For obtaining the second relation in Eq. (3.34) we take into account that for every finite Ω the exponential $\exp(-x^2/4 - i\Omega x)$ is a holomorphic function in the complex x -plane and, therefore, the integration does not depend on the particular integration path. Hence, we can write that

$$\int_{-\infty}^0 e^{-x^2/4 - i\Omega x} dx = 2e^{-\Omega^2} \int_{-\infty + i\Omega}^{i\Omega} e^{-y^2} dy = 2e^{-\Omega^2} \underbrace{\int_{-\infty + i\Omega}^{-\infty} e^{-y^2} dy}_{=0} + 2e^{-\Omega^2} \int_{-\infty}^{i\Omega} e^{-y^2} dy = -iZ(\Omega), \quad (\text{A.5})$$

where the integral from $(-\infty - \Omega_i, \Omega_r)$ to $(-\infty, 0)$ vanishes since along that path the real part of the integrand is zero.

Appendix B

Range of the disparity parameter S

For the study of the locality of nonlinear interactions in Section 4.4 we introduced in analogy to the classical theory of Navier-Stokes turbulence the so-called disparity parameter S which in a one-dimensional formulation depends on only two of the interacting modes, say k and p , i.e., $S = S(k, p)$. Here we shall prove that $S \in [1, \infty)$ which we used in the main work. Recall that the disparity parameter is defined as

$$S := \frac{\max\{|k|, |p|, |k - p|\}}{\min\{|k|, |p|, |k - p|\}}. \quad (\text{B.1})$$

Evidently, S takes only non-negative values and can attain $+\infty$ only if one of the wave numbers is zero. Thus, we need to determine the lowest possible value of S . Note that S remains the same in the case of simultaneously interchanging $k \leftrightarrow -k$ and $p \leftrightarrow -p$. Therefore, it suffices to consider only half of the (k, p) -plane, say where $k \geq 0$. Let us fix one of the modes and write $k = k_0$. If $k_0 = 0$, then the value of S depends solely on p . For $p \neq 0$, we have that $S = +\infty > 1$. If also $p = 0$, then $|k| = |p| = |k - p|$, meaning that $\max\{|k|, |p|, |k - p|\} = \min\{|k|, |p|, |k - p|\}$ and $S = 1$. This represents a rather pathological case in one dimension, since then all modes are 0. In a higher-dimensional spectral space, one can have $S = 1$ without any of the wave numbers to be zero. This corresponds simply to an equal-sided triangle. Consider also that in any number of dimensions we have that

$$||k| - |p|| \leq |k - p| \leq |k| + |p|, \quad (\text{B.2})$$

which we shall often use.

Now, let us assume that $k = k_0 > 0$. There are three possibilities for p .

1. Case: $p = k_0$

$$\Rightarrow S = \frac{\max\{k_0, k_0, 0\}}{\min\{k_0, k_0, 0\}} = \infty > 1. \quad (\text{B.3})$$

2. Case: $p < k_0$

$$\Rightarrow S = \frac{\max\{k_0, |k_0 - p|\}}{\min\{|p|, |k_0 - p|\}} \quad (\text{B.4})$$

Here, we have to distinguish between three different possibilities for p .

(a) $p = 0$

$$\Rightarrow S = \frac{k_0}{0} = \infty > 1 \quad (\text{B.5})$$

(b) $p < 0 \Rightarrow |k_0 - p| > k_0$ and $|k_0 - p| > |p|$.

From that follows that $\max\{k_0, |k_0 - p|\} = |k_0 - p|$ and $\min\{|k_0 - p|, |p|\} = |p|$, meaning that

$$S = \frac{|k_0 - p|}{|p|} > 1. \quad (\text{B.6})$$

(c) $p > 0 \Rightarrow |k_0 - p| < k_0$ and, therefore, $\max\{k_0, |k_0 - p|\} = k_0$. Thus, we have that

$$S = \frac{k_0}{\min\{|p|, |k_0 - p|\}} > 1, \quad (\text{B.7})$$

since both $|k_0 - p| < k_0$ and $|p| < k_0$ are simultaneously fulfilled.

3. Case: $p > k_0$

Here p can be only positive, since we already assumed that $k_0 > 0$. In this case it follows that $\max\{|p|, |k_0 - p|\} = |p|$. Thus, the disparity parameter is given by

$$S = \frac{\max\{|p|, |k_0 - p|\}}{\min\{k_0, |k_0 - p|\}} = \frac{p}{k_0} > 1. \quad (\text{B.8})$$

Hence, in all possible cases $1 \leq S$, implying that $S \in [1, \infty)$.

Appendix C

Symmetries of the shell-to-shell coupling terms

In Chapter 5 we analysed the nonlinear terms by dividing the spectral space into circular shells. Applying such a decomposition on the nonlinear terms let to identifying a matrix structure that produces a coupling between the different shells. Recall that the two nonlinearities in the equation of motion lead to two coupling matrices \mathbf{T}^{NS} and \mathbf{T}^C the elements of which are to be calculated by the velocity field according to

$$T_{IJ}^{NS} = \lambda_0 \frac{1}{V} \int_{\Omega} \langle \mathbf{v} \rangle_J \cdot ((\mathbf{v} \cdot \nabla) \langle \mathbf{v} \rangle_I) d\Omega \quad (\text{C.1a})$$

$$T_{IJ}^C = \beta \frac{1}{V} \int_{\Omega} \langle \mathbf{v} \rangle_I \cdot (|\mathbf{v}|^2 \langle \mathbf{v} \rangle_J) d\Omega. \quad (\text{C.1b})$$

Here the brackets $\langle \cdot \rangle_I$ and $\langle \cdot \rangle_J$ represent a shorthand notation for the projection operators P_I and P_J as defined in the main text and the indices I and J denote the corresponding shells. As discussed in detail in Section 5.2, the symmetry properties of the interaction terms given above play an essential role in obtaining their physical interpretation. One can see immediately and without any additional rewriting that the coupling T_{IJ}^C produced by the cubic interaction is symmetric with respect to an interchange of the roles of shells S_I and S_J . This is due to the fact that $|\mathbf{v}|^2$ is simply a non-negative scalar function the value of which is independent of the spectral shells involved. Thus, the contribution T_{IJ}^C depends essentially on the scalar product $\langle \mathbf{v} \rangle_I \cdot \langle \mathbf{v} \rangle_J$ which is symmetric with respect to the two vector fields. Hence, the interaction T_{IJ}^C produces the same effect in the energy balance equations of both shells S_I and S_J .

Eq. (C.1a) that gives the mathematical form of the Navier-Stokes coupling T_{IJ}^{NS} , on the other hand, is a little bit more involved. In Section 5.2 we claimed that it is antisymmetric with respect to the indices I and J . However, this property holds only under the requirements that the velocity field is incompressible and that appropriate boundary conditions

apply. Here we shall present a proof of the antisymmetry of T_{IJ}^{NS} . In order to simplify the notation, we shall set the parameters λ_0 and V to one, since their exact value is not essential for the computation. Additionally, for brevity we consider a two-dimensional velocity field $\mathbf{v} = (v_x, v_y)$ but the reasoning can be generalised to an arbitrary number of dimensions (greater than one) in a straightforward fashion. Writing the vector \mathbf{v} componentwise, taking into account that the projection operator P is linear and integrating by parts, one can rewrite Eq. (C.1a) as

$$\begin{aligned}
T_{IJ}^{NS} &= \int_{\Omega} \langle \mathbf{v} \rangle_J \cdot ((\mathbf{v} \cdot \nabla) \langle \mathbf{v} \rangle_I) d\Omega = \\
&= \int_{\Omega} \left(\langle v_x \rangle_J v_x \frac{\partial \langle v_x \rangle_I}{\partial x} + \langle v_x \rangle_J v_y \frac{\partial \langle v_x \rangle_I}{\partial y} + \langle v_y \rangle_J v_x \frac{\partial \langle v_y \rangle_I}{\partial x} + \langle v_y \rangle_J v_y \frac{\partial \langle v_y \rangle_I}{\partial y} \right) d\Omega = \\
&= - \int_{\Omega} \left(\langle v_x \rangle_I \frac{\partial (\langle v_x \rangle_J v_x)}{\partial x} + \langle v_x \rangle_I \frac{\partial (\langle v_x \rangle_J v_y)}{\partial y} + \right. \\
&\quad \left. + \langle v_y \rangle_I \frac{\partial (\langle v_y \rangle_J v_x)}{\partial x} + \langle v_y \rangle_I \frac{\partial (\langle v_y \rangle_J v_y)}{\partial y} \right) d\Omega = \\
&= - \int_{\Omega} \langle \mathbf{v} \rangle_I \cdot ((\mathbf{v} \cdot \nabla) \langle \mathbf{v} \rangle_J) d\Omega - \int_{\Omega} (\langle \mathbf{v} \rangle_J \cdot \langle \mathbf{v} \rangle_I) \underbrace{(\nabla \cdot \mathbf{v})}_{=0} d\Omega = -T_{JI}^{NS}. \tag{C.2}
\end{aligned}$$

The second step involves integration by parts and relies on the vanishing of the boundary terms which are of the form $\langle v_i \rangle_J v_j \langle v_l \rangle_I |_{\partial\Omega}$ where the indices i, j and l denote either x or y . The contribution of such terms is zero for both periodic and no-slip ($\mathbf{v}(\mathbf{r} \in \partial\Omega, t) = 0$) boundary conditions. The antisymmetry of T_{IJ}^{NS} implies that, if the Navier-Stokes coupling between shells S_I and S_J leads to a positive contribution in the energy equation for the shell S_J , then the same coupling is responsible to a negative contribution of the same magnitude in shell S_I . Thus, the Navier-Stokes nonlinearity only moves energy from one shell to another in a globally conservative manner.

Appendix D

Derivation of Eqs. (5.25)

For the sake of completeness we shall give here the derivation of the four equations in Eqs. (5.25) involving the tensor $D_{ij}(\mathbf{k})$ which are needed in order to derive the approximation obtained in Eq. (5.24) after applying the Millionshchikov hypothesis. The relations follow from the definition of $D_{ij}(\mathbf{k})$ given in Chapter 2.2. The first one represents the trace of \mathbf{D} and can be derived as

$$\sum_{j=1}^N D_{jj}(\mathbf{k}) = \sum_{j=1}^N \left(\delta_{jj} - \frac{k_j k_j}{k^2} \right) = \sum_{j=1}^N 1 - \frac{1}{k^2} \sum_{j=1}^N k_j^2 = N - 1 \quad (\text{D.1})$$

which is the result in Eq. (5.25a). Similarly, Eq. (5.25b) can be computed as

$$\begin{aligned} \sum_{i=1}^N D_{ij}(\mathbf{k}) D_{il}(\mathbf{k}) &= \sum_{i=1}^N \left(\delta_{ij} - \frac{k_i k_j}{k^2} \right) \left(\delta_{il} - \frac{k_i k_l}{k^2} \right) = \\ &= \sum_{i=1}^N \delta_{ij} \delta_{il} - \frac{1}{k^2} \sum_{i=1}^N \delta_{ij} k_i k_l - \frac{1}{k^2} \sum_{i=1}^N \delta_{il} k_i k_j + \frac{k_j k_l}{k^4} \sum_{i=1}^N k_i^2 = \\ &= \delta_{jl} - \frac{k_j k_l}{k^2} - \frac{k_j k_l}{k^2} + \frac{k_j k_l}{k^2} = \delta_{jl} - \frac{k_j k_l}{k^2} = D_{jl}(\mathbf{k}). \end{aligned} \quad (\text{D.2})$$

Eq. (5.25c) derives as a consequence of Eq. (5.25a) and Eq. (5.25b), namely

$$\sum_{i,j=1}^N D_{ij}(\mathbf{k}) D_{ij}(\mathbf{k}) = \sum_{j=1}^N \left(\sum_{i=1}^N D_{ij}(\mathbf{k}) D_{ij}(\mathbf{k}) \right) = \sum_{j=1}^N D_{jj}(\mathbf{k}) = N - 1, \quad (\text{D.3})$$

which can also be viewed as a special case of Eq. (5.25d) when $\mathbf{k} = \mathbf{p}$. The last relation in Eq. (5.25) can be deduced as follows

$$\begin{aligned}
\sum_{j,l=1}^N D_{jl}(\mathbf{k}) D_{jl}(\mathbf{p}) &= \sum_{j,l=1}^N \left(\delta_{jl} - \frac{k_j k_l}{k^2} \right) \left(\delta_{jl} - \frac{p_j p_l}{p^2} \right) = \\
&= \sum_{j,l=1}^N \delta_{jl} \delta_{jl} - \frac{1}{p^2} \sum_{j,l=1}^N \delta_{jl} p_j p_l - \frac{1}{k^2} \sum_{j,l=1}^N \delta_{jl} k_j k_l + \frac{1}{k^2 p^2} \sum_{j=1}^N k_j p_j \sum_{l=1}^N k_l p_l = \\
&= N - 2 + \frac{(\mathbf{k} \cdot \mathbf{p})^2}{k^2 p^2}, \tag{D.4}
\end{aligned}$$

which is the result in Eq. (5.25d).

Bibliography

- [1] L. F. Richardson. *Weather Prediction by Numerical Process*. Cambridge University Press, 1922, p. 66.
- [2] U. Frisch. *Turbulence: The legacy of A. N. Kolmogorov*. Cambridge University Press, 1995.
- [3] R. Ecke. ‘The Turbulence Problem, An Experimentalist’s Perspective’. In: *Los Alamos Science* 29 (2005), pp. 124–141.
- [4] G. I. Taylor. ‘The Spectrum of Turbulence’. In: *Proc. R. Soc. Lond. A: Math. Phys. Eng. Sci.* 164 (1938), pp. 476–490.
- [5] J. Zhang, B. Tao and J. Katz. ‘Turbulent flow measurement in a square duct with hybrid holographic PIV’. In: *Exp. Fluids* 23 (1997), pp. 373–381.
- [6] B. W. Zeff et al. ‘Measuring intense rotation and dissipation in turbulent flows’. In: *Nature* 421 (2003), pp. 146–149.
- [7] A. La Porta et al. ‘Fluid particle accelerations in fully developed turbulence’. In: *Nature* 409 (2001), pp. 1017–1019.
- [8] C. Y. Wang. ‘Exact Solutions of the Unsteady Navier-Stokes Equations’. In: *Appl. Mech. Rev.* 42 (1989), pp. 269–282.
- [9] C. Y. Wang. ‘Exact Solutions of the Steady-State Navier-Stokes Equations’. In: *Annu. Rev. Fluid Mech.* 23 (1991), pp. 159–177.
- [10] O. Ladyzhenskaya. *The Mathematical Theory of Viscous Incompressible Flows*. 2nd ed. New York: Gordon and Breach, 1969.
- [11] M. E. Taylor. *Partial Differential Equations III*. Springer, 2010.
- [12] J. M. Burgers. ‘Correlation problems in a one-dimensional model of turbulence I-IV’. In: *Proc. Acad. Sci. Amst.* 53 (1950), pp. 247–742.
- [13] J. M. Burgers. *The non-linear diffusion equation*. Reidel, Dordrecht, 1974.
- [14] J. D. Cole. ‘On a quasilinear parabolic equation occurring in aerodynamics’. In: *Quart. Appl. Math.* 9 (1951), pp. 225–236.
- [15] E. Hopf. ‘The partial differential equation $u_t + u u_x = x x$ ’. In: *Comm. Pure Appl. Math.* 3 (1950), pp. 201–230.
- [16] E. Hopf. ‘A mathematical example displaying features of turbulence’. In: *Comm. Pure Appl. Math.* 1 (1948), pp. 303–322.
- [17] L. D. Landau and E. M. Lifshitz. *Fluid Mechanics*. Vol. 6. translation from Russian. Pergamon, 1959.

- [18] D. Ruelle and F. Takens. ‘On the nature of turbulence’. In: *Commun. Math. Phys.* 20 (1971), pp. 167–192.
- [19] M. J. Feigenbaum. ‘Quantitative universality for a class of nonlinear transformations’. English. In: *J. Stat. Phys.* 19 (1978), pp. 25–52.
- [20] J. P. Gollub and S. V. Benson. ‘Many routes to turbulent convection’. In: *J. Fluid Mech.* 100 (1980), pp. 449–470.
- [21] S. A. Orszag. ‘Numerical methods for the simulation of turbulence’. In: *Phys. Fluids* 12 (1969), pp. 250–257.
- [22] S. A. Orszag and G. S. Patterson. ‘Numerical simulation of three-dimensional homogeneous isotropic turbulence’. In: *Phys. Rev. Lett.* 28 (1972), pp. 76–79.
- [23] G. K. Batchelor. *The theory of homogeneous turbulence*. 2nd ed. Cambridge University Press, Cambridge, 1971.
- [24] K. R. Sreenivasan. ‘On the scaling of the turbulence energy dissipation rate’. In: *Phys. Fluids* 27 (1984), pp. 1048–1051.
- [25] B. R. Pearson, P. Krogstad and W. Van De Water. ‘Measurements of the turbulent energy dissipation rate’. In: *Phys. Fluids* 14 (2002), pp. 1288–1290.
- [26] D. A. Donzis, K. R. Sreenivasan and P. K. Yeung. ‘Scalar dissipation rate and dissipative anomaly in isotropic turbulence’. In: *J. Fluid Mech.* 532 (2005), pp. 199–216.
- [27] K. R. Sreenivasan. ‘An update on the energy dissipation rate in isotropic turbulence’. In: *Phys. Fluids* 10 (1998), pp. 528–529.
- [28] T. Gotoh, D. Fukayama and T. Nakano. ‘Velocity field statistics in homogeneous steady turbulence obtained using a high-resolution direct numerical simulation’. In: *Phys. Fluids* 14 (2002), pp. 1065–1081.
- [29] Y. Kaneda et al. ‘Energy dissipation rate and energy spectrum in high resolution direct numerical simulations of turbulence in a periodic box’. In: *Phys. Fluids* 15 (2003), pp. 21–24.
- [30] W. J. Bos, L. Shao and J. J.-P. Bertoglio. ‘Spectral imbalance and the normalized dissipation rate of turbulence’. In: *Phys. Fluids* 19, 045101 (2007).
- [31] A. N. Kolmogorov. ‘The local structure of turbulence in incompressible viscous fluid for very large Reynolds number’. In: *Dokl. Akad. Nauk SSSR* 30 (1941), pp. 299–303.
- [32] W. D. McComb. *The physics of fluid turbulence*. Oxford University Press, 1990.
- [33] P. G. Saffman. ‘The large-scale structure of homogeneous turbulence’. In: *J. Fluid Mech.* 27 (1967), pp. 581–593.
- [34] P. A. Davidson. ‘On the large-scale structure of homogeneous two-dimensional turbulence’. In: *J. Fluid Mech.* 580 (2007), pp. 431–450.
- [35] W. Heisenberg. ‘Zur statistischen Theorie der Turbulenz’. In: *Z. Phys.* 124 (1948), pp. 628–657.
- [36] S. Corrsin. ‘Further generalization of Onsager’s cascade model for turbulent spectra’. In: *Phys. Fluids* 7 (1964), pp. 1156–1159.
- [37] Y.-H. Pao. ‘Structure of turbulent velocity and scalar fields at large wavenumbers’. In: *Phys. Fluids* 8 (1965), pp. 1063–1075.

- [38] W. D. McComb. ‘A local energy-transfer theory of isotropic turbulence’. In: *J. Phys. A* 7 (1974), pp. 632–649.
- [39] J. von Neumann. *Recent theories in turbulence, in Collected Works*. Vol. 6. A. H. Taub, Pergamon Press, New York, 1963, pp. 437–472.
- [40] C. Foias, O. Manley and L. Sirovich. ‘Empirical and Stokes eigenfunctions and the far-dissipative turbulent spectrum’. In: *Phys. Fluids A-Fluid* 2 (1990), pp. 464–467.
- [41] L. Sirovich, L. Smith and V. Yakhot. ‘Energy spectrum of homogeneous and isotropic turbulence in far dissipation range’. In: *Phys. Rev. Lett.* 72 (1994), pp. 344–347.
- [42] F. Anselmet et al. ‘High-order velocity structure functions in turbulent shear flows.’ In: *J. Fluid Mech.* 140 (1984), pp. 63–89.
- [43] D. P. Ruelle. ‘Hydrodynamic turbulence as a problem in nonequilibrium statistical mechanics’. In: *Proc. Natl. Acad. Sci. U.S.A.* 109 (2012), pp. 20344–20346.
- [44] G. Boffetta and R. E. Ecke. ‘Two-dimensional turbulence’. In: *Annu. Rev. Fluid Mech.* 44 (2011), pp. 427–451.
- [45] R. Fjørtoft. ‘On the changes in the spectral distribution of kinetic energy for two-dimensional, nondivergent flow’. In: *Tellus* 5 (1953), pp. 225–230.
- [46] R. H. Kraichnan. ‘Inertial ranges in two-dimensional turbulence’. In: *Phys. Fluids* 10 (1967), pp. 1417–1423.
- [47] G. K. Batchelor. ‘Computation of the energy spectrum in homogeneous two-dimensional turbulence’. In: *Phys. Fluids* 12.12 (1969), pp. 233–239.
- [48] C. E. Leith. ‘Diffusion approximation for two-dimensional turbulence’. In: *Phys. Fluids* 11 (1968), pp. 671–672.
- [49] R. H. Kraichnan. ‘Inertial-range transfer in two- and three-dimensional turbulence’. In: *J. Fluid Mech.* 47 (1971), pp. 525–535.
- [50] P. Constantin and F. Ramos. ‘Inviscid limit for damped and driven incompressible Navier-Stokes equations in 2D’. In: *Commun. Math. Phys.* 275 (2007), pp. 529–551.
- [51] L. A. K. Blackbourn and C. V. Tran. ‘Effects of friction on forced two-dimensional Navier-Stokes turbulence’. In: *Phys. Rev. E* 84 (2011).
- [52] K. Nam et al. ‘Lagrangian chaos and the effect of drag on the enstrophy cascade in two-dimensional turbulence’. In: *Phys. Rev. Lett.* 84 (2000), pp. 5134–5137.
- [53] T. Gotoh. ‘Energy spectrum in the inertial and dissipation ranges of two-dimensional steady turbulence’. In: *Phys. Rev. E* 57 (1998), pp. 2984–2991.
- [54] K. R. Sreenivasan. ‘On the universality of the Kolmogorov constant’. In: *Phys. Fluids* 7 (1995), pp. 2778–2784.
- [55] F. Jenko et al. ‘Electron temperature gradient driven turbulence’. In: *Phys. Plasmas* 7 (2000), pp. 1904–1910.
- [56] A. J. Brizard and T. S. Hahm. ‘Foundations of nonlinear gyrokinetic theory’. In: *Rev. Mod. Phys.* 79 (2007), pp. 421–468.
- [57] T. Görler and F. Jenko. ‘Multiscale features of density and frequency spectra from nonlinear gyrokinetics’. In: *Phys. Plasmas* 15, 102508 (2008).
- [58] A. Banñón Navarro et al. ‘Free energy balance in gyrokinetic turbulence’. In: *Phys. Plasmas* 18, 092303 (2011).

- [59] B. Teaca, A. Bañón Navarro and F. Jenko. ‘The energetic coupling of scales in gyrokinetic plasma turbulence’. In: *Phys. Plasmas* 21 (2014).
- [60] L. Landau. ‘On the vibration of the electronic plasma’. In: *J. Phys. USSR* 10 (1946), pp. 25–34.
- [61] N. G. Van Kampen. ‘On the theory of stationary waves in plasmas’. In: *Physica* 21 (1955), pp. 949–963.
- [62] K. M. Case. ‘Plasma oscillations’. In: *Ann. Phys.* 7 (1959), pp. 349–364.
- [63] D. R. Hatch et al. ‘Saturation of Gyrokinetic Turbulence through Damped Eigenmodes’. In: *Phys. Rev. Lett.* 106, 115003 (2011).
- [64] G. G. Plunk et al. ‘Two-dimensional gyrokinetic turbulence’. In: *J. Fluid Mech.* 664 (2010), pp. 407–435.
- [65] D. R. Hatch et al. ‘Transition between Saturation Regimes of Gyrokinetic Turbulence’. In: *Phys. Rev. Lett.* 111 (2013), p. 175001.
- [66] V. Bratanov et al. ‘Aspects of linear Landau damping in discretized systems’. In: *Phys. Plasmas* 20, 022108 (2013).
- [67] M. J. Pueschel, T. Dannert and F. Jenko. ‘On the role of numerical dissipation in gyrokinetic Vlasov simulations of plasma microturbulence’. In: *Comput. Phys. Commun.* 181 (2010), pp. 1428–1437.
- [68] C. S. Ng, A. Bhattacharjee and F. Skiff. ‘Kinetic Eigenmodes and Discrete Spectrum of Plasma Oscillations in a Weakly Collisional Plasma’. In: *Phys. Rev. Lett.* 83 (1999), pp. 1974–1977.
- [69] A. Lenard and I. B. Bernstein. ‘Plasma oscillations with diffusion in velocity space’. In: *Phys. Rev.* 112 (1958), pp. 1456–1459.
- [70] P. L. Bhatnagar, E. P. Gross and M. Krook. ‘A model for collision processes in gases. I. Small amplitude processes in charged and neutral one-component systems’. In: *Phys. Rev.* 94 (1954), pp. 511–525.
- [71] R. E. LaQuey et al. ‘Nonlinear saturation of the trapped-ion mode’. In: *Phys. Rev. Lett.* 34 (1975), pp. 391–394.
- [72] B. I. Cohen et al. ‘Non-linear saturation of the dissipative trapped-ion mode by mode coupling’. In: *Nucl. Fusion* 16 (1976), pp. 971–992.
- [73] A. Hasegawa and K. Mima. ‘Stationary spectrum of strong turbulence in magnetized nonuniform plasma’. In: *Phys. Rev. Lett.* 39 (1977), pp. 205–208.
- [74] A. Hasegawa and K. Mima. ‘Pseudo-three-dimensional turbulence in magnetized nonuniform plasma’. In: *Phys. Fluids* 21 (1978), pp. 87–92.
- [75] Y. Kuramoto. ‘Diffusion-induced chaos in reaction systems’. In: *Progr. Theor. Phys. Suppl.* 64 (1978), pp. 346–367.
- [76] G. I. Sivashinsky. ‘Nonlinear analysis of hydrodynamic instability in laminar flames I. Derivation of basic equations’. In: *Acta Astronautica* 4 (1977), pp. 1177–1206.
- [77] G. I. Sivashinsky. ‘On self-turbulization of a laminar flame’. In: *Acta Astronautica* 6 (1979), pp. 569–591.
- [78] B. Nicolaenko and B. Scheurer. ‘Remarks on the Kuramoto-Sivashinsky equation’. In: *Physica D* 12 (1984), pp. 391–395.

- [79] E. Tadmor. ‘The well-posedness of the Kuramoto-Sivashinsky equation’. In: *SIAM J. Math. Anal.* 17 (1986), pp. 884–893.
- [80] R. Conte and M. Musette. ‘Painlevé analysis and Bäcklund transformation in the Kuramoto-Sivashinsky equation’. In: *J. Phys. A-Math. Gen.* 22 (1989), pp. 169–177.
- [81] R. Temam. *Infinite-dimensional dynamical systems in mechanics and physics*. Springer-Verlag, Applied Mathematical Sciences, Volume 68, 1988.
- [82] P. Collet et al. ‘A global attracting set for the Kuramoto-Sivashinsky equation’. English. In: *Commun. Math. Phys.* 152 (1993), pp. 203–214.
- [83] J. Goodman. ‘Stability of the Kuramoto-Sivashinsky and related systems’. In: *Commun. Pure and Appl. Math.* 47 (1994), pp. 293–306.
- [84] C. Foias et al. ‘Inertial manifolds for the Kuramoto-Sivashinsky equation and an estimate of their lowest dimension’. In: *J. Math. Pures Appl.* 67 (1988), pp. 197–226.
- [85] V. Bratanov et al. ‘Nonuniversal power-law spectra in turbulent systems’. In: *Phys. Rev. Lett.* 111, 075001 (2013).
- [86] Tobias Görler. personal communication.
- [87] S. M. Cox and P. C. Matthews. ‘Exponential time differencing for stiff systems’. In: *J. Comput. Phys.* 176 (2002), pp. 430–455.
- [88] A. Kassam and L. Trefethen. ‘Fourth-order time-stepping for stiff PDEs’. In: *SIAM J. Sci. Comput.* 26 (2005), pp. 1214–1233.
- [89] P. Collet et al. ‘Analyticity for the Kuramoto-Sivashinsky equation’. In: *Physica D* 67 (1993), pp. 321–326.
- [90] S. S. Girimaji and Y. Zhou. ‘Spectrum and energy transfer in steady Burgers turbulence’. In: *Phys. Lett. A* 202 (1995), pp. 279–287.
- [91] Y. Zhou. ‘Interacting scales and energy transfer in isotropic turbulence’. In: *Phys. Fluids A-Fluid* 5 (1993), pp. 2511–2524.
- [92] B. Teaca et al. ‘Locality and universality in gyrokinetic turbulence’. In: *Phys. Rev. Lett.* 109, 235003 (2012).
- [93] G. G. Howes et al. ‘Astrophysical gyrokinetics: Basic equations and linear theory’. In: *Astrophys. J.* 651 (2006), pp. 590–614.
- [94] H. H. Wensink et al. ‘Meso-scale turbulence in living fluids’. In: *Proc. Natl. Acad. Sci. U.S.A.* 109 (2012), pp. 14308–14313.
- [95] J. Dunkel et al. ‘Minimal continuum theories of structure formation in dense active fluids’. In: *New J. Phys.* 15 (2013), p. 045016.
- [96] J. Dunkel et al. ‘Fluid dynamics of bacterial turbulence’. In: *Phys. Rev. Lett.* 110, 228102 (2013).
- [97] P. C. Swift J. and Hohenberg. ‘Hydrodynamic fluctuations at the convective instability’. In: *Phys. Rev. A* 15 (1977), pp. 319–328.
- [98] R. A. Simha and S. Ramaswamy. ‘Hydrodynamic fluctuations and instabilities in ordered suspensions of self-propelled particles’. In: *Phys. Rev. Lett.* 89, 058101 (2002).
- [99] J. Toner and Y. Tu. ‘Flocks, herds, and schools: A quantitative theory of flocking’. In: *Phys. Rev. E* 58 (1998), pp. 4828–4858.

- [100] J. Toner, Y. Tu and S. Ramaswamy. ‘Hydrodynamics and phases of flocks’. In: *Ann. Phys.* 318 (2005), pp. 170 –244.
- [101] M. C. Marchetti et al. ‘Hydrodynamics of soft active matter’. In: *Rev. Mod. Phys.* 85 (2013), pp. 1143–1189.
- [102] V. Bratanov, F. Jenko and E. Frey. *Self-organization in active fluids: A new class of turbulence*. submitted to Proc. Natl. Acad. Sci. U.S.A.
- [103] S. Gama, U. Frisch and H. Scholl. ‘The two-dimensional Navier-Stokes equations with a large-scale instability of the Kuramoto-Sivashinsky type: Numerical exploration on the Connection Machine’. English. In: *J. Sci. Comput.* 6 (1991), pp. 425–452.
- [104] A. S. Monin and A. M. Yaglom. *Statistical fluid mechanics*. MIT Press, Cambridge, Mass., 1975.
- [105] M. D. Millionshchikov. ‘Theory of homogeneous isotropic turbulence’. In: *Dokl. Akad. Nauk SSSR* 32 (1941), pp. 611–614.
- [106] B. D. Fried and S. D. Conte. *The Plasma Dispersion Function*. Academic Press, London, 1961.

Acknowledgements

First and foremost I would like to express my gratitude to my supervisor Prof. Frank Jenko, who supported me during my work and made it possible in the first place. It has been a great pleasure to conduct my research at the Max-Planck-Institut für Plasmaphysik in Garching and this I owe to him. Further, I would like to thank my supervisor at the LMU, Prof. Erwin Frey, for kindly providing his expertise in the area of biophysics which greatly improved the quality of the present work. Sincere thanks go also to David Hatch, PhD, and Dr. Alejandro Bañón Navarro for the numerous discussions on turbulence and the gyrokinetic theory. I also appreciate discussions with Dr. Hauke Doerk and Dr. Tobias Görler as well as their effort in reading parts of this work and providing suggestions for improvements. In that regard let me further acknowledge Daniel Grošelj and Ivan Erofeev for sacrificing some of their time to read chapters of this thesis and give constructive ideas. I thank also Dr. Omar Maj who was always there and ready to help when I was struggling with mathematical problems. Last but not least, my sincere gratitude deserves Michael Oberparleiter for his unlimited helpfulness when I experienced some of the numerous programming difficulties during this work. His invaluable pieces of advice regarding C++, Vim or L^AT_EX, to name a few, saved me hours of tedious searching on the Internet. It were those various little tips which helped me achieve the best of my numerical tools and obtain my results in the form they are presented here.

Lebenslauf

Vasil Bratanov

persönliche Information

Geburtsdatum: 04.05.1987
Geburtsort: Burgas, Bulgarien
Staatsangehörigkeit: bulgarisch

Schulbildung

09/1994 - 06/2001 Schule „Naiden Gerov“, Burgas
09/2001 - 05/2006 Fremdsprachengymnasium „Goethe“, Burgas

Studium

10/2006 - 09/2009 Bachelor of Science, Physik, Humboldt-Universität zu Berlin
Gesamtnote 1,4
10/2009 - 09/2011 Master of Science, Theoretische and Mathematische Physik,
Ludwig-Maximilians-Universität München
Gesamtnote 1,3

Promotionsstudium

11/2011 - 10/2014 Doktorand am Max-Planck-Institut für Plasmaphysik, Garching

Publications (peer-reviewed)

1. **Aspects of linear Landau damping in discretized systems**
V. Bratanov, F. Jenko, D. R. Hatch, and S. Brunner, Physics of Plasmas 20, 022108 (2013)
2. **Nonuniversal power-law spectra in turbulent systems**
V. Bratanov, F. Jenko, D. R. Hatch, and M. Wilczek, Phys. Rev. Lett. 111, 075001 (2013)
3. **Transition between saturation regimes of gyrokinetic turbulence**
D. R. Hatch, F. Jenko, A. B. Navarro, V. Bratanov, Phys. Rev. Lett. 111, 175001 (2013)
4. **Phase space scales of free energy dissipation in gradient-driven gyrokinetic turbulence**
D. R. Hatch, F. Jenko, V. Bratanov, A. B. Navarro, Journal of Plasma Physics 80, pp 531-551 (2014)